Evaluation of instantaneous and cumulative models for reactivity ratio estimation with multiresponse scenarios

by

Xiaoqin Zhou

A thesis

presented to the University of Waterloo

in fulfillment of the

thesis requirement for the degree of

Master of Applied Science

in

Chemical Engineering

Waterloo, Ontario, Canada, 2004

I hereby declare that I am the sole author of this thesis. This is a true copy of the thesis, including any required final revisions, as accepted by my examiners.

I understand that my thesis may be made electronically available to the public.

ABSTRACT

Estimating reactivity ratios in multicomponent polymerizations is becoming increasingly important. At the same time, using cumulative models is becoming imperative, as some multicomponent systems are inherently so fast that instantaneous "approximate" models can not be used.

In the first part of the thesis, triad fractions (sequence length characteristics) are employed in a multiresponse scenario, investigating different error structures and levels. A comparison is given between instantaneous triad fraction models and instantaneous composition model, which represent the current state-of-the-art.

In the second part of the thesis, extensions are discussed with cumulative composition and triad fraction models over the whole conversion range, thus relating the problem of reactivity ratio estimation to the optimal design of experiments (i.e. optimal sampling) over polymerization time and conversion.

The performance of cumulative multiresponse models is superior to that of their instantaneous counterparts, which can be explained from an information content point of view. As a side-project, the existence of azeotropic points is investigated in terpolymer (Alfrey-Goldfinger equation) and tetrapolymer (Walling-Briggs equation) systems.

Acknowledgements

First of all, I want to express my grateful appreciation to my supervisor, Prof. Alex Penlidis, and to Prof. Tom Duever for their time, guidance, generosity, patience, and most of all their kindness.

I would like to thank every member of our research group for all the help. Jennifer Chen, Matthew Scorah, Nahlar Sahloul, Joy Jie Cheng, Ramin Khesareh, all of them gave me selfless help.

Finally, I would like to thank my parents and my husband Yu. They gave me plentiful supports.

Table of contents

List of Tables

List of figures

1. Introduction and Objectives

Reactivity ratios are important parameters used to describe the characteristics of a copolymerization system. The basic model used to estimate reactivity ratios is Mayo-Lewis equation. In early years, because of its complicated form, investigators had to resort to graphic and linear regression methods to estimate the reactivity ratios. But these approaches had inherent faults. From a statistical point of view, they violated the basic assumptions for linear regression. Tidwell et al. (1965) used nonlinear least square (NLLS) to get more precise results. Patino-Leal et al. (1980) applied the Error-in-Variables model (EVM), which takes into account the error in every measured variable used by the model. Rossignoli and Duever (1995) discussed and compared these two methods. From a statistical point of view, both methods are better than linear methods in that they consider the nonlinear nature of the model structure. With the introduction of better and easy to use computing tools, both methods have gained in popularity.

Despite these advances, there are several aspects of reactivity ratio estimation that need to be addressed. One of the most important aspects is related to the fact that the Mayo-Lewis model relates instantaneous properties. What we in fact measure most often are cumulative properties. If the cumulative properties do not change considerably with conversion, then the Mayo-Lewis model can often be used. The deviation between cumulative and instantaneous composition is called composition drift. Usually a small composition drift occurs near the low conversion, which means the experiment should be run at low conversions. For some systems, because the reaction is fast, it is difficult to stop at low conversion. For those systems, where the monomers have very different reactivity ratios, even at low conversion, there is considerable composition drift. To deal with this problem, a more complicated model, which calculates cumulative properties, is required.

Second, other physical measurement related to reactivity ratio can be used, such as sequence length distributions (triad fractions), propagation rate constant etc.. Also, on-line detection of monomer concentration has been investigated. Although the precision still does not satisfy industrial needs and the applications are only limited to special systems, researchers have investigated the combination of models with real time data.

1.1. Objectives

The requirement of controlling the reaction at very low conversion to avoid composition drift may pose limitations for certain systems. At present, experimental composition data often accompany conversion data (Zerroukhi et al., 1999; Erbil et al., 2000; Fernández-Monreal et al., 1999; Zaldivar et al., 1997; Ziaee et al., 1998; Gauthier et al., 2002; Fernández-García et al., 2000; Kucharski et al., 1997). It is therefore suitable to use a cumulative copolymer composition model to deal with this situation. Hautus et al. (1985), Plaumann(1989) and Van Den Brink et al.(1999) investigated in detail the analytical integrated form of the copolymerization composition equation with nonlinear regression. One of our research objectives is to continue to improve the estimation at high conversions with NLLS and/or EVM using the full copolymer composition model in an ordinary differential equation form. This can be further extended for application to the sequence length distribution model as well.

In addition, in order to modify the mechanical properties of a polymer, research has progressed on multicomponent polymerization (terpolymerization). Thus, it is very interesting to extend the estimation schemes from copolymer systems to terpolymer systems, and to test these schemes against experimental data from our group.

2. Copolymerization Models

There are four steps during the propagation stage of free radical copolymerization. Equations 2.1 to 2.4 represent these four steps, whereas Equations 2.5 and 2.6 give the definitions of reactivity ratios.

$$R_1 * + M_1 \xrightarrow{k_{11}} R_1 * \quad (2.1)$$

$$R_1 * + M_2 \xrightarrow{k_{12}} R_2 * \quad (2.2)$$

$$R_2 * + M_1 \xrightarrow{k_{21}} R_1 * \quad (2.3)$$

$$R_2 * + M_2 \xrightarrow{k_{22}} R_2 * \quad (2.4)$$

$$r_1 = \frac{k_{11}}{k_{12}}; \quad (2.5)$$

$$r_2 = \frac{k_{22}}{k_{21}} \quad (2.6)$$

Here R^*_i are radicals, M_i are monomers and r_i are reactivity ratios. Based on their time scale, mathematical models are classified into instantaneous and cumulative models. The instantaneous model describes the composition variation from time t to t+dt, while the cumulative model describes the composition variation from time 0 to time t.

2.1. Instantaneous composition model

The most widely used copolymerization model is the Mayo-Lewis model given by Equation 2.7 and 2.8 in its two popular alternative forms. The model relates copolymer composition (F1) with feed composition (f_1 or $[M_1]$) via the reactivity ratios r_1 and r_2, which are the parameters to be estimated. $[M_1]$ is concentration of monomer 1 in the reactor, f_1 is the mole fraction of (unreacted, unbound, free) monomer 1, and F_1 is the corresponding mole fraction of monomer 1 incorporated (bound) in the copolymer chains.

$$\frac{d[M_1]}{d[M_2]} = \frac{[M_1]}{[M_2]} \cdot \frac{r_1[M_1] + [M_2]}{[M_1] + r_2[M_2]} \quad (2.7)$$

$$F_1 = \frac{(r_1 - 1) f_1^{\,2} + f_1}{(r_1 + r_2 - 2) f_1^{\,2} + 2(1 - r_2) f_1 + r_2} \tag{2.8}$$

Here:

$$F_1 = \frac{d[M_1]}{d[M_1] + d[M_2]} \tag{2.9}$$

$$f_1 = \frac{[M_1]}{[M_1] + [M_2]} \tag{2.10}$$

2.2. Instantaneous sequence length model

Sequence length usually characterizes polymer chain microstructure. Rudin(1981) used average sequence length models to estimate reactivity ratios:

$$\overline{n}_1 = \frac{N_{11} + 1/2\, N_{12}}{1/2\, N_{12}} = \frac{N_{212} + N_{211} + N_{111}}{N_{212} + N_{211}/2} \tag{2.11}$$

$$\overline{n}_2 = \frac{N_{22} + 1/2\, N_{12}}{1/2\, N_{12}} = \frac{N_{121} + N_{221} + N_{222}}{N_{121} + N_{221}/2} \tag{2.12}$$

$\overline{n}_1$ is number average sequence length, N_{ij} is the diad quantity and N_{ijk} is the triad quantity. When normalized, the above equations are given as follows :

$$\overline{n}_1 = \frac{A_{11} + 1/2\, A_{12}}{1/2\, A_{12}} = \frac{A_{212} + A_{211} + A_{111}}{A_{212} + A_{211}/2} = \frac{1}{A_{212} + A_{211}/2} \tag{2.13}$$

$$\overline{n}_2 = \frac{A_{22} + 1/2\, A_{12}}{1/2\, A_{12}} = \frac{A_{121} + A_{221} + A_{222}}{A_{121} + A_{221}/2} = \frac{1}{A_{121} + A_{221}/2} \tag{2.14}$$

A_{ij}, A_{ijk} are mole fractions of the diad and the triad fraction respectively (i,j,k=1,2). There are six triad mole fractions for copolymer.

The number average sequence length can be related to reactivity ratios as follows:

$$\overline{n}_1 = r_1 \frac{[M_1]}{[M_2]} + 1 \tag{2.15}$$

$$\overline{n}_2 = r_2 \frac{[M_2]}{[M_1]} + 1 \tag{2.16}$$

O'Driscoll (1980) pointed out that if one uses one set of triad data only, the r_1 and r_2 estimates will not have the same precision. In his work the triad data were all monomer-

1-centered triads, and the average number sequence length of monomer 2 was defined by $\overline{n}_1 . \overline{n}_2 = F_2 / F_1 \cdot \overline{n}_1$. In the average number sequence length- composition plot, $\overline{n}_1$ was less scattered than $\overline{n}_2$, *i.e.*, r_1 was estimated more closely to the true value than r_2 was. This implies that the estimate calculated from all triad data will be better. From the above equations, based on the number average sequence length, a direct relationship is found between sequence distribution and reactivity ratios.

The typical triad fraction model is described by equations 2.17 - 2.22.

$$A_{211+112} = \frac{2r_1 f_1 f_2}{r_1^{\,2} f_1^{\,2} + 2r_1 f_1 f_2 + f_2^{\,2}} \tag{2.17}$$

$$A_{212} = \frac{f_2^{\,2}}{r_1^{\,2} f_1^{\,2} + 2r_1 f_1 f_2 + f_2^{\,2}} \tag{2.18}$$

$$A_{111} = \frac{r_1^{\,2} f_1^{\,2}}{r_1^{\,2} f_1^{\,2} + 2r_1 f_1 f_2 + f_2^{\,2}} \tag{2.19}$$

$$A_{122+221} = \frac{2r_2 f_1 f_2}{r_2^{\,2} f_2^{\,2} + 2r_2 f_1 f_2 + f_1^{\,2}} \tag{2.20}$$

$$A_{121} = \frac{f_2^{\,2}}{r_2^{\,2} f_2^{\,2} + 2r_2 f_1 f_2 + f_1^{\,2}} \tag{2.21}$$

$$A_{222} = \frac{r_2^{\,2} f_2^{\,2}}{r_2^{\,2} f_2^{\,2} + 2r_2 f_1 f_2 + f_1^{\,2}} \tag{2.22}$$

Hill et al. (1989) used all six triad fractions to estimate reactivity ratios for styrene (STY) and acrylonitrile (AN). Comparing with the composition model, the triad fraction data give better estimates, even though the measurements are determined with relatively lower accuracy. Cheetham (1994) also used the triad fractions of acrylonitrile (AN) and vinyl acetate (VAc) copolymerization to estimate reactivity ratios. Burke (1994) performed a model discrimination study for reactivity ratios using the triad fraction model.

Pentad fraction model is more complicated than diad and triad fraction model due to the longer sequences involved. For pentad model:

$$\overline{n}_1 = 1/(1-\alpha_1) = r_1 \frac{[M_1]}{[M_2]} + 1 \tag{2.23}$$

$$\overline{n}_2 = 1/(1-\alpha_2) = r_2 \frac{[M_2]}{[M_1]} + 1 \tag{2.24}$$

Rudin(1981) gave an example for α_1:

$$\alpha_1 = \frac{0}{2}s_1 + \frac{2}{16}s_2 + \frac{2}{8}s_3 + \frac{8}{14}s_4 + \frac{8}{12}s_5 + s_6 \tag{2.25}$$
$$s_1 = N_{22122};\ s_2 = 2N_{22121} + N_{12121} + 2N_{22112};\ s_3 = 2N_{12112};$$
$$s_4 = 2N_{11122} + 2N_{11121};\ s_5 = N_{21112} + 2N_{11112};\ s_1 = N_{11111}$$

where N_{ijkmn} is the pentad mole quantity.

2.3. Cumulative composition model

2.3.1. Analytically integrated model

The Meyer-Lowry equation is obtained by integrating the Mayo-Lewis equation and is given as follows..

$$x = 1 - \left(\frac{f_1}{f_{1,0}}\right)^{\alpha}\left(\frac{1-f_1}{1-f_{1,0}}\right)^{\beta}\left(\frac{f_{1,0}-\delta}{f_1-\delta}\right)^{\gamma} \tag{2.26}$$

where:

$$\alpha = \frac{r_2}{1-r_2};\ \beta = \frac{r_1}{1-r_1};\ \gamma = \frac{1-r_2}{2-r_1-r_2};\ \delta = \frac{1-r_1r_2}{(1-r_1)(1-r_2)}$$

$$x = 1 - \frac{N_1 + N_2}{N_{10} + N_{20}} \tag{2.27}$$

$$\overline{F_1} = \frac{f_{10} - f_1(1-x)}{x} \tag{2.28}$$

Here *x* is total molar conversion defined by equation 2.27. This cumulative model relates conversion, x, to f_1, and via the Mayo-Lewis model, to F_1. The Mayo-Lewis model (i.e. the instantaneous copolymer composition model given by equation 2.8) is integrated between feed compositions f_{10} to f_1. Van den Brink et al. (1999) and Garcia-Rubio et al. (1985) used the cumulative analytical composition model to estimate reactivity ratios.

2.3.2. Numerically integrated model

There is an assumption for Meyer-Lowry equation that the reactivity ratios do not change during the whole conversion range. In fact, reactivity ratios may change at high conversion, due to diffusion effects on the propagation rate constants. Hence, solving the cumulative composition equation numerically becomes a more general approach.

Shawki and Hamielec (1979) tried to obtain estimates directly from the integrated form of the copolymer equation:

$$\ln(1-x) = \int_{f_{10}}^{f_1} \frac{df_1}{F_1 - f_1} \tag{2.29}$$

Here x is overall mole conversion defined by Equation 2.27. Runge-Kutta method was used to numerically integrate Equation 2.29. As the authors mentioned, this algorithm is easy to handle. However, there exist singularities at either the azeotropic point or at x=1. To simplify the calculation, an alternative form of equation 2.29 is given as follows

$$\frac{df_1}{dx} = \frac{f_1 - F_1}{1-x} \tag{2.30}$$

This equation avoids problems associated with the azeotropic point in the algorithm. The cumulative polymer composition $\overline{F_1}$ is determined by Equation 2.28 or alternatively by the following equation:

$$\frac{d\left(x\overline{F_1}\right)}{dx} = F_1 \tag{2.31}$$

2.4. Cumulative sequence length model

The definition of cumulative triad fraction is via Equation 2.32, so the relationship between cumulative triad fraction and instantaneous monomer mole fraction and mole conversion can be formulated as follows. Triad fractions centered on monomer 2 have similar equations.

$$\frac{dx\overline{A}_{ijk}}{dx} = A_{ijk} \tag{2.32}$$

$$\frac{dx\overline{A}_{211+112}}{dx} = A_{211+112} = \frac{2r_1 f_1 f_2}{r_1^{\,2} f_1^{\,2} + 2r_1 f_1 f_2 + f_2^{\,2}} \tag{2.33}$$

$$\frac{dx\overline{A}_{212}}{dx} = A_{212} = \frac{f_2^{\,2}}{r_1^{\,2} f_1^{\,2} + 2r_1 f_1 f_2 + f_2^{\,2}} \tag{2.34}$$

2.5. Extensions to terpolymerization

For terpolymerization, after the stationary state assumption is applied,

$$k_{12}[R_1][M_2] + k_{13}[R_1][M_3] = k_{21}[R_2][M_1] + k_{31}[R_3][M_1] \tag{2.35}$$

$$k_{21}[R_2][M_1] + k_{23}[R_2][M_3] = k_{12}[R_1][M_2] + k_{32}[R_3][M_2] \tag{2.36}$$

$$k_{31}[R_3][M_1] + k_{32}[R_3][M_2] = k_{13}[R_1][M_3] + k_{23}[R_2][M_3] \tag{2.37}$$

the Alfrey-Goldfinger equation (Equation 2.38) is finally obtained. The definition of reactivity ratios is the same as that of the copolymer, so the reactivity ratios of the constituent copolymer are also applied to the terpolymer system.

$$\begin{aligned} F_1 : F_2 : F_3 = {} & f_1\left[\frac{f_1}{r_{31}r_{21}} + \frac{f_2}{r_{21}r_{32}} + \frac{f_3}{r_{31}r_{23}}\right]\left[f_1 + \frac{f_2}{r_{12}} + \frac{f_3}{r_{13}}\right] \\ & : f_2\left[\frac{f_1}{r_{12}r_{31}} + \frac{f_2}{r_{12}r_{32}} + \frac{f_3}{r_{32}r_{13}}\right]\left[\frac{f_1}{r_{21}} + f_2 + \frac{f_3}{r_{23}}\right] \\ & : f_3\left[\frac{f_1}{r_{13}r_{21}} + \frac{f_2}{r_{23}r_{12}} + \frac{f_3}{r_{13}r_{23}}\right]\left[\frac{f_1}{r_{31}} + \frac{f_2}{r_{32}} + f_3\right] \end{aligned} \tag{2.38}$$

For a multi-component system, similar analysis results in the multi-component copolymerization (Walling-Briggs) equation:

$$
\begin{aligned}
d[M_1]:d[M_2]:\cdots:d[M_n] &= F_1:F_2:\cdots:F_n \\
&= [M_1]D_1\left\{[M_1]+\frac{[M_2]}{r_{12}}+\frac{[M_3]}{r_{13}}+\cdots+\frac{[M_n]}{r_{1n}}\right\} \\
&:[M_2]D_2\left\{\frac{[M_1]}{r_{21}}+[M_2]+\frac{[M_3]}{r_{23}}+\cdots+\frac{[M_n]}{r_{2n}}\right\} \\
&\vdots \\
&:[M_n]D_n\left\{\frac{[M_1]}{r_{n1}}+\frac{[M_2]}{r_{n2}}+\frac{[M_3]}{r_{n3}}+\cdots+[M_n]\right\}
\end{aligned}
\tag{2.39}
$$

where

$$
D_1 = \begin{vmatrix}
-\frac{1}{r_{n1}} & \frac{1}{r_{21}} & \frac{1}{r_{31}} & \cdots & \frac{1}{r_{n-1,1}} \\
-\frac{[M_2]}{r_{n2}} & -\left(\frac{[M_1]}{r_{21}}+\frac{[M_3]}{r_{23}}+\cdots+\frac{[M_n]}{r_{2n}}\right) & \frac{[M_2]}{r_{32}} & \cdots & \frac{[M_2]}{r_{n-1,2}} \\
-\frac{[M_3]}{r_{n3}} & \frac{[M_3]}{r_{23}} & -\left(\frac{[M_1]}{r_{31}}+\frac{[M_2]}{r_{32}}+\cdots+\frac{[M_n]}{r_{3n}}\right) & \cdots & \cdots \\
\vdots & & & \cdots & \\
-\frac{[M_{n-1}]}{r_{n,n-1}} & & & \cdots & -\left(\frac{[M_1]}{r_{n-1,1}}+\frac{[M_2]}{r_{n-1,2}}+\cdots+\frac{[M_n]}{r_{n-1,n}}\right)
\end{vmatrix}
\tag{2.40}
$$

D_2 to D_n have analogous forms to D_1.

3. Reactivity Ratio Estimation: Literature Update

3.1. Introduction

Reactivity ratios are important parameters for describing copolymerization and terpolymerization characteristics. Their estimation is an area of interest to both academia and industry (Polic et al.,1998). Traditionally, reactivity ratios are estimated using the instantaneous copolymer composition equation, usually referred to as the Mayo-Lewis equation (Equation 2.7 or its equivalent form Equation 2.8), based on copolymer composition data, obtained by running polymerizations at low conversions i.e. if usually conversion levels of less than 5%, although the value may range from 5% to 10% depending on the copolymer system. Experiments are designed, for the unconstrained case, using Tidwell-Mortimer methodology (Tidwell and Mortimer, 1965; Dube et al., 1991), or, if there are constraints with respect to comonomer feed composition, via the methodology described by Burke et al. (1993).

Compared to methods using copolymer composition data, efforts to use sequence length (triad fraction) data for estimation are scarce. This was maybe understandable in the past, due to experimental complications with collecting triad fraction data, but it should not be an obstacle nowadays.

Here we build upon Polic et al. (1998) and present recent papers where reactivity ratios are estimated, published during the period 1997 to date.

3.2. Case studies dealing with reactivity ratio estimation reported between 1997 to date

Polic et al. (1998) presented a comprehensive literature survey on reactivity ratio estimation before 1997. Table 3.1 lists recent articles (1997 to date) where reactivity ratios are estimated. Copolymer systems, estimation methods used and brief related comments are listed. Table 3.2 contains a list of abbreviations used in the commentary of Table 3.1

Table 3.1 A listing of recent articles (1997 to date) where reactivity ratios are estimated (see Table 3.2 for a list of abbreviations)

Reference	Date	Method	System/Comments
Aguilar et al.	2002	NLLS	HEMA/AMPS,DMAA/AMPS,low conversion data, integrated model.
Belleney et al	2002	FR,KT,TM	MMA,PMEM,PEEM/MA; MMA,PMEM,PEEM,MA/NaSS for terpolymer MMA/PMEM(PEEM)/MA (NaSS)
Bernhardt et al.	2001	NLO	Methylated b-cyclodextrin with hydrophobic acrylates; in water medium
Brar and Dutta	1998	KT,	AN/ Hexyl methacrylate; low conversion
Brar and Hekmatyar	1999		AN/STY/MMA;microstructure determination
Brar and Yadav	2003	KT,EVM	GMA/Vinylidene chloride
Buback and Wittkowski	2000	NLO	Ethene with AA and MAA; high pressures and temperatures
Buback et al.	1999	NLO	Ethene with acrylic and methacrylic acid;high pressure
Camail et al.	1998	ML	acrylamide, acrylic acid and N-(1,1-dimethyl-3-oxobutyl)acrylamide; terpolymer system
Catalgil-Giz et al.	2002	EVM	STY/MMA; on-line monitoring issues
Chambard et al	1999	NLLS	Sty/BA
Coote	1997		STY/MMA
Coskun and Ilter	2002	FR,KT	(2-phenyl-1,3-dioxolane-4-yl)MMA with alkyl methacrylates

Table 3.1(Cont'd)

Reference	Date	Method	System/Comments
Coskun et al.	2002	KT,FR, ML	3-phthalimido-2-HPMA/STY; thermal analysis studies
Czerwinski	1997	KT	STY/methyl α-cyanocinnamate
Czerwinski	1998	NLLS	Low and high conversion; general copolymer system
De and Sathyanarayana	2002a	NLO	Indene/alkyl acrylates;Tg information
De and Sathyanarayana	2002b	NLO	Indene/p-tert-butylstyrene; thermal degradation; Tg studies
De and Sathyanarayana	2002c	FR,KT	MMA/VAc/Molecular Oxygen (the copolyperoxide of MMA and VAc)
Demirelli et al.	2000	FR,KT	(3-mesityl-3-methylcyclobutyl)-2-HEMA with AN
Erbil et al.	2000	TM	itaconic acid/ acrylamide; conductometric titration method; conversion less than 15%
Erol and Soykan	2002	FR,KT	MMA/2-methylbenzyl methacrylate and 4-methylbenzyl methacrylate
Fernandez-Garcia et al.	2000a	NLLS	2-HEMA/BMA;low conversions;Tg data as well
Fernandez-Garcia et al.	2000b	TM	STY/BA; solvent effects
Fernandez-Monreal et al	1999	TM	2-HEMA/ STY in DMF solvent, triad fraction data
Filley et al.	2002		Ethylene/VAc; transition state theory
Galimberti et al.	1999	NLO	Ethene/propene with metallocenes; correlation between reactivity ratio and zirconocene structure
Galimberti et al.	1998	NLO	Ethene/propene; use of C^{13}-NMR data

Table 3.1(Cont'd)

Reference	Date	Method	System/Comments
Gauthier et al.	2002	EVM,NLLS	Sulfobetaine zwitterionomers based on n-BA and 2-ethoxyethyl acrylate; Low and high conversions
Grockner and Ritter	1999	NLO	Methylated b-cyclodextrim with isoboruyl acrylate and BA in aqueous medium
Habibi et al.	2003	GLS	i-BMA/LMA; linear least squares adjusted by variance-covariance matrix
Habibi et al.	2003		lauryl methacrylate–isobutyl methacrylate in bulk
Haddleton et al.	1997	NLO	MMA and BMA in anionic radical and living radical polymerizations
Hagiopol et al.	2003	Simplex algorithm	Several systems with different characters of reactivity ratios.
Hakim et al.	2000	EVM,NLLS	BA/MMA; solution polymerization; elevated temperatures; depropagation
Ito et al.	2000	KT	Hydroxystyrene derivatives with t-BMA and t-BA
Jo and Lee	2001	Monte Carlo	Effect of reactivity ratios on hyperbranched polymer microstructure; simulation
Kaim	2000	NLO	STY/AN; solvent effect
Kaim and Oracz	1999	NLO	STY/MMA; solvent effect
Kaim	1998	Simplex algorithm	STY/MMA; bulk
Kaim and Oracz	1998	Simplex algorithm	STY/AN terminal and penultimate model; solvent effect

Table 3.1(Cont'd)

Reference	Date	Method	System/Comments
Kucharski and Lubczak	1997	KT,FR	Hydroxyalkyl methacrylates with acrylamide and methacrylamide;low conversion
Lousenburg and Shoichet	2000	EVM	Trifluorovinyl ethers with Vac; low conversion
Manders et al.	1997	TM	MMA/BMA
McManus et al.	2002	EVM	AMS/BA; bulk
McManus et al.	1999	EVM	BA/MMA; bulk elevated temperature
McManus et al.	1998a	EVM	AN/VAc; bulk
McManus et al.	1998b	EVM	STY/HEA;STY/HEA/EA
Mohammed et al.	1998	KT;NLLS	Dimethyl meta- isopropenyl benzyl isocyanate with STY,MMA and BA
Monett et al.	2002	FR,KT,TM, GA	MMA/MVE; low conversion
Ni and Hunkeler	1997	ANN	High conversion
Oliva et al.	1997	NLO	Ethylene/STY with zirconocene-based catalyst
Oracz and Kaim	2001		Maximum likelihood methodology;general copolymer system
Palmer et al.	2001	EVM	AMS/MMA; solution; depropagation
Palmer et al.	2000	EVM	AMS/MMA; bulk; depropagation
Prevost et al.	1999	EKT	Oxidative copolymerization of aniline with alkoxysulfonated anilines
Rainaldi et al.	2000	KT	AA/HEMA; template polymerization
Roos et al.	1999	NLO	BA/MMA and poly(MMA) macromers; comparison with ATRP
Ryttel	1999	FR,KT	EMA with halophenyl maleimides
Sanghvi et al.	2000	FR, KT,TM	STY /AN; microemulsion; low conversions

Table 3.1(Cont'd)

Reference	Date	Method	System/Comments
Sarzotti et al.	2002	ML	Ethylene/1-hexene
Scorah et al.	2001	EVM	MMA/VAc;bulk/solution; low conversions
Senthilkumar et al.	2001	FR,KT	(Phthalimido)EMA/GMA
Shan et al.	2000		STY/phenylmaleimide; charge transfer complex
Smith and Klier	1998	NLO	Methacrylic acid with poly(ethylene glycel) mono methacrylate
Stergiou et al.	2002	FR,KT	STY/alkyl methacrylates; thermal properties
Thamizharasi et al.	1999a	FR,KT,EKT	4-Nitrophenyl Acrylate/MMA
Thamizharasi et al.	1999b	FR,KT,EKT	MA with CPA; applications in leather industry
Thamizharasi et al.	1997a	FR,KT,EKT	MMA and BA with acetylphenyl acrylate
Thamizharasi et al.	1997b	FR,KT,EKT	GMA with nitrophenyl acrylate
Van Den Brink et al.	1999a	NLLS	General system
Van Den Brink et al.	1999b	NLLS	MMA/MBL; on-line Raman Spectroscopy
Vijayanand et al.	2003	KT,FR,EVM	BCPA/MMA; solution; low conversions
Vijayanand et al.	2002	KT,FR,EVM	DMPMA/MMA; low conversion
Yamada et al.	2000	KT,Qe	Vinyl Esters in Fluoroalcohols as solvents; conversions 10-40%;solvent effect
Zaldivar et al	1997	KT,TM,ML	Acrylic acid/VAc; low conversion
Zerroukhi et al.	1999	KT,MH	Substituted STY/Manh; low and high conversion
Zhao et al.	2002	NLO	STY/n-butyl maleimide; charge transfer complex
Ziaee and Nekoomanesh	1997	FR,KT,EKT,MH	STY/BA

Table 3.2 Abbreviation tables

Abbreviation	Description
AA	Acrylic acid
AMS	α-methyl styrene
AN	Acrylonitrile
ANN	Artificial Neural Network
BA	Butyl acrylate
BCPA	Benzyloxycarbonylphenyl acrylate
BCPM	4-benzyloxycarbonylphenyl
BMA	Butyl methacrylate
CPA	Chlorophenyl acrylate
DMF	N,N'-dimethylformamide
DMPMA	3,5-Dimethylphenyl methacrylate
EA	Ethyl acrylate
EKT*	Extended Kelen-Tudos
EMA	Ethyl methacrylate
EVM*	Error-in-variables-model
FR*	Fineman-Ross
GA	Genetic Algorithm
GLS	General Linear Squares
GMA	Glycidyl methacrylate
HEA	Hydroxyethyl acrylate
HEMA	2-hydroxyethyl methacrylate

Table 3.2(Cont'd)

Abbreviation	Description
HPMA	Hydroxypropyl methacrylate
KT*	Kelen-Tudos
MA	Methyl acrylate
MAA	Methacrylic acid
MAN	Methacrylonitrile
MAnh	Maleic Anhydride
MBL	α-mehtylene-γ-butyrolactone
MH*	Mao-Huglin
ML*	Mayo-Lewis
MMA	Methyl methacrylate
NLLS*	Nonlinear least squares
NLO*	Nonlinear optimization
Qe*	Q-e scheme
STY	Styrene
TM*	Tidwell-Mortimer
VAc	Vinyl Acetate

* Basic references for the methods identified by an asterisk can be found in Polic et al. (1998)

4. Parameter Estimation and Experimental Design

4.1. Nonlinear least squares (NLLS)

Because the nonlinear least squares (NLLS) method is widely accepted by researchers and it is easy to understand, it was used in this work initially to estimate the reactivity ratios. The model structure of NLLS is:

$$y_i = f(x_i, \boldsymbol{\theta}^*) + \varepsilon_i \qquad (4.1)$$

where y_i is the experiment measurement for the i^{th} trial, $f(x_i; \boldsymbol{\theta})$ is the predicted value of the measurement, x_i represents the value of independent variate describing the reaction condition, ε_i is the random error and $\boldsymbol{\theta}^*$ is the true parameter value. The sum of the squared residuals is given by Equation 4.2. The objective is to minimize the sum of squared residuals.

$$S(\boldsymbol{\theta}) = \sum_i (y_i - f(x_i, \boldsymbol{\theta}))^2 \qquad (4.2)$$

The values of $\boldsymbol{\theta}$ that minimize $S(\boldsymbol{\theta})$ are known as the least squares parameter estimates, $\hat{\boldsymbol{\theta}}$. The bold characters indicate vectors or matrices here.

There are three assumptions made for the application of least squares:

1. The independent variables are perfectly known. In reality, if the error for an independent variable is much less than that of a dependent variable, this assumption is still valid.
2. The random errors in the dependent variable are statistically independent from run to run.
3. The variance of the dependent variable is constant

If the error distribution is $N(0, \sigma^2)$, a maximum likelihood estimation can be obtained. If the error distribution is heterogeneous, it violates assumption 3. Under this condition, the

Box-Cox transformation is often used. Common transformations are log(y), 1/y or $\sqrt{y}$. Alternatively, a weighted nonlinear least squares method can be used given as follows:

$$S(\boldsymbol{\theta}) = \sum w_i \left(y_i - f(x_i;\boldsymbol{\theta})\right)^2 \quad . \tag{4.3}$$

Where w_i are the weights assigned to each observation.

The initial guess is important to NLLS. Without a good initial guess, NLLS may not converge or may converge to a local minimum. Van Herk and Dröge (1997) applied the visualization method to plot the local reactivity ratio space to help determine the suitable initial guess. K-T, EKT results or literature values are also used as possible initial guesses. Given the initial value, the Marquardt-Levenberg optimization method is used to obtain the final parameter estimates.

With NLLS, the measurement error of an independent variable is not considered. If the errors in both independent and dependent variables are of similar magnitude the best solution is to resort to the EVM method.

4.2. Box-Draper

Box and Draper (1965) used a Bayesian approach to derive the determinant criterion for multiresponse parameter estimation. Given the general multiresponse model:

$$y_{iu} = f_i(\mathbf{x}_u, \boldsymbol{\theta}^*) + \varepsilon_{iu}, i = 1\ldots k, u = 1\ldots n \tag{4.4}$$

where y_{iu} is u^{th} observation on the i^{th} response. f_i is the predicted value of the i^{th} response; x_u is the set of input variables for observation u and ε_{ui} is the random normally distributed error of response i observation u. Through the Bayesian approach, the posterior probability $p(\boldsymbol{\theta}|y)$ is:

$$p(\boldsymbol{\theta}|\mathbf{y}) = C|\boldsymbol{\nu}|^{-n/2} \qquad i,j=1\ldots k \tag{4.5}$$

where C is the normalizing constant ; $\boldsymbol{\nu}$ is the estimated measurement covariance matrix defined as follows:

$$\mathbf{v} = \begin{bmatrix} v_{11} & \cdots & v_{1j} \\ \vdots & \ddots & \vdots \\ v_{i1} & \cdots & v_{ij} \end{bmatrix} \tag{4.6}$$

v_{ij} is the sum of the product of the deviations of responses *i* and *j* as follows:

$$v_{ij} = \sum_{u=1}^{n} \{y_{iu} - f_i(\boldsymbol{\theta})\}\{y_{ju} - f_j(\boldsymbol{\theta})\} \tag{4.7}$$

To obtain the parameter estimates the p($\boldsymbol{\theta}$ |**y**) should be maximized, which is equivalent to minimizing $|v_{ij}|$.

4.3. D-optimal design

The objective of experimental design methodologies is to yield parameter estimates of maximum precision (smallest joint confidence region). D-optimal design is suitable for NLLS. It either minimizes the inverse of the determinant of the NLLS information matrix **M** (Equation 4.8), which is proportional to the volume of joint confidence region of the parameters or maximizes the determinant of the information matrix **M**. **M** is given by Equation 4.9, where **J** is Jacobian matrix and $\mathbf{j}_i$ is the value of Jacobian at i^{th} trial shown as Equation 4.10. Hence, maximizing Equation 4.9 is equivalent to minimizing the volume of the joint confidence region. Note that this design offers no protection against lack of fit and therefore assumes model adequacy (Rossignoli and Duever, 1995).

$$\varphi = \min|\mathbf{M}|^{-1} \tag{4.8}$$

$$|\mathbf{M}| = |\mathbf{J}'\mathbf{J}| \tag{4.9}$$

$$\mathbf{j}_i = \left[\frac{\partial f}{\partial \theta_1} \quad \frac{\partial f}{\partial \theta_2} \quad \cdots \quad \frac{\partial f}{\partial \theta_p} \right] \tag{4.10}$$

There are two types of design: sequential design and non-sequential design. The D-optimal design is a model- dependent experimental design technique, and it consequently needs the prior knowledge of estimated parameters. So a sequential design is a suitable scheme to update the parameter values. The non-sequential design is useful to provide an initial experiment. It finds the suitable experiment support points and provides for increasing precision by using replicate experiments.

For the models in this work, there is a problem in that there are a large number of local optima. This causes many optimization problems. Here we use a graphical approach

(design locus) to getting an approximate initial design. If necessary, the approximation can be used as initial values to obtain a more accurate design in a sequential fashion.

The number of support point of D-optimal design is usually between *p* and *p(p+1)/2*. Generally, for a non-sequencial experimental design, *n* equals *p* so that the Jacobian matrix becomes a square matrix where $|\mathbf{J}'\mathbf{J}| = |\mathbf{J}|^2$. Thus maximizing $|\mathbf{J}'\mathbf{J}|$ is equivalent to maximizing the volume in the derivative space of the simplex formed by *p* points $\mathbf{j}(\boldsymbol{x}_i)(i=1,\ldots,p)$ and the origin (Atkinson and Donev, 1992).

For reactivity ratio estimation, n equals 2 and **J** is 2 by 2 square matrix. The region of the derivative space is in a plane. That permits the optimization surface to be easily visualized and understood.

4.4. Multivariate D-optimal design

The use of triad fractions, for example, results in a multivariate estimation problem; hence a multivariate D-optimal design is required. The criterion is to minimize the determinant of the information matrix **M**, as follows:

$$|\mathbf{M}| = \left| \sum_{i=1}^{r} \sum_{j=1}^{r} \sigma^{ij} \mathbf{J}_i' \mathbf{J}_j \right|^{-1} \tag{4.11}$$

where r is the number of responses, $\mathbf{J}_i$ is the Jacobian matrix of i^{th} response for p run experiments (Equation 4.12) and σ^{ij} is the element of the inverse variance-covariance matrix.

$$\mathbf{J}_i = \begin{bmatrix} \dfrac{\partial f_i^{(1)}}{\partial \theta_1} & \dfrac{\partial f_i^{(1)}}{\partial \theta_2} & \cdots & \dfrac{\partial f_i^{(1)}}{\partial \theta_p} \\ \vdots & \vdots & \vdots & \vdots \\ \dfrac{\partial f_i^{(p)}}{\partial \theta_1} & \dfrac{\partial f_i^{(p)}}{\partial \theta_2} & \cdots & \dfrac{\partial f_i^{(p)}}{\partial \theta_p} \end{bmatrix} \tag{4.12}$$

Draper and Hunter's research (1966) show that in their examples the design points are not strongly influenced by their measurement correlation. This indicates that if the error structure is unknown, a design that ignores the weights of the variance-covariance values can still be a good approximation. Burke (1994) also reported this stability property of

the design point for the triad fraction model when the correlations of the triad fractions varied. This property is very useful since it simplifies the design for multi response models.

4.5. Benchmarking tests

Our NLLS program is based on routines from the IMSL library functions. The Marquardt-Levenberg method is used to search for the minimum value. Runge-Kutta 4^{th} order and Adams predictor-corrector algorithms are used to solve the ordinary differential equations (ODE) for the cumulative model.

In the triad fraction model, the set of monomer-1-centered triad fraction data, corresponding to two independent responses, would be a function of one reactivity ratio, r_1, only, while monomer-2-centered triad fractions are functions only of r_2. Therefore the question arises. Is it necessary to use all the triad data at once? The two examples that follow try to address this.

4.5.1. Multiple responses for one parameter (triad fraction data)

The copolymerization system, STY-AN, is evaluated. The experimental data are simulated through the reaction kinetics in Burke's Ph.D. thesis (1994). They are triad fraction data centered on monomer 1, styrene. For the styrene-acrylonitrile system, the value of r_1 =0.4545 obtained from the article by Hill et al. (1982) is taken as the true value for the simulation. The additive error is assumed to be uniformly distributed.

The posterior distribution plots are presented as Figures 4.1a,b, c. When the random error is small (Figure 4.1a), the point estimates obtained based on a single response and based on multiple responses are both close to the true value. As the random error increased (Figure 4.1b and 4.1c), the point estimate based on a single response increasingly deviates from the true value, while the estimate from multiple responses is still close to the true value. From the above analysis, it can be conclude that when the error becomes larger, single response based estimation is less precise than the estimation using multiple responses. See also Table 4.1. The point estimate deviation at high error level from multiresponse is less than that from single response.

Table 4.1 Triad fraction simulation data with different level of error

	error 1%		error 5%		error 10%	
f1	$A_{112+211}$	A_{212}	$A_{112+211}$	A_{212}	$A_{112+211}$	A_{212}
0.1	0.092	0.908	0.095	0.934	0.096	0.953
0.2	0.184	0.814	0.188	0.817	0.197	0.867
0.3	0.274	0.701	0.285	0.73	0.285	0.712
0.4	0.358	0.589	0.374	0.6	0.384	0.618
0.5	0.433	0.475	0.441	0.489	0.455	0.506
0.6	0.483	0.356	0.493	0.354	0.518	0.359
0.7	0.503	0.236	0.521	0.239	0.528	0.239
0.8	0.459	0.126	0.476	0.13	0.465	0.135
0.9	0.316	0.039	0.331	0.04	0.329	0.04

Response	Point estimation of r_1		
$A_{112+211}$, A_{212}	0.4529	0.4424	0.4369
$A_{112+211}$	0.4567	0.4629	0.4846
A_{212}	0.4512	0.4332	0.4159

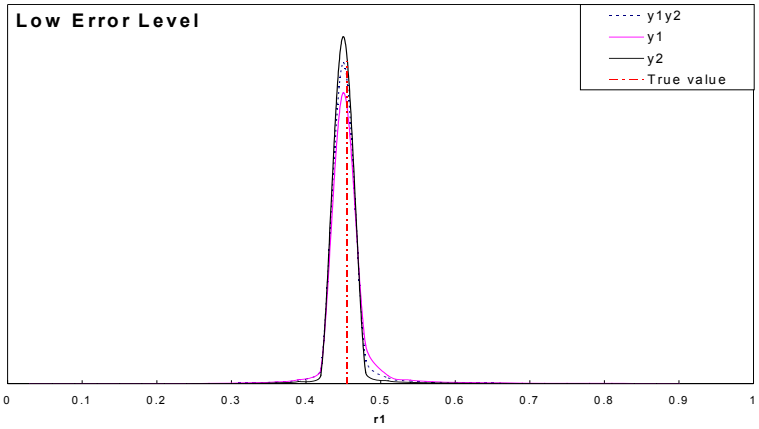

a :Additive error is 1%

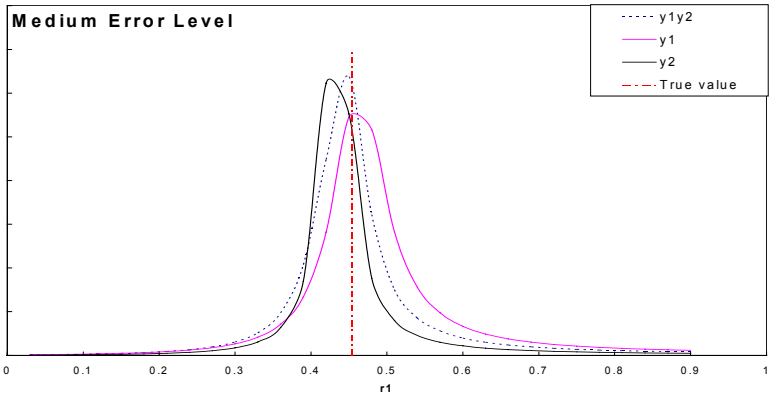

b: Additive error is 5%

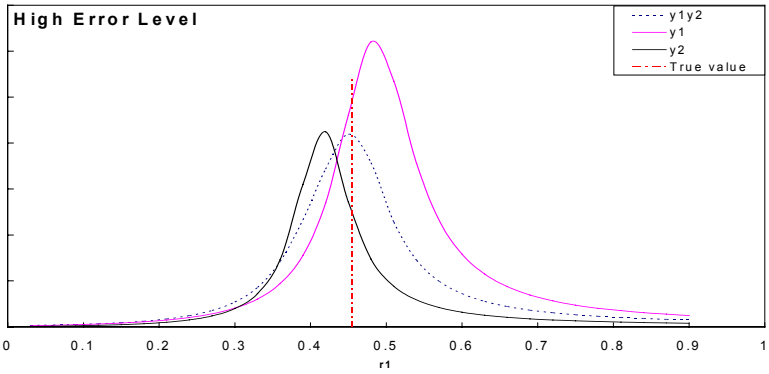

c: Additive error is 10%

Figure 4.1 Posterior distribution for one parameter, with different responses, different errors. y1 is posterior distribution from $A_{112+211}$; y2 is posterior distribution from A_{212}; y1y2 is posterior distribution from the mixed data of $A_{112+211}$ and A_{212}.

4.5.2. Multiple responses for two parameters

The example here is from Box and Draper's paper (1965). For the sequence of first order irreversible reactions:

$A \rightarrow B \rightarrow C$

the equations describing the amount of A (y_1), B (y_2), and C (y_3) are given by:

$$\dot{y}_1 = -\phi_1 y_1 \tag{4.13}$$

$$\dot{y}_2 = \phi_1 y_1 - \phi_2 y_2 \tag{4.14}$$

$$\dot{y}_3 = \phi_2 y_2 \tag{4.15}$$

Initial Condition: t=0, y_1=1,y_2 =y_3 =0

Because ϕ_i must be positive, let θ_i=lnϕ_i so that θ can be distributed from -∞ to +∞

Table 4.2 summarizes the estimation results.

Table 4.2 Results for the two-parameter estimation problem described in Box nd Draper (1965)

	θ_1	θ_2
y1,y2,y3:	-1.5844	-0.6953
y2,y3:	-1.5743	-0.8463
y3*:	-1.6556	-0.5108
y2:	-1.6610	-0.7168

Initial guess value for (ϕ1,ϕ2)= (0.3,0.6), unless otherwise noted *(ϕ_1, ϕ_2)=(0.6,0.6).

Figure 4.2 shows the 95% joint confidence region in good agreement with the paper by Box and Draper (1965). The confidence region corresponding to the multiresponse (y1,y2,y3) case is the smallest.

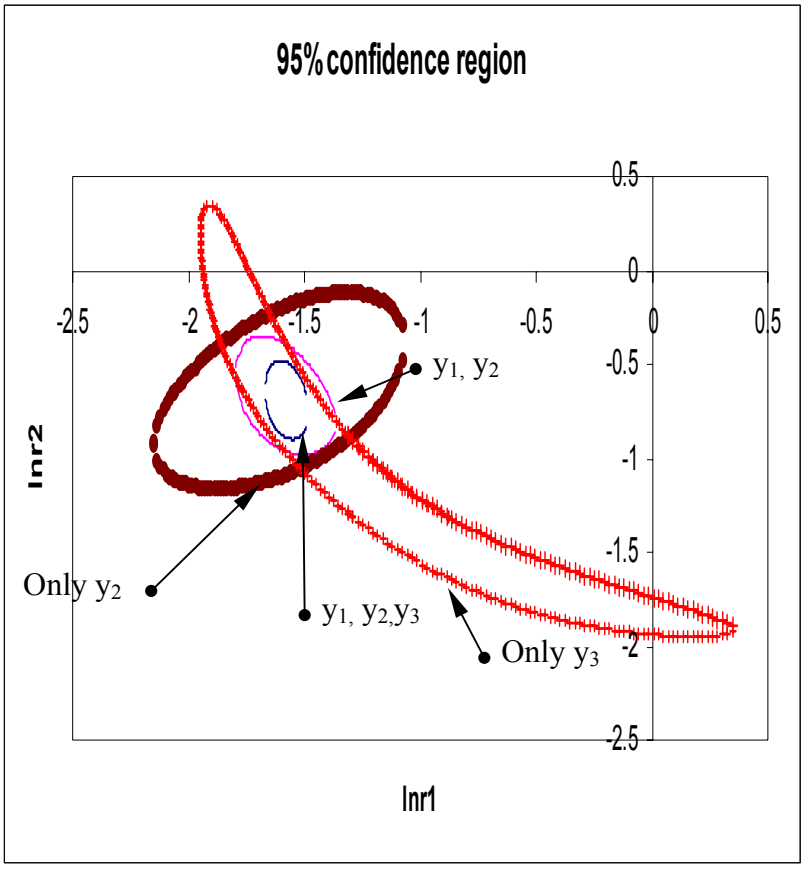

Figure 4.2 95% joint confidence regions for θ_1 and θ_2; for Box example

Considering the above two examples, all available sequence distribution data will be used to improve the estimate's precision. However, for triad fraction data, there exist two linear dependencies: $A_{111}+ A_{112}+A_{212}=1$ and $A_{222}+ A_{221}+A_{121}=1$. This type of dependency is known to introduce instabilities into the estimation problem. Hence, we can only choose $A_{112+211}$, A_{212}, $A_{221+122}$ and A_{121} (i.e., four out of six triads) to estimate reactivity ratios.

5. Copolymer Systems and Data Generation

5.1. General simulation models

In this section, the general model equations used to simulate copolymerization reactions are briefly described. The mass balances describing the monomer consumption are given by Equation 5.1-5.4. There is an assumption that the activity of the free radicals has no relationship with the polymer chain length.

$$\frac{dN_1}{dt} = -\left(k_{11}\phi\cdot_1 + k_{21}\phi\cdot_2\right)N_1\left[R\cdot\right] + F_{1,in} - F_{1,out} \tag{5.1}$$

$$\frac{dN_2}{dt} = -\left(k_{22}\phi\cdot_2 + k_{12}\phi\cdot_1\right)N_2\left[R\cdot\right] + F_{2,in} - F_{2,out} \tag{5.2}$$

where N_i is the amount of monomer *i*; k_{ij} is the propagation constant of radical *i* and monomer *j*; $F_{i,in}$ and $F_{i,\ out}$ are the flow rates of component *i* in and out of the reactor ; $\phi\cdot_i$ is given by the following equations:

$$\phi\cdot_1 = \frac{\left[R\cdot_1\right]}{\left[R\cdot\right]} = \frac{k_{21}f_1}{k_{21}f_1 + k_{12}f_2} \tag{5.3}$$

$$\phi\cdot_2 = \frac{\left[R\cdot_2\right]}{\left[R\cdot\right]} = \frac{k_{12}f_2}{k_{21}f_1 + k_{12}f_2} \tag{5.4}$$

The subscript 1,2 and p indicate monomer 1, 2 and polymer respectively. For a batch operation

$F_{1,in}=F_{2,in}=F_{1,out}=F_{2,out}=0$

Hence, Equation 5.1 and 5.2 can be rewritten as

$$\frac{dN_1}{dt} = -\frac{k_{11}k_{22}\left(r_1N_1 + N_2\right)}{k_{22}r_1N_1 + k_{11}r_2N_2}\cdot N_1\left[R\cdot\right] \tag{5.5}$$

$$\frac{dN_2}{dt} = -\frac{k_{11}k_{22}\left(r_2N_2 + N_1\right)}{k_{22}r_1N_1 + k_{11}r_2N_2}\cdot N_2\left[R\cdot\right] \tag{5.6}$$

According to radical stationary state hypothesis, the total radical concentration is determined by:

$$[R\cdot]=\left(\frac{2fk_dN_I}{k_tV}\right)^{1/2} \tag{5.7}$$

where k_d is the initiator decomposition rate constant; V is the total volume; f is the initiator efficiency; k_t is overall termination rate constant; N_I is the quantity of initiator, which is given by Equation 5.8.

$$\frac{dN_I}{dt}=-k_dN_I \tag{5.8}$$

The total volume change is determined by the density change when the monomer turns into polymer.

$$\frac{dV}{dt}=\frac{dN_1}{dt}MW_1\left(\frac{1}{\rho_1}-\frac{1}{\rho_P}\right)\frac{1}{1000}+\frac{dN_2}{dt}MW_2\left(\frac{1}{\rho_2}-\frac{1}{\rho_P}\right)\frac{1}{1000} \tag{5.9}$$

where ρ is density and MW is molecular weight. Due to the assumption that all the monomer is consumed for polymerization, the overall conversion can be written as

$$\frac{dx}{dt}=\frac{dN_P}{dt}\frac{1}{N_{1,0}+N_{2,0}}=-\left(\frac{dN_1}{dt}+\frac{dN_2}{dt}\right)\frac{1}{N_{1,0}+N_{2,0}} \tag{5.10}$$

Equations 5.5-5.10 describe the kinetics of bulk copolymerization at low conversion in a batch reaction.

As conversion increases, diffusion starts to control the reaction. The gel effect will occur with the increase in conversion. The termination rate constant k_t will decrease greatly. When the glass transition temperature is below the reaction temperature, the glass effect occurs. The free volume model can be used to describe the kinetics. The termination rate constant k_t and propagation rate constant k_p start to decrease at two specific critical free volume fraction values. For homopolymerization, the decrease of these kinetic rate constants is expressed as:

$$k_t=k_{t0}\left(\frac{\overline{M}_{wCr}}{\overline{M}_w}\right)^n\exp\left(-A\left(\frac{1}{V_F}-\frac{1}{V_{FCr1}}\right)\right) \tag{5.11}$$

$$k_p = k_{p0} \exp\left(-B\left(\frac{1}{V_F} - \frac{1}{V_{FCr2}} \right) \right) \tag{5.12}$$

In Equation 5.11 and 5.12, A and B are constants indicating how fast the rate constant decreases. k_{t0} and k_{p0} are the termination and propagation rate constants at low conversion. V_{FCr1} and V_{FCr2} are the two critical free volume fractions at which k_t and k_p begin to decrease respectively. The critical molecular weight $\overline{M}_{wCr}$ can be determined by Equation5.13, where K_3 can be determined theoretically or experimentally, and the free volume fraction V_F is determined by Equation 5.14, where T_g is the glass transition temperature and α is the expansion coefficient.

$$K_3 = \overline{M}_{wCr}^{\,0.5} \exp\left(\frac{A}{V_{FCr1}} \right) \tag{5.13}$$

$$V_F = \left[0.025 + \alpha_P \left(T - T_{gP}\right)\right]\frac{V_P}{V} + \left[0.025 + \alpha_1 \left(T - T_{g1}\right)\right]\frac{V_1}{V} \tag{5.14}$$

For copolymerization, each propagation rate constant decreases at a different speed as shown in Equation 5.15. Because there are many adjustable parameters, B is usually assumed to be equal to 1.

$$k_{ij} = k_{ij0} \exp\left(-B\left(\frac{1}{V_F} - \frac{1}{V_{FCr2ij}} \right) \right) \tag{5.15}$$

The total free volume fraction is still defined in the same way by including all component free volume fractions as follows.

$$V_F = \left[0.025 + \alpha_P \left(T - T_{gP}\right)\right]\frac{V_P}{V} + \left[0.025 + \alpha_1 \left(T - T_{g1}\right)\right]\frac{V_1}{V} + \left[0.025 + \alpha_2 \left(T - T_{g2}\right)\right]\frac{V_2}{V} \tag{5.16}$$

The difficulty is that those critical parameters for copolymerization are not easily obtained from experiments directly and there is few data reported in the literature. The second critical free volume fraction, $V_{FCr2,ii}$ can be obtained from homopolymerization data. Based on the fact that the product of two reactivity ratios approaches 1 when the conversion is close to one, $V_{FCr2,ij}$ ($i \neq j$) can be expressed as

$$V_{FCr,12} = \frac{B}{B/V_{FCr,22} + \ln\left(k_{220.} r_1 / k_{110}\right)} \tag{5.17}$$

k_{110}, k_{220} are homopolymerization propagation rate constant at low conversion. As for the first critical free volume fraction and critical molecular weight, they are usually calculated through K_3 using an iterative method.

The molecular weight is calculated by the method of moments. Equation 5.18-5.23 show the moment calculation, and Equation 5.24-26 give the relationship between moments and molecular weight, where k_{td} is the disproportionation termination rate constant; γ is the proportion of free radical chains terminated by disproportionation and Q_0, Q_1, Q_2 are the first three moments of the polymer molecular weight distribution respectively.

$$\tau = \frac{k_{td}[R\cdot] + k_{fm}[M]}{k_p[M]} = \frac{\gamma k_t[R\cdot] + k_{fm}[M]}{k_p[M]} \tag{5.18}$$

$$\beta = \frac{k_{tc}[R\cdot]}{k_p[M]} = \frac{(1-\gamma)k_t[R\cdot]}{k_p[M]} \tag{5.19}$$

$$[M] = \frac{N_1 + N_2}{V} \tag{5.20}$$

$$\frac{dVQ_0}{dt} = \frac{dN_p}{dt}\left(\tau + \frac{\beta}{2}\right) \tag{5.21}$$

$$\frac{dVQ_1}{dt} = \frac{dN_p}{dt} \tag{5.22}$$

$$\frac{dVQ_2}{dt} = \frac{dN_p}{dt}\left(\frac{2\tau + 3\beta}{(\tau+\beta)^2}\right) \tag{5.23}$$

$$\overline{M}_n = MW\frac{Q_1}{Q_0} \tag{5.24}$$

$$\overline{M}_w = MW\frac{Q_2}{Q_1} \tag{5.25}$$

$$MW = MW_1 \times \overline{F}_1 + MW_2 \times (1 - \overline{F}_1) \tag{5.26}$$

5.2. STY/AN system

This system is widely used in industry as it produces a material with excellent mechanical properties. It is a typical system with an azeotropic point and relatively low composition drift. Homo-polymerization information of styrene and acrylonitrile is listed in Table 5.1 and 5.2. The monomer reactivity ratios used to model low conversion experiments are those given by Hill et al. (1982); r_1=0.4545, r_2=0.0912. For high conversion, the reactivity ratios are from Garcia-Rubio et al. (1985); r_1=0.36, r_2=0.078. The overall termination rate constant and other parameters for the free volume theory are also supplied in their papers and reproduced in Table 5.3. Table 5.4 gives the values of k_d and f for the initiator AIBN.

Table 5.1 Homopolymerization parameters for Styrene

Parameter		Unit
MW	104.1512	g/mol
k_p	$1.09\times10^{7}\exp(-7051/RT)$	L $mol^{-1}s^{-1}$
k_t	$1.703\times10^{9}\exp(-2268/RT)$	L $mol^{-1}s^{-1}$
k_{fm1}	$1.096482\times10^{7}\exp(-134268.8/RT)$	L $mol^{-1}s^{-1}$
ρ_m	$0.924-9.18\times10^{-4}(T-273.15)$	g/cm^3
ρ_p	$1.084-6.05\times10^{-4}(T-273.15)$	g/cm^3
$V_{fcrit,2}$	$0.311052\exp(-671.76/RT)$	
α	1.00×10^{-3}	
Tg	-88.2	°C

Table 5.2 Homopolymerization parameters for Acrylonitrile

Parameter		Unit
MW	53.0634	g/mol
k_{22}	$1.047\times10^{8}\exp(-7278.38/RT)$	L $mol^{-1}s^{-1}$
k_{t2}	$2.95\times10^{11}\exp(-5396.88/RT)$	L $mol^{-1}s^{-1}$
k_{fm2}	$1.090932\times10^{6}\exp(-10972.4/RT)$	L $mol^{-1}s^{-1}$
ρ_m	$0.835546-1.38286\times10^{-3}(T-273.15)$	g/cm^3
ρ_p	1.17	g/cm^3
$V_{fcrit,2}$	$5.32770\exp(3059.04/RT)$	
α	1.25×10^{-3}	
Tg	-82.8	°C

Table 5.3 Copolymerization parameters for STY/AN

Parameter		Unit
kt0	6.78×109.exp(-6335/R(1/T-1/333.2))	
A	0.307	
B	1.7	
n	1.75	
α	25×10-3	
Tg	105	°C

Table 5.4 Data for 2,2'azobisisobutyronitrile (AIBN)

kd	1.03833×1015exp(-30706/R/T)	s^{-1}
f	2.47×10-2exp(2166/R/T)	

According to Garcia-Rubio's observation, the termination reaction is diffusion controlled right from the start, i.e. $V_{fcrit,1}=V_f$ at conversion zero. This simplified model can fit their experimental data (Garcia-Rubio et al., 1985) in the range of 40-60°C and for different initiator AIBN concentrations very well. In this study we here only simulated STY/AN system in bulk copolymerization at 60°C.

Several runs at feed ratios of 0.5, 0.7 and 0.9 are simulated. Figure 5.1, a conversion vs. time plot, shows that the free volume theory predicts the behavior of STY/AN system well. The three feed ratios are located on both sides of the azeotropic point. When the monomer feed ratio is above the azeotropic point, the monomer residual mole fraction increases and tends to unity at high conversion. Below the azeotropic point, the monomer residual mole fraction decreases and tends to a limiting mole fraction at high conversion (Figure 5.2).

5.3. MMA/VAc system

This is a system which exhibits a large composition drift. It is not easy to estimate reactivity ratios for this system with the instantaneous model, because the conversion would have to be controlled to very low levels to satisfy the assumptions of the instantaneous model. Figure 5.3 shows the estimation results for the instantaneous model and cumulative model. The experimental data came from Scorah et al. (2001). It is for a bulk polymerization experiment at 60°C with initiator AIBN at 0.05 mol/L. Although the conversion was controlled to 1% or so, the estimation results between the two models are significantly different.

The homopolymerization information of MMA/VAc system is listed in Tables 5.5 and 5.6. The copolymerization information uses the parameters reported in the paper of Dube and Penlidis (1995) and the Watpoly database (Table 5.7). The model prediction for the MMA rich in feed fits very well with the experimental data. However, when VAc is rich in feed, the gel effect transition result a little deviation. The experimental data at a feed ratio 0.3 is from Dube and Penlidis paper (1995); other experimental data is obtained from Scorrah (1999). Overall, the free volume model can describe the kinetic behavior of MMA/VAc system well (Figure 5.4).

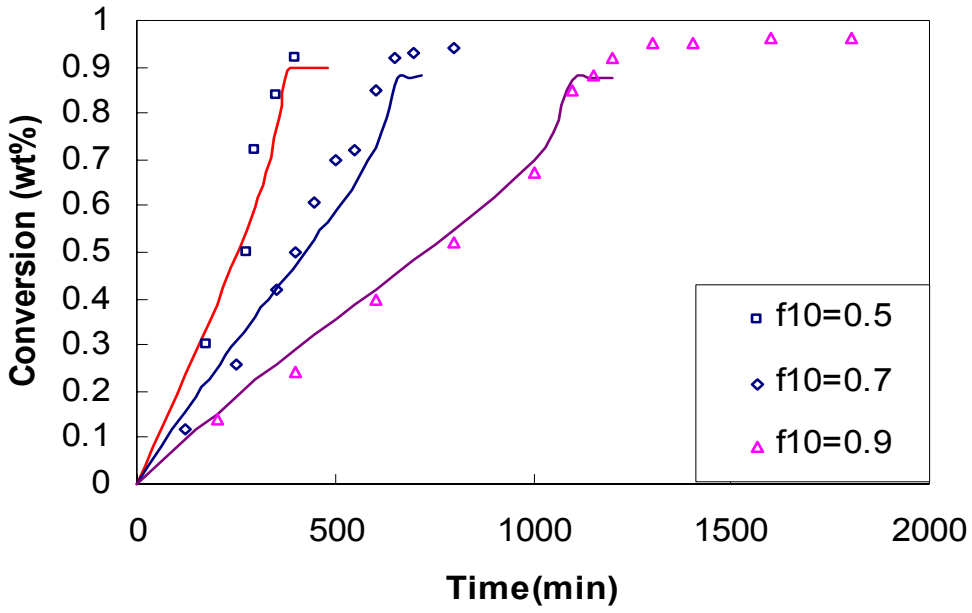

Figure 5.1 Conversion vs. time for STY/AN copolymerization at 60°C and $[I]_0$=0.01M AIBN. The line is the model prediction

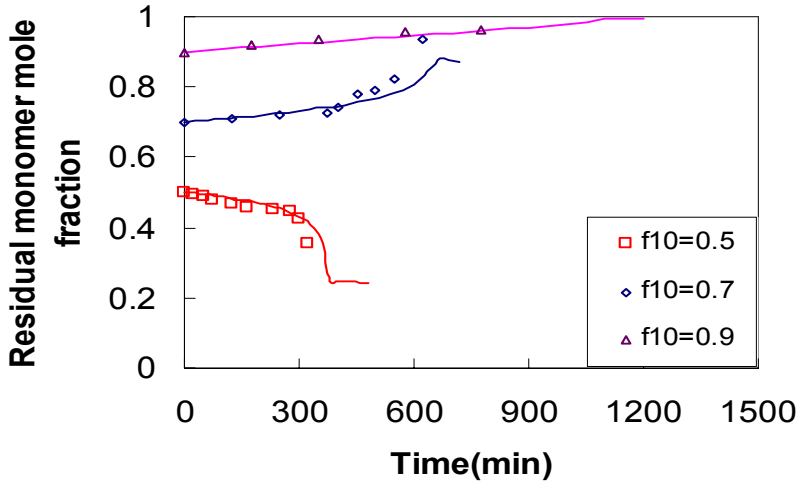

Figure 5.2 Residual mole fraction vs. time for STY/AN copolymerization at 60°C and $[I]_0$=0.01M AIBN. The line is the model prediction

Table 5.5 Homopolymerization parameters for Methyl Methacrylate

Parameter		Unit
MW	100.1162	g/mol
k_p	$5.365859\times10^{5}\exp(-4353/RT)$	L $mol^{-1}s^{-1}$
k_t	$9.8\times10^{7}\exp(-701/RT)$	L $mol^{-1}s^{-1}$
k_{fm1}	$1.557243\times10^{3}\exp(-7475.06/RT)$	L $mol^{-1}s^{-1}$
ρ_m	$0.966471-1.16\times10^{-3}(T-273.15)$	g/cm^3
ρp	1.1950-3.3×10-4(T-273.15)	g/cm3
Vfcrit,2	0.0671	
α	1.00×10-3	
Tg	-106.05	°C

Table 5.6 Homopolymerization parameters for Vinyl Acetate

Parameter		Unit
MW	86.09	g/mol
k_p	$1.3\times10^{9}\exp(-8403.5/RT)$	L $mol^{-1}s^{-1}$
k_t	$1.64\times10^{10}\exp(-3401.4/RT)$	L $mol^{-1}s^{-1}$
k_{fm1}	$1.8617\times10^{5}\exp(-9895/RT)$	L $mol^{-1}s^{-1}$
ρ_m	$0.95741-1.2713\times10^{-3}(T-273.15)$	g/cm^3
ρ_p	$1.21447-8.7493\times10^{-4}(T-273.15)$	g/cm^3
$V_{fcrit,2}$	0.060	
α	1.00×10^{-3}	
Tg	-164	°C

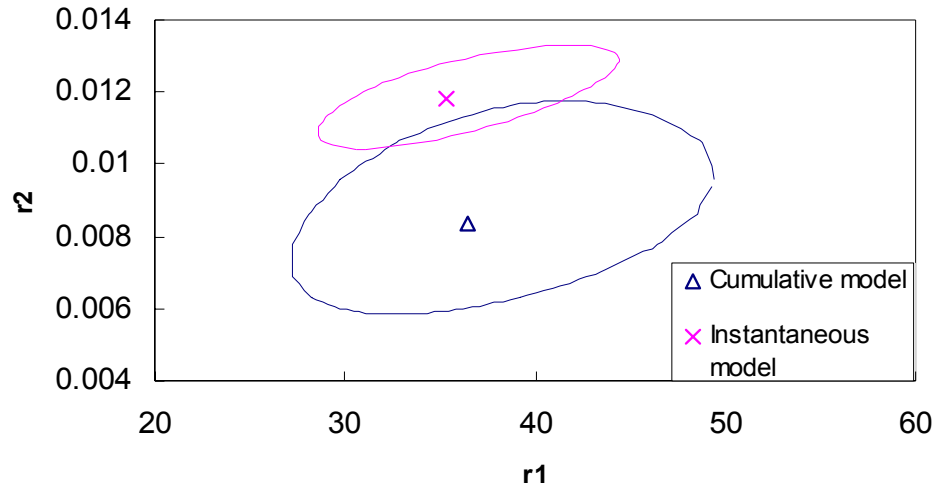

Figure 5.3 95% Joint confidence region for estimation of reactivity ratios of MMA/VAc at low conversion. The cross and its corresponding contour is for instantaneous composition model (RREVM); The triangle and its corresponding contour is for cumulative composition model. Experimental data are from Scorah et al. (2001)

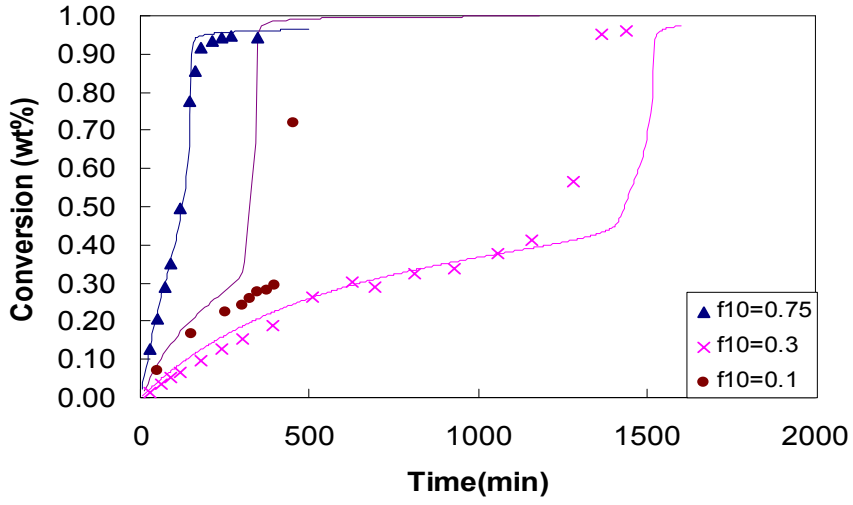

Figure 5.4 Conversion history of copolymer system MMA/VAc. The line is model prediction. Experimental data at f_{10}=0.3 come from Dube and Penlidis (1995), other experimental data come from Scorah et al. (2001).

Table 5.7 Copolymerization parameters for MMA/VAc

Parameter		Unit
A	0.307	
B	1.0	
n	1.75	
α	48×10^{-3}	
Tg	81.85	°C

5.4. Copolymerization of functional methacrylates: case studies for reactivity ratio estimation

Copolymerizations of functional methacrylates have not been extensively studied. Methacrylic copolymers have been used in various industrial applications (Payne, 1964; Marten, 1968; Vijayaraghavan and Reddy, 1996; Warson, 1972). Copolymerizations of functional methacrylates with other monomers provide simple routes for synthesizing biologically active materials and coatings formulations (Batz et al. 1973; Gendy et al. 1991). Copolymers from MMA are used in the formation of biologically active films and production of materials for optical telecommunication applications (Pandeya et al. 1999; Johnca et al. 2000). The use of alkyl and phenyl-meth-acrylates as binders in protective coatings because of their excellent durability,white color in water and transparency, has been reported (Otsu et al. 1966; Tamizharasi et al. 1999). Poly(phenyl methacrylates) are harder polymers of high tensile strength and their Tg is higher than their acrylate counterparts because of restricted freedom of rotation. The application is found in laser photoresist materials (Ichimura and Nishio 1987)

The accurate estimation of copolymer composition and determination of monomer reactivity ratios are significant for “tailoring” copolymers. In the first case we discuss reactivity ratio estimation for copolymerization of 3,5-dimethylphenyl methacrylate (DMPMA) with MMA, followed by the copolymerization of 4-benzyloxycarbonylphenyl (BCPM) with glycidyl methacrylate (GMA).

5.4.1. Copolymerization of DMPMA with MMA

The copolymerization of DMPMA with MMA in EMK solution was studied over a wide composition range with the mole fraction of DMPMA in the feed range from 0.15 to 0.90. The copolymerization schematic is shown as follows:

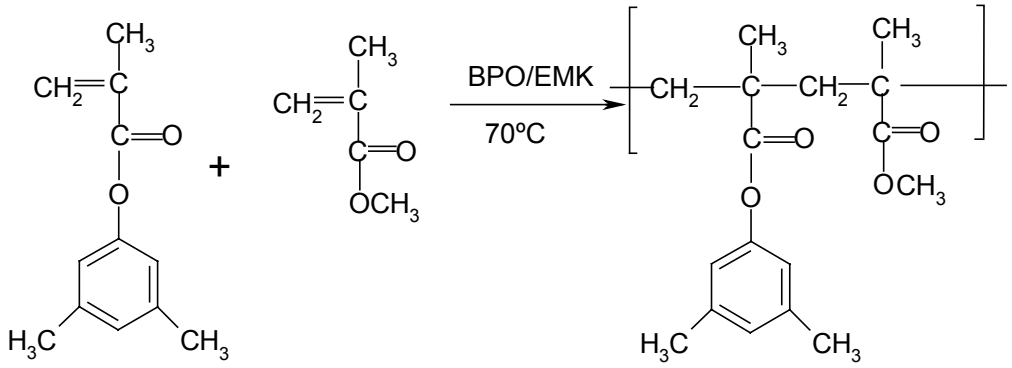

(5.27)

Copolymerization data are shown in Table 5.8 (A. Penlidis, personal communication).

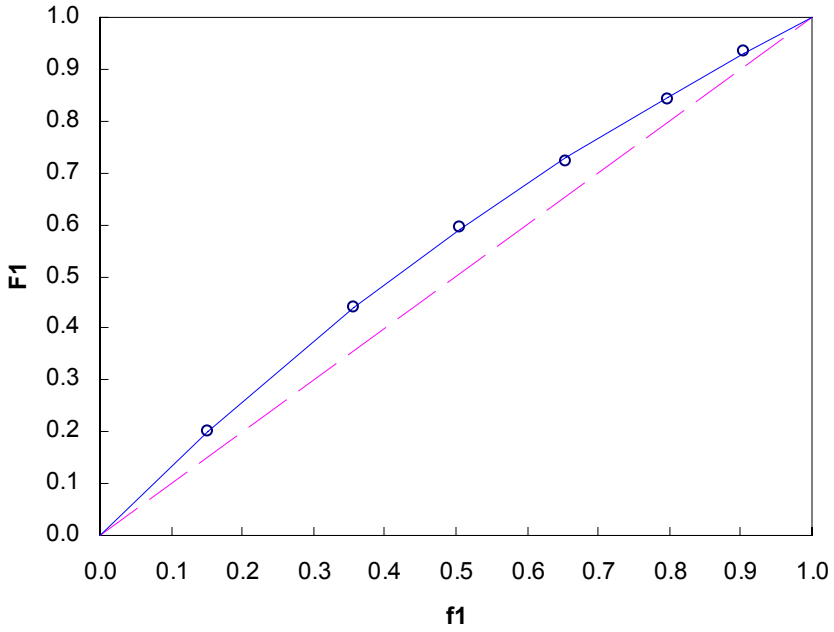

Figure 5.5 Copolymer composition diagram for poly(DMPMA-co-MMA)

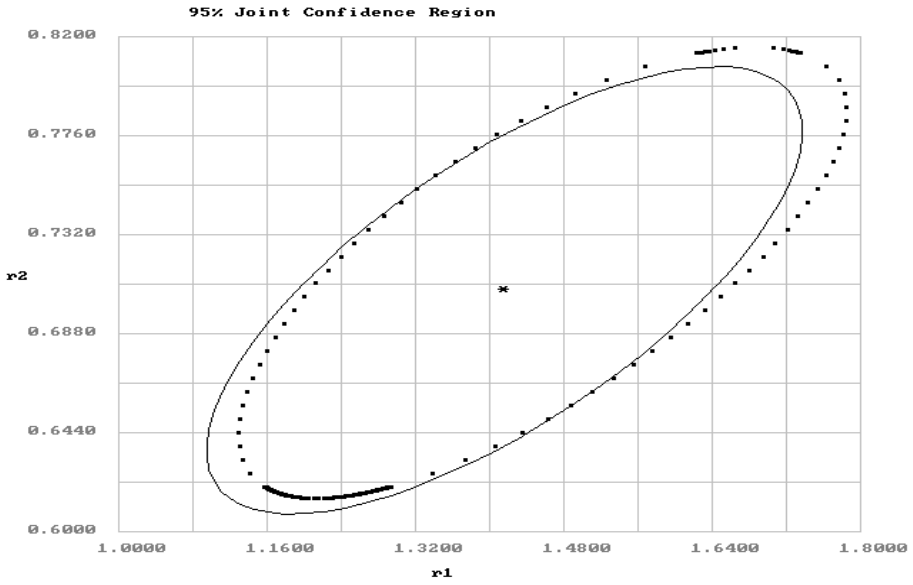

Figure 5.6 95%Joint confidence region for r_1 and r_2 for DMPMA/MMA

Table 5.8 Composition Data for free radical polymerization of DMPMA(1) with MMA(2) in EMK solution at 70°C

Experiment run	f_1^*	Conversion (%)	F_1^*
1	0.1518	9.31	0.2013
2	0.3560	9.84	0.4420
3	0.5058	8.72	0.5933
4	0.6540	8.96	0.7238
5	0.7968	7.85	0.8416
6	0.9051	9.18	0.9325

* f1 and F1 are the mole fraction of DMPMA in the feed and in the copolymer, respectively.

The plot of the mole fraction of DMPMA in the copolymer (F1) versus the mole fraction in the feed (f1) is shown in Figure 5.5. The plot indicates that the composition of DMPMA in the copolymer is always higher than that in the feed, hence one is expecting

the reactivity ratios to be $r_1>1$ and $r_2<1$. This is confirmed in Figure 5.6, which shows the 95% posterior probability contour for the estimated r_1 and r_2. In this case, the point estimates from RREVM (Polic et al. 1997) are: $r_1=1.4160$ and $r_2=0.7073$. The product r_1 r_2 is 1.0015, ideal copolymerization, suggesting a random distribution of monomer units in the copolymer.

5.4.2. Copolymerization of BCPM/GMA

Copolymerization data are shown in Table 5.9.

The composition plot is shown in Figure 5.7 .The plot indicates that the composition with respect to BCPM in the copolymer is always slight higher than that in the feed, thus one would expect the reactivity ratios to be $r_1> 1$ and $r_2<1$.

This is confirmed in Figure 5.8, which shows the 95% JCR corresponding to the estimated r_1 and r_2 values using the RREVM method. The point estimates are: $r_1=1.1655$ and $r_2=0.7892$ (BCPM=1, GMA=2). The product $r_1 \times r_2$ is 0.9198, very close to unity, suggesting a random distribution of monomer units in the copolymer with slightly longer sequences of BCPM. Copolymers of BCPA/GMA find applications as leather adhesives.

Table 5.9 Composition data for free radical copolymerization of BCPM(1) with GMA(2) in EMK solution at 70°C

Experiment run	f_1^*	Conversion(%)	F_1^*
1	0.1527	7.56	0.1849
2	0.3002	8.25	0.3419
3	0.5028	9.12	0.5498
4	0.6456	9.46	0.6900
5	0.8028	9.13	0.8256
6	0.9023	8.94	0.9221

* f_1 and F_1 are the mole fraction of BCPM in the feed and copolymer, respectively.

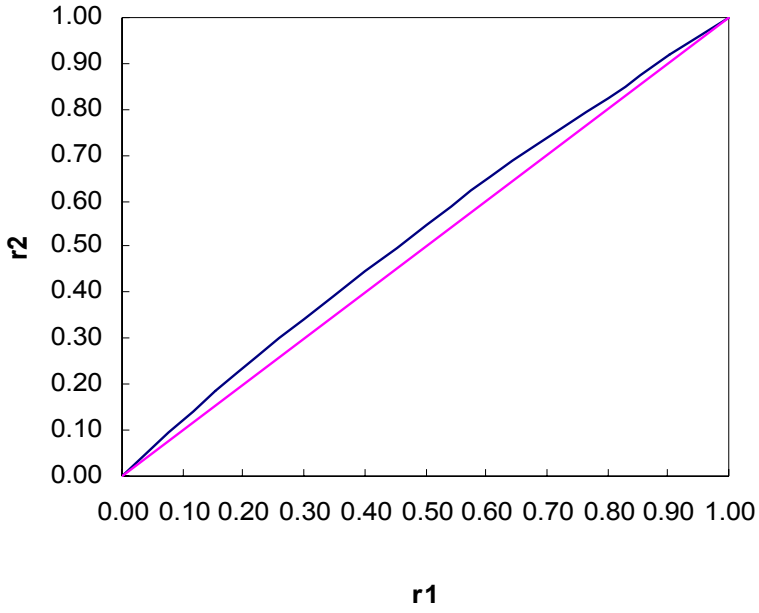

Figure 5.7 Copolymer composition diagram for poly(BCPM-co-GMA)

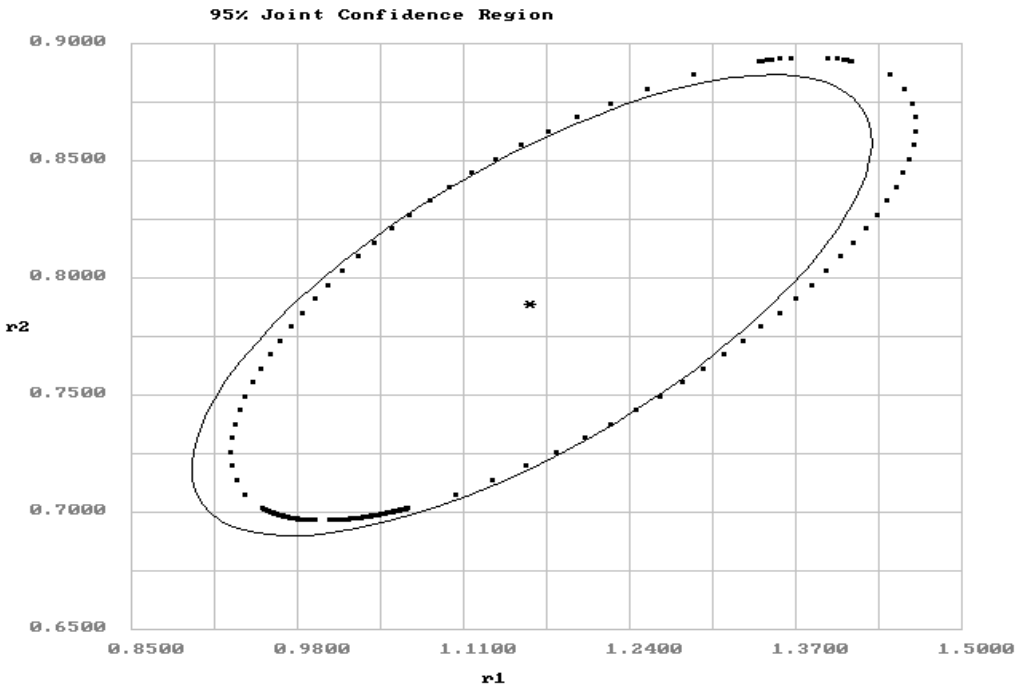

Figure 5.8 95%Joint confidence region for r_1 and r_2 for BCPM/GMA

6. Case Studies

6.1. Instantaneous triad fraction model

Copolymer reactivity ratios are usually estimated via the instantaneous composition model (Mayo-Lewis equation). Although statistically correct methods are used to estimate reactivity ratios, the question still exists of whether one can improve the estimates using possibly more information from the polymerization data. Sequence length data are a good choice for such an alternative. The sections that follow show how sequence distribution data (triad fractions) can be used as a viable alternative for reactivity ratio estimation.

The simulated system is STY/AN at 60°C in bulk copolymerization. The true reactivity ratio values are 0.4545 and 0.0912, based on Hill et al. (1982) experimental results. The monomer feed ratio ranges from 0.1 to 0.9 at intervals of 0.1. There are nine data points totally. Various error levels are listed in Table 6.1, based on Burke's thesis (1994). The effect of error structure is discussed below.

Table 6.1 Error levels

	Low error	Medium error	High error
Monomer fraction	0	0	0
Triad fraction	0.00833	0.01667	0.03333

* all of these values are standard deviations.

6.1.1. Simulation results with additive error

For additive error, $\mathrm{Var}(\varepsilon_i)=\mathbf{I}\sigma^2$.The confidence interval is given by $\hat{A}_{ijk} \pm Z_{\alpha/2}\sigma$. The significance level $\alpha = 0.0026$ when $Z_{\alpha/2} \approx 3$.σ is the standard deviation. The Z factor is the inverse value of the cumulative standard normal distribution at a certain significance level.

The point estimates are listed in Table 6.2. The 95% joint confidence regions (JCRs) are plotted in Figure 6.1. From the JCR plot, we can see that the estimates at different error

level have no significant difference from the true values. But the uncertainty of the estimates increases at high error level, as expected.

Furthermore, the joint confidence contours are almost horizontal in Figure 6.1, because each reactivity ratio only relates with one monomer centered triad fraction, and hence they are not correlated with each other.

Table 6.2 The estimates with additive error

	r1	r2
True Value	0.4545	0.0912
Low error	0.4579	0.0900
Medium error	0.4509	0.0918
High error	0.4683	0.0897

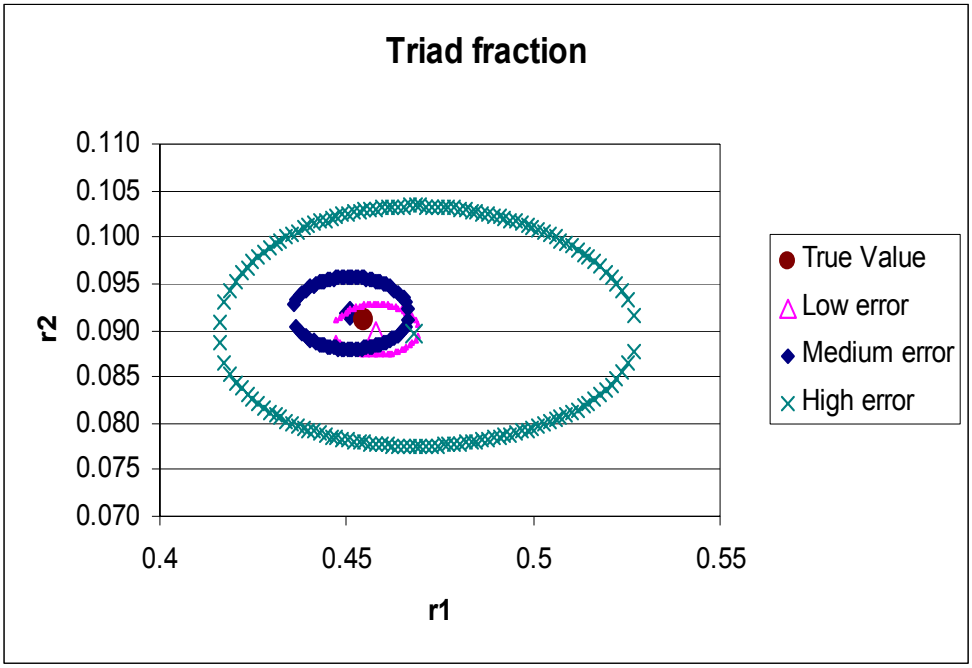

Figure 6.1 95% joint confidence region for instantaneous triad fractions with additive error

6.1.2. Simulation results with multiplicative error

The confidence interval of estimates with multiplicative error is

$$A_{ijk} = \hat{A}_{ijk}\left(1 \pm Z_{\alpha/2}\sigma\right) \qquad (6.1)$$

The symbols are the same as those in additive error.

After transformating to the additive form

$$\begin{aligned} \ln A_{ijk} &= \ln \hat{A}_{ijk} + \ln(1 \pm \varepsilon) \qquad (6.2) \\ &\approx \ln \hat{A}_{ijk} \pm \varepsilon \\ \varepsilon &= Z_{\alpha/2}\sigma \end{aligned}$$

where ε<10% which results in σ to be less than 0.033. This still satisfies the model structure of NLLS.

The point estimates are listed in Table 6.3. The 95% joint confidence regions (JCRs) are plotted in Figure 6.2. From the JCR plot, we can see that the estimates at different error level have no significant difference from the true values. Once again, the uncertainty of the estimates increases greatly at high error level, as expected.

Table 6.3 The estimates with multiplicative error

	r1	r2
True Value	0.4545	0.0912
Low error	0.4550	0.0915
Medium error	0.4551	0.0913
High error	0.4555	0.0897

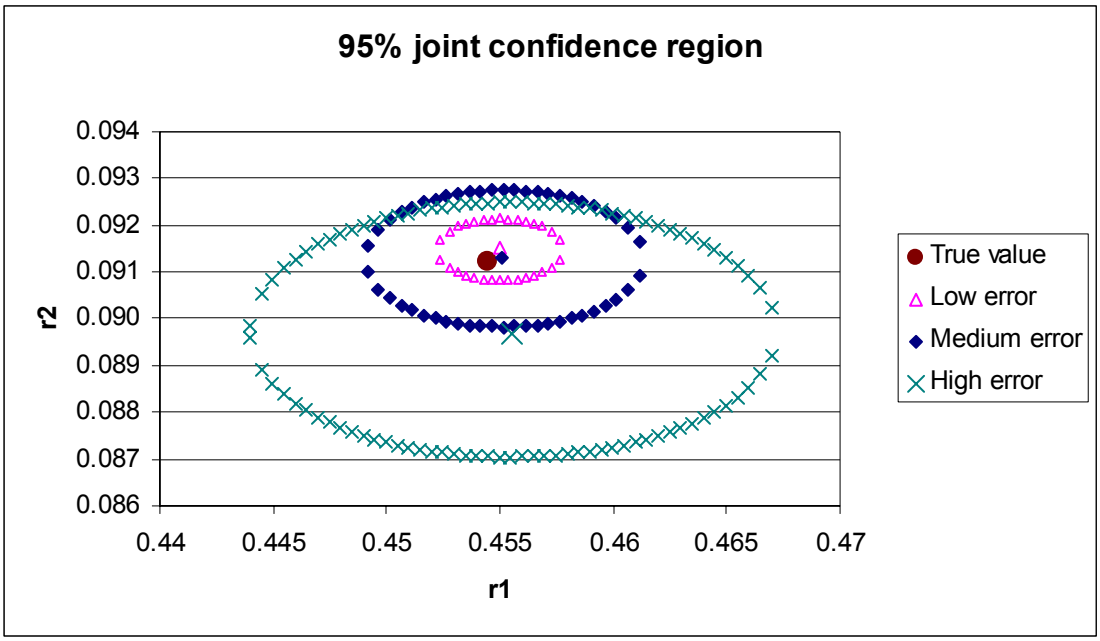

Figure 6.2 95% joint confidence region with multiplicative error

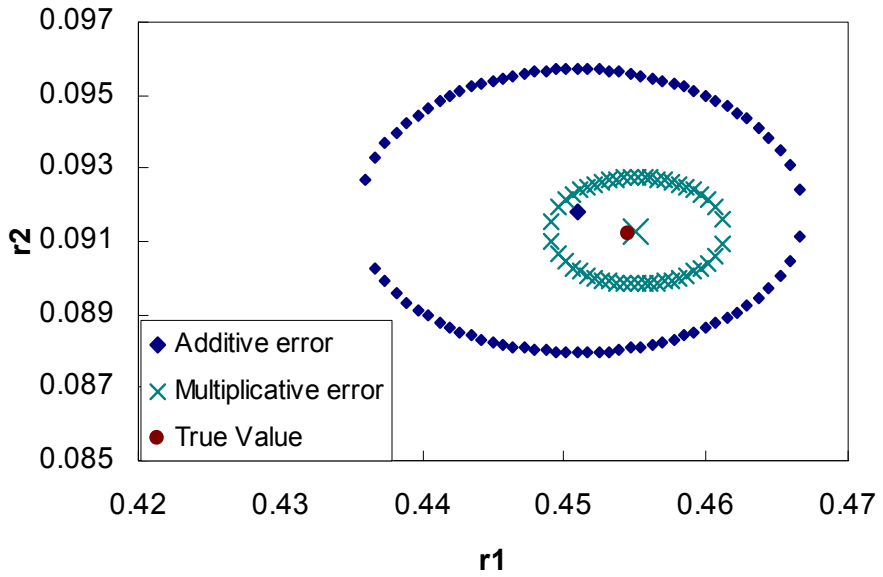

Figure 6.3 95% joint confidence region for estimation with multiplicative error and additive error at medium error level

At medium error level, both error structures yield precise estimates compared to high error level. For the additive error structure, the small reactivity ratio is estimated more accurately, while for multiplicative error structure, the large reactivity ratio is estimated more accurately. That shows the influence of the error structure on the estimates.

Interestingly, the medium error level is close to the real error level (Burke, 1994). The estimates agree very well with the true value. Since the multiplicative error is a type of relative error, the corresponding absolute error is much smaller than the additive error at the same error level considered in this example. Hence, it is not surprising to get more accurate estimation with multiplicative error than with additive error data (see Figure 6.3).

A potential problem with the multiplicative error structure is that when the experimental data are very small (close to 0), this may make the algorithm unstable. The weighted NLLS is a good choice to deal with this situation.

6.1.3. Simulation results with correlated error using the Box-Draper method

For correlated error: Var (ε_i)=$\mathbf{V}\sigma^2$ (6.3)

$$\because Var(\varepsilon)_{ii} = v(\varepsilon_i)\sigma^2 = R_{ii}\sigma^2 \tag{6.4}$$

$$Var(\varepsilon)_{ij} = \mathrm{cov}(\varepsilon_i\varepsilon_j) = \frac{\mathrm{cov}(\varepsilon_i\varepsilon_j)}{\sqrt{v(\varepsilon_i)v(\varepsilon_j)}}\sigma^2 = R_{ij}\sigma^2 \tag{6.5}$$

$$\therefore \ \mathbf{V}=\mathbf{R} \tag{6.6}$$

Here the **V** matrix is just the correlation matrix **R**. This is closer to reality, because in one experiment all triad fractions come from the same NMR spectrum.

With Cholesky decomposition, **R** is factored as $\mathbf{L}^T\mathbf{L}$, where **L** is a lower triangular matrix.

$$\mathbf{A}_u = \hat{\mathbf{A}}_u \pm \mathbf{Z}_{\alpha/2}\mathbf{L} \tag{6.7}$$

where u is the experiment trial. The correlated error used is again obtained from Burke's thesis (1994) and is listed in Table 6.4

Table 6.4 Simulated correlation of triad fraction

	A_{212}	$A_{112+211}$	A_{121}	$A_{122+221}$
A_{212}	1.000	-0.823	0.000	0.000
$A_{112+211}$	-0.823	1.000	0.000	0.000
A_{121}	0.000	0.000	1.000	-0.291
$A_{122+221}$	0.000	0.000	-0.291	1.000

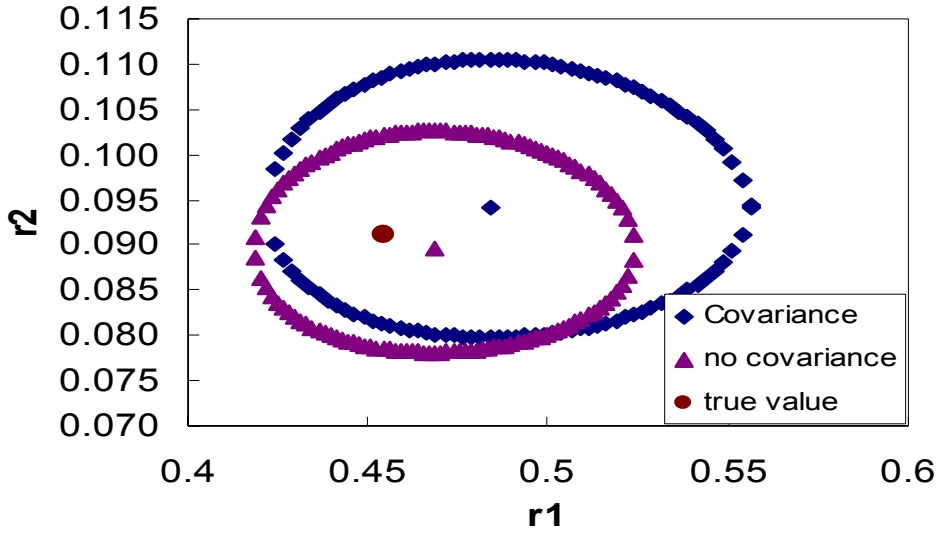

Figure 6.4 95% joint confidence region for triad fractions with correlated error at high error level; the non-correlated-error data are with additive error structure

From Figure 6.4, the estimation with correlated error is not as good as the estimation without correlated error (additive error). The point estimate of r_1 deviates from the true value more than r_2 because of the highly correlated error between A_{212} and $A_{112+211}$.

Figure 6.5 shows the JCRs for different error levels. The question is whether the estimation could be improved if the error covariance is taken into account.

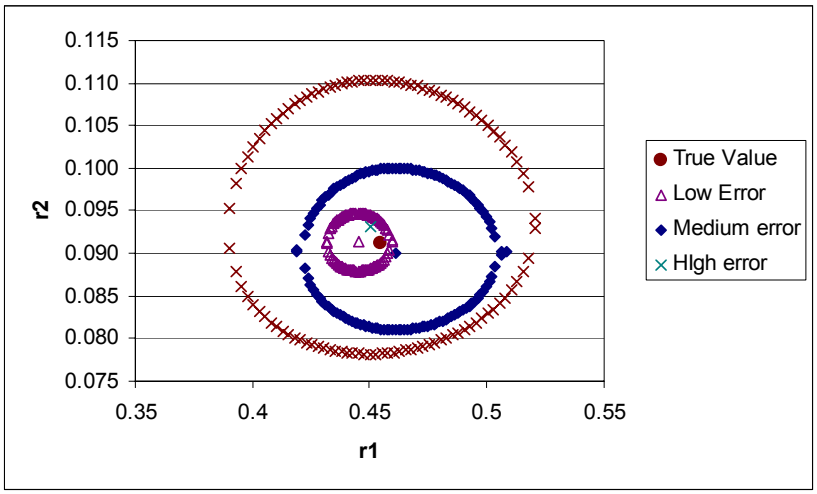

Figure 6.5 The plot for 95% joint confidence region at different error levels with correlated error

Here we still simulate the STY/AN system at 60°C in bulk copolymerization. The point estimates of reactivity ratios are listed in Table 6.5 and Table 6.6. In Table 6.5, the simulated data have no correlated error. NLLS and Box_Draper have no significant difference, because the covariance is so small that it can be neglected. In Figure 6.6, the 95% joint confidence regions (JCRs) also show this point. The shape and position of JCRs for the two methods are close except at high error level (Figure 6.6c). That is due to the sensitivity of Box_Draper method to the data perturbation. When experimental errors are high, the covariance structure cannot be obtained from few data points. That may distort the JCR and result in larger deviation.

In Table 6.6, the experimental data have correlated error. The point estimates from Box_Draper are better than NLLS. This is more obvious from the 95% JCR's plots(Figure 6.7a,b,c). The JCRs from Box_Draper method are smaller than those from NLLS. That means the estimation from Box_Draper has less uncertainty, since the Box_Draper method takes into account the error correlation of the experimental data.

Table 6.5 Point estimates of reactivity ratios through NLLS and Box_Draper method; Simulated data without correlated error

	NLLS		Box_Draper	
	r_1	r_2	r_1	r_2
True Value	0.4545	0.0912		
Low error level	0.4579	0.0900	0.4570	0.0907
Medium error level	0.4509	0.0918	0.4551	0.0913
High error level	0.4683	0.0897	0.4658	0.1014

Table 6.6 Point estimates of reactivity ratios through NLLS and Box_Draper method; simulated data with correlated error

	NLLS		Box_Draper	
	r_1	r_2	r_1	r_2
True Value	0.4545	0.0912		
Low error level	0.4540	0.0909	0.4546	0.0909
Medium error level	0.4472	0.0890	0.4452	0.0925
High error level	0.4838	0.0942	0.4715	0.0935

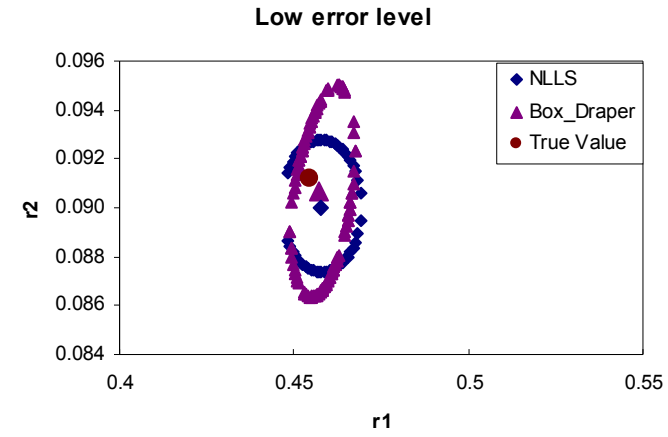

a)

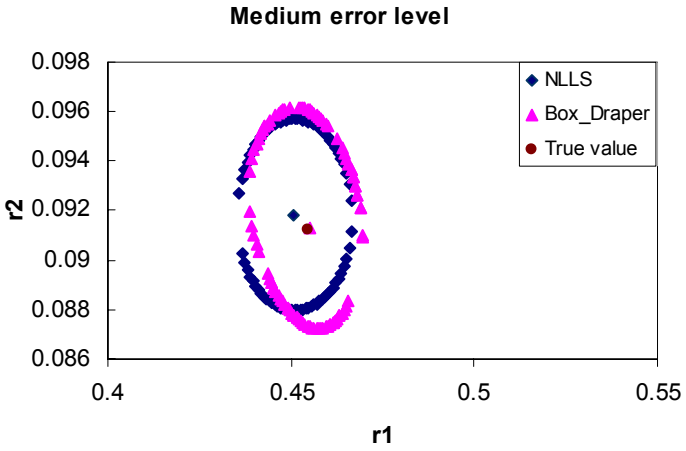

b)

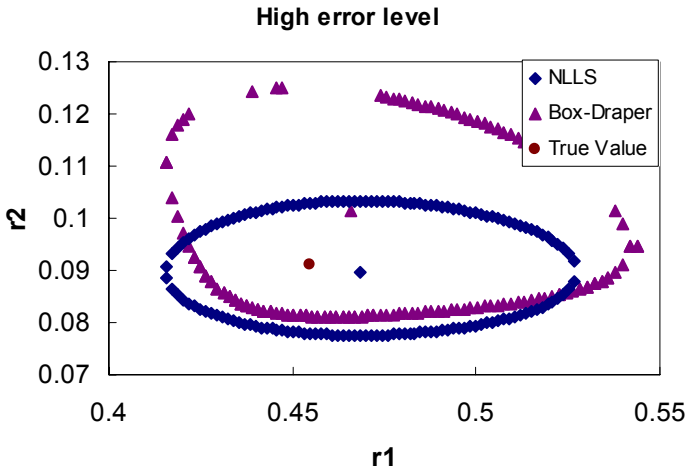

c)

Figure 6.6 Comparison of 95% joint confidence regions for estimation with Box-Draper method and NLLS. The simulated data have no correlated error

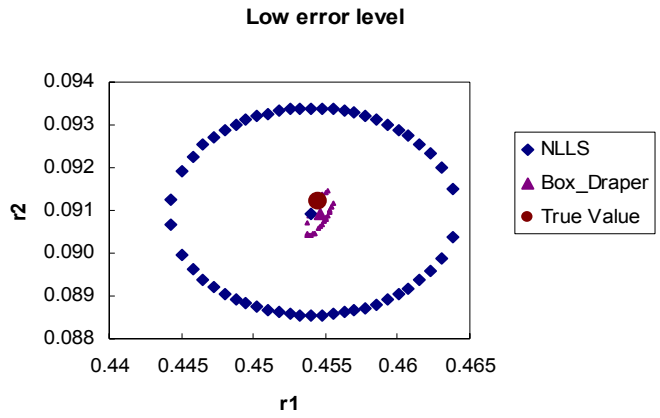

a)

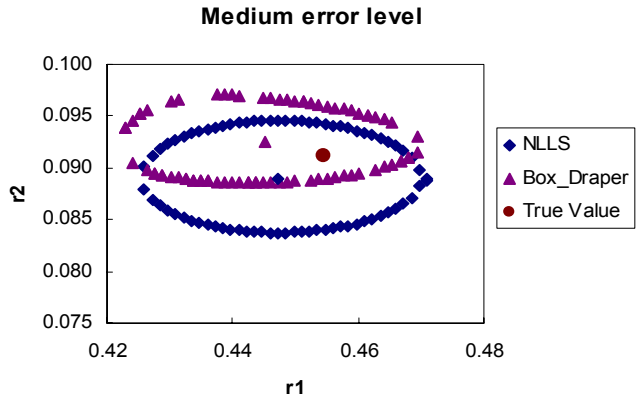

b)

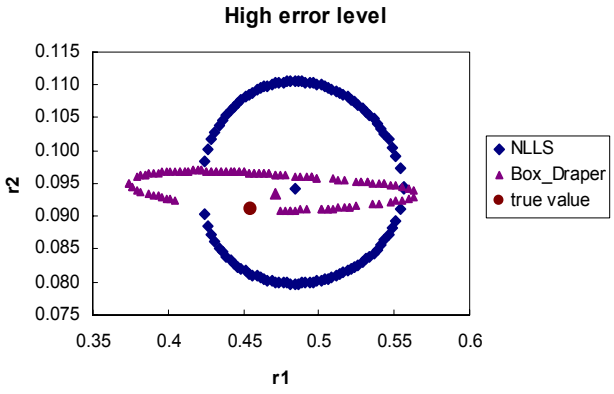

c)

Figure 6.7 Comparison of 95% joint confidence regions for estimation with Box-Draper method and NLLS. The simulated data have correlated error

6.1.4. Summary

The classical NLLS is reliable with both additive and multiplicative error. However, the true experimental triad distribution data usually come from the same NMR spectrum. Thus, they contain correlated error to some extent. If the correlation is considered, the estimation precision will be improved greatly. That is proved via the results using the Box_Draper method. But this method has its own drawback being more sensitive to the data perturbation. Thus, it needs more experimental data points at high error level. Furthermore, when covariance matrix is used in Box-Draper method, the stable region of estimation shrinks, so the initial value should be carefully chosen to obtain good estimates.

6.1.5. Experimental data verification-STY/MMA and STY/AN

In order to check whether the instantaneous sequence distribution model works well for the estimation of reactivity ratios, experimental data from the literatures are used to re-estimate the reactivity ratios.

The copolymer systems of STY/MMA and STY/AN have been extensively researched because of their wide applications in industry. Fukuda et al. (1985) published a set of experimental data on triad fractions, often cited by researchers. O'Driscoll et al. (1980, 1989) and Maxwell et al. (1993) published experimental data on the low conversion kinetics of STY/MMA system. The estimates of reactivity ratios are listed in Table 6.7

Table 6.7 Estimates of reactivity ratios of STY/MMA system

	r_1	r_2
Estimates from O'Driscoll et al. (1980)	0.472	0.454
Estimates from triad fraction model	0.4421	0.4723

Using these two sets of reactivity ratios, the triad fraction distributions are calculated again and plotted in Figure 6.8. The predicted triad fractions from the two sets of reactivity ratios are very close. Almost all of the experimental data are located on the predicted curves. Hill et al. (1982, 1989) investigated the STY/AN system in bulk

polymerization at 60°C. Triad fraction data were analyzed. Sanghvi et al. (2000) and Garcia-Rubio et al. (1985) also studied the STY/AN system in bulk.

The estimation results for STY/AN are listed in Table 6.8. The triad fractions calculated from those estimates are compared to the experimental data in Figures 6.9 and 6.10.

Table 6.8 Estimated reactivity ratios for STY/AN at 60 °C

	r_1	r_2
Hill et al. (1982)	0.47	0.08
Our estimates based on data from Hill et al.(1982)	0.4545	0.0912
Our estimates based on data from Hill et al.(1989)	0.4663	0.0859

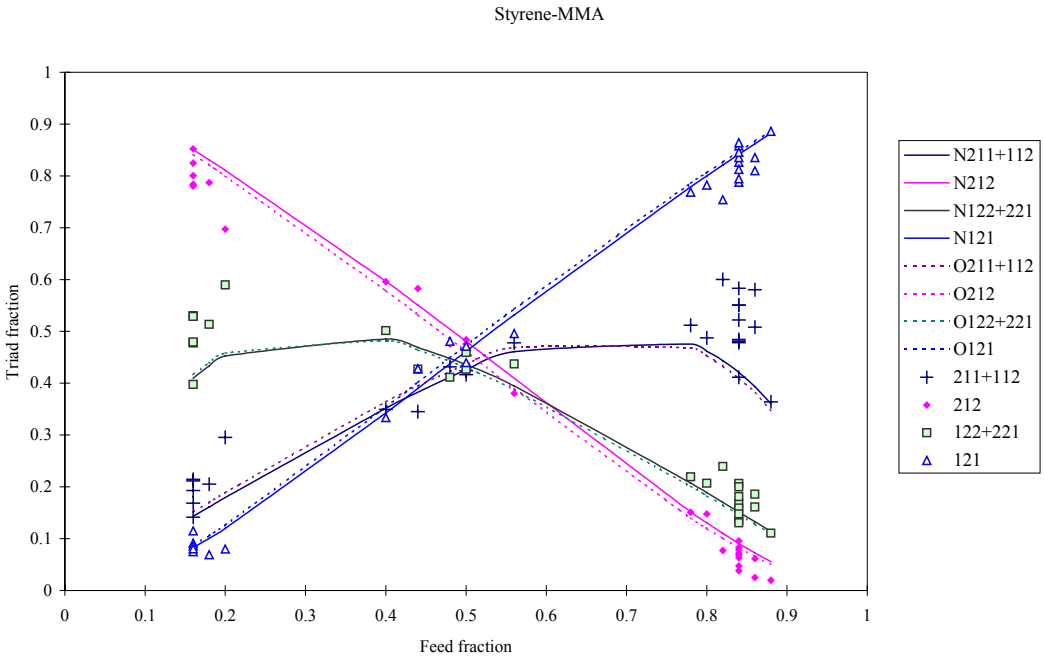

Figure 6.8 Triad fractions of Styrene/MMA system; N~ are the predictions of triad fractions from our simulation. O~ are the predictions from the simulation of O'Driscoll et al. (1980); Experimental data from Burke (1994)

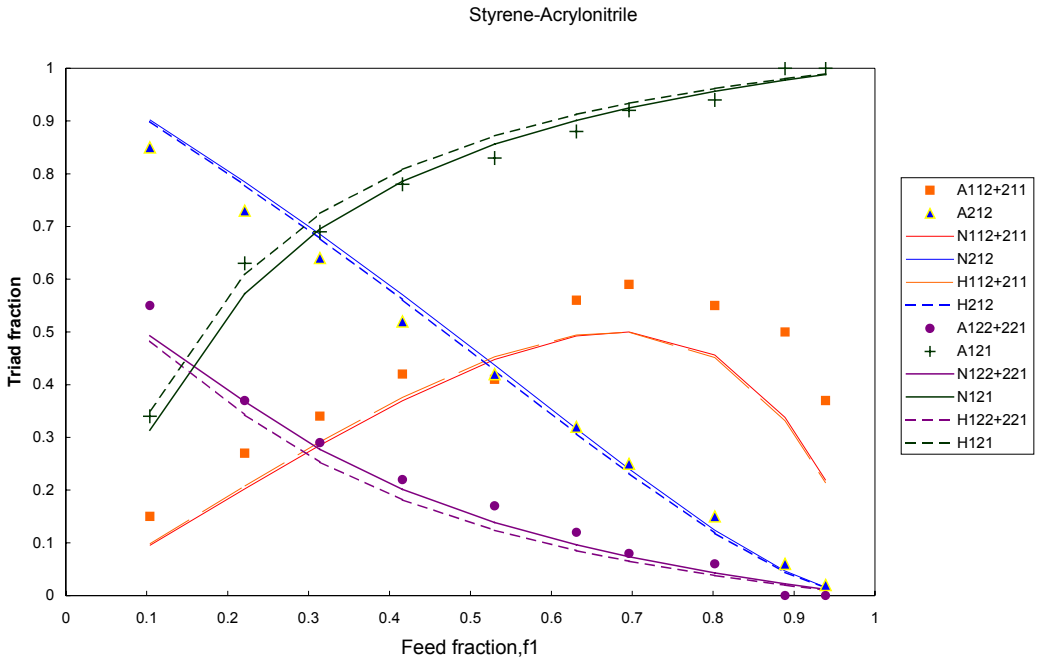

Figure 6.9 Triad fractions of Styrene/ Acrylonitrile system; N~ are the predictions of triad fraction from simulation. H~ are the predictions of triad fractions with reactivity ratios from Hill et al. (1982). Experimental data are obtained from Hill et al. (1982)

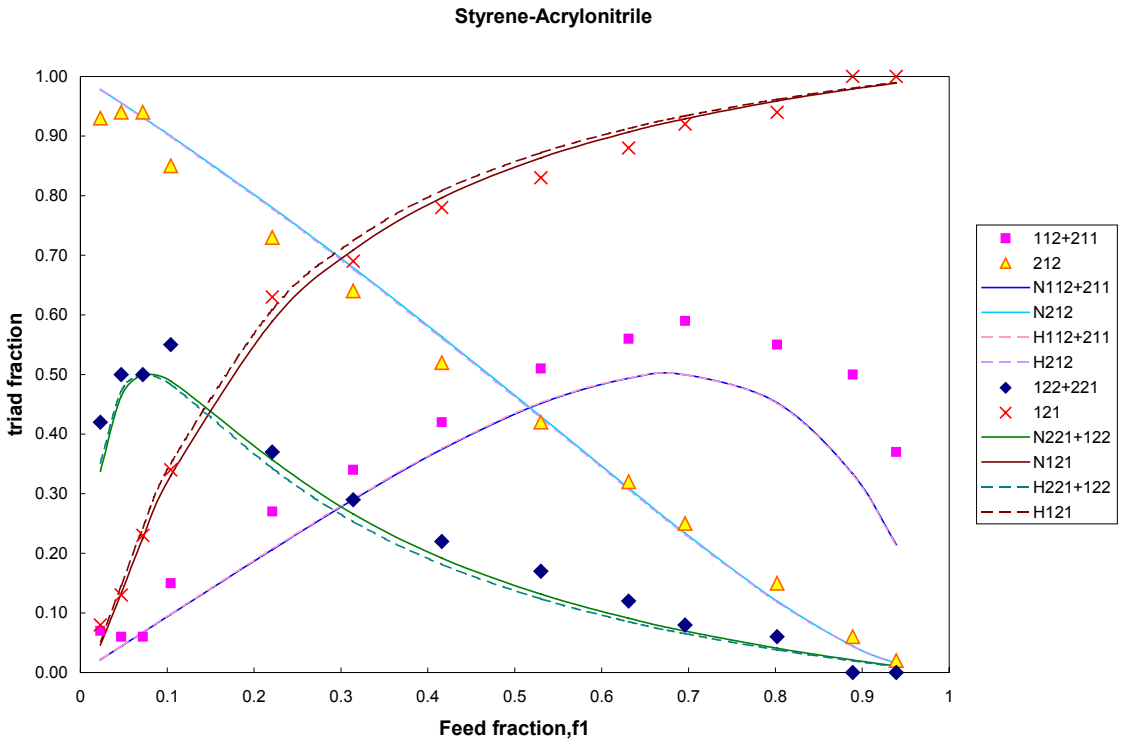

Figure 6.10 Triad fractions of Styrene/Acrylonitrile system; N~ are the predictions of triad fractions from simulation. H~ are the predictions of triad fractions with reactivity ratios from Hill et al. Experimental data are obtained from Hill et al.(1989)

From Figures 6.9 and 6.10, the triad fractions centered on monomer 2 (AN) agree well with the predictions. The triad fractions centered on monomer 1 (STY) show slight deviations.

From Figures 6.8-6.10, the predicted curve generated using the reactivity ratios estimated by nonlinear least squares agrees well with that from the reactivity ratios in the literature. This is a good indication that the multiresponse NLLS in combination with a triad fraction distribution instantaneous model are suitable for estimating reactivity ratios at low conversion.

6.2. Combination of triad fraction data and composition data (NLLS_IMFT)

6.2.1. Introduction

The instantaneous model of triad fraction (IMT) improves the estimation of reactivity ratios greatly compared with the Mayo-Lewis equation (see Figure 6.11). However, triad fractions usually come from the same NMR spectrum. That causes correlated error in the experimental data. This decreases the accuracy of estimation, because classical NLLS does not consider the correlation in the experimental data. Composition data are usually obtained from different sources, such as elemental analysis, etc.. If the two kinds of data are combined together, the estimation may be improved further.

The NLLS_IMFT program combines the responses of copolymer composition and triad fractions together. Here F refers to the copolymer composition and T refers to the triad fractions. This method has been checked by the simulation data of STY/AN (60°C) in bulk copolymerization. The errors are in the medium level, as per Burke's thesis (1994) (see Table 6.9).

Table 6.9 Different error level of measurment

	Low	Medium	High
Polymer composition	0.005	0.010	0.015
Triad fraction (mole)	0.00833	0.01667	0.0333

All of these are standard deviations.

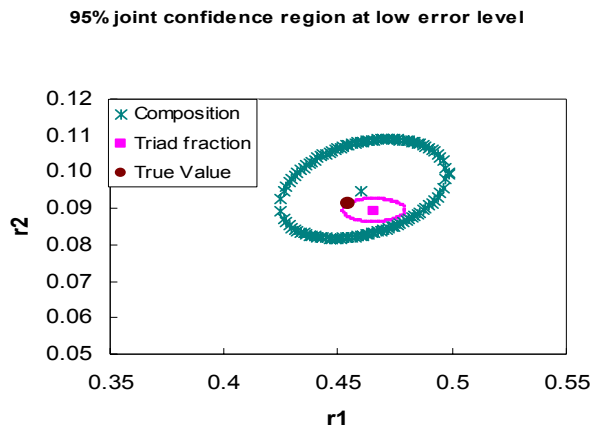

a

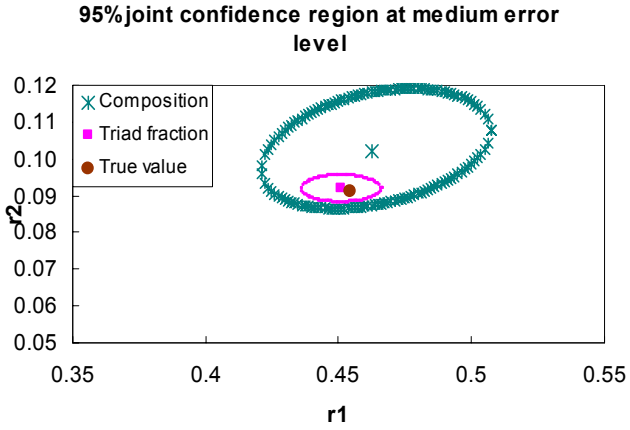

b

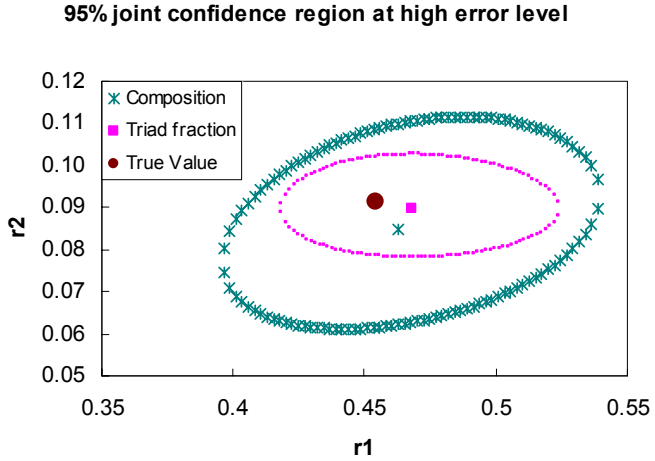

c

Figure 6.11 95% joint confidence region (exact contour)

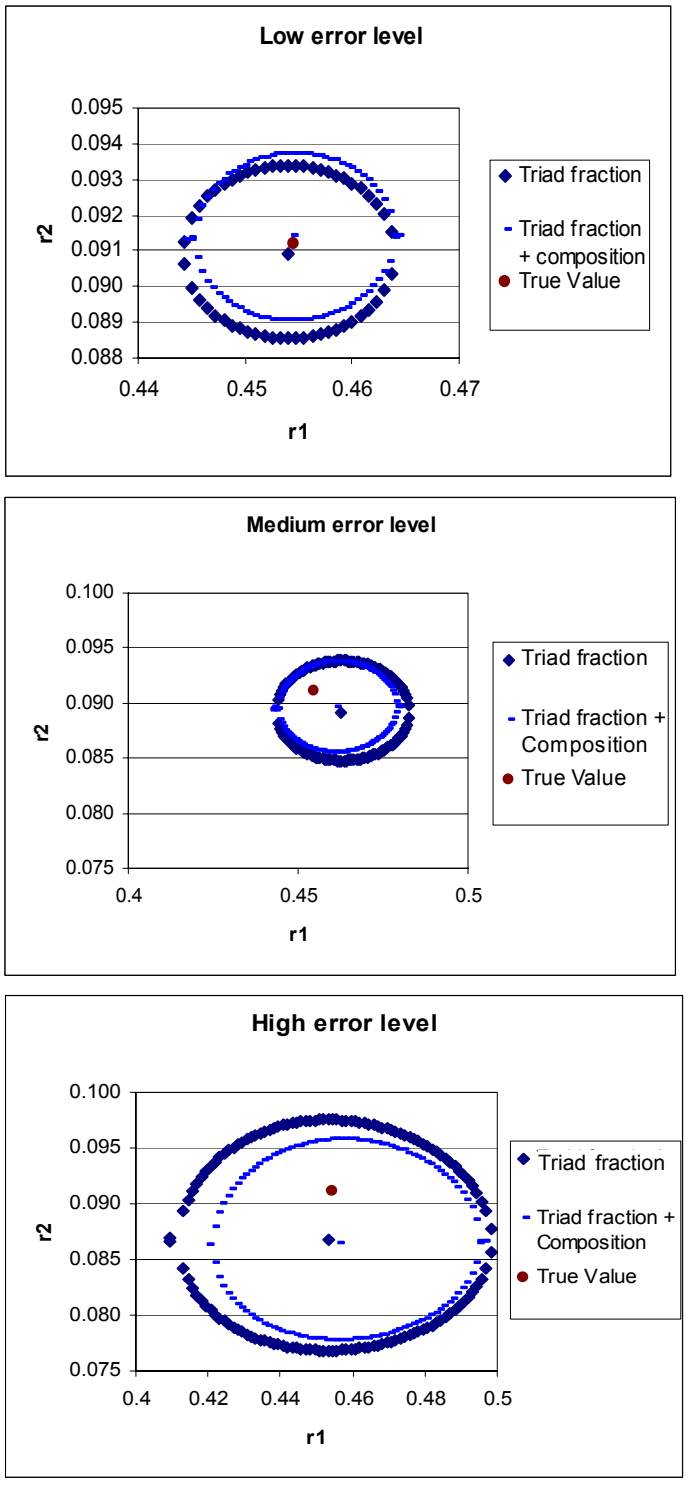

Figure 6.12 95% joint confidence region. Experimental data have correlated error

Figure 6.12 shows there is no large improvement in the point estimates as we expected. Thus, the benefit of adding a response of composition is rather small.

6.2.2. IMFT with experimental data

The experimental data come from Brar et al. (1993) (see Table 6.10). The system is styrene/butyl acrylate in bulk copolymerization at at 70°C.

Table 6.10 Experimental data for Styrene (STY) _Butyl acrylate (BA) copolymerization in bulk at 70°C

fs	Fs	A112	A212	A221	A121
0.20	0.35	0.37	0.56	0.51	0.32
0.30	0.51	0.40	0.50	0.43	0.47
0.40	0.62	0.46	0.30	0.39	0.54
0.50	0.65	0.49	0.23	0.30	0.67
0.60	0.70	0.47	0.13	0.20	0.79
0.70	0.78	0.37	0.06	0.14	0.84
0.80	0.85	0.30	0.02	0.08	0.92

Table 6.11 Estimates for STY/BA system

		r1	r2
Brar et al.	KT	1.17	0.15
	EVM	1.21	0.17
This work	NLLS	1.39	0.29
	EVM	1.59	0.35
	IMT	1.15	0.21
	IMFT	1.16	0.21

The EVM results in our work differ from Brar's results (see Table 6.11). In the composition plot (Figure 6.13), it is possible to see that there is a point at f_{10}=0.2 that greatly deviates from the curve predicted by Brar's EVM result. If this point is eliminated, the same result as Brar's is obtained. The interesting point is that this point has no obvious influence on the estimates from the triad fraction model. The joint confidence regions with this point are shown in Figure 6.14. The triad fractions calculated by the estimates using the IMFT method give the best fit of the experimental data (Figure 6.15).

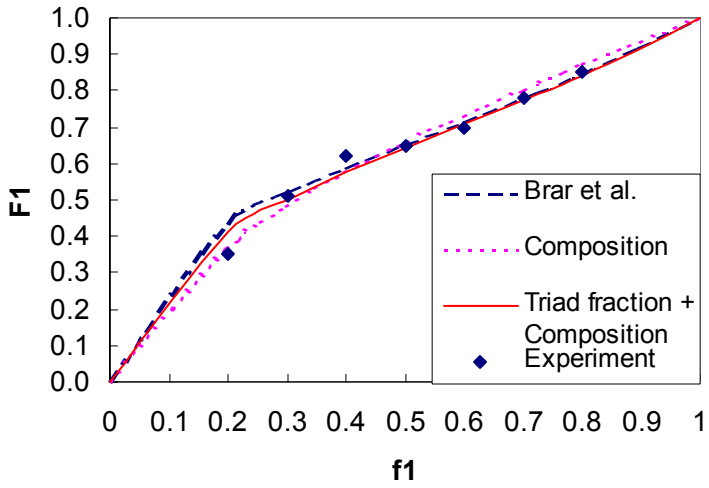

Figure 6.13 Composition Curve for STY/BA system. Scattered data are experimental data (Brar et al. 1992); Solid line predicted by reactivity ratios from triad fraction + composition data method.

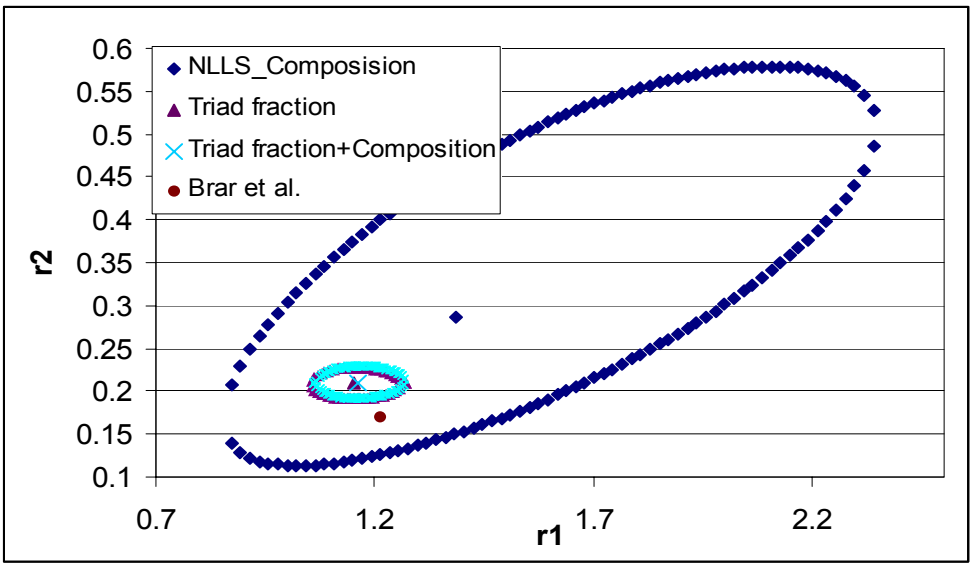

Figure 6.14 95% joint confidence region for STY_BA system(exact contour)

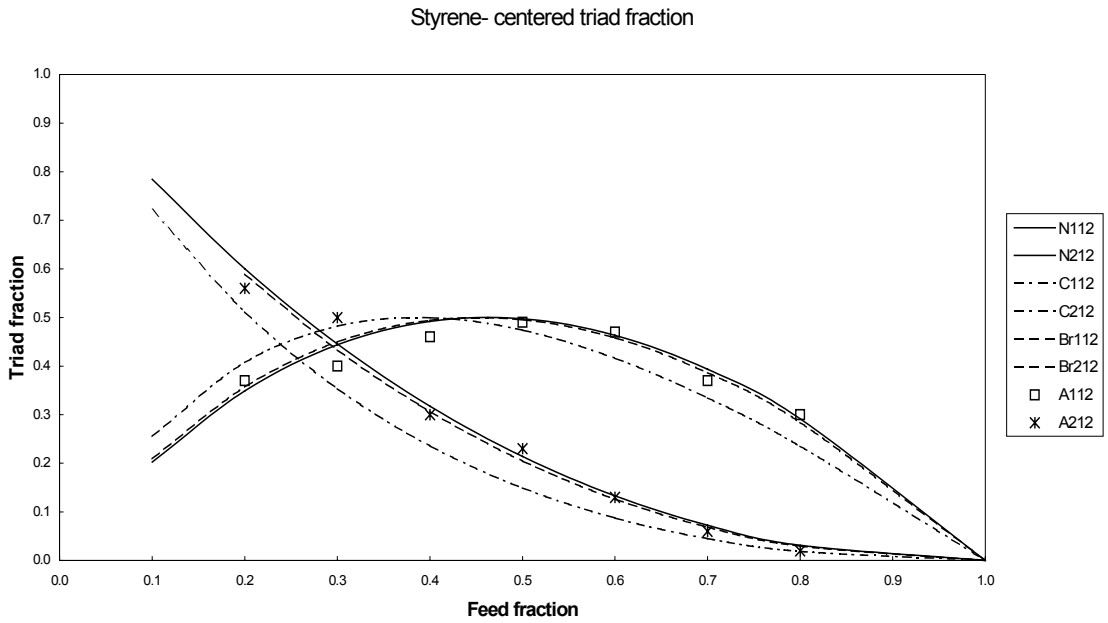

a)

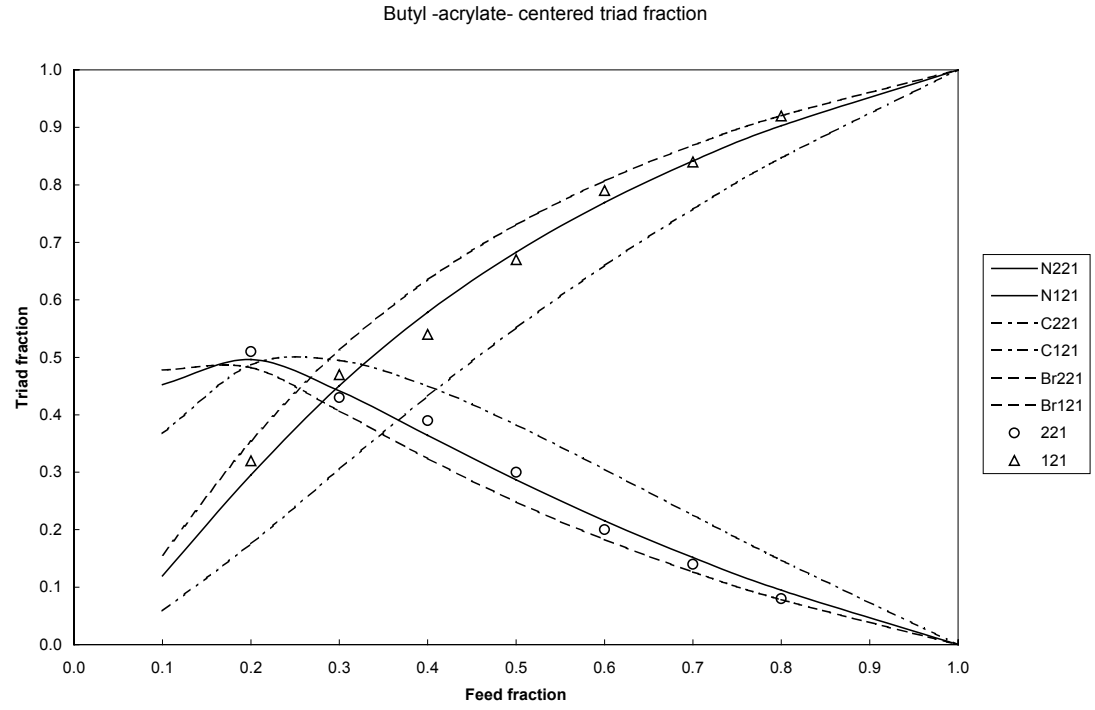

b)

Figure 6.15 Triad fraction curves. "N" stands for the triad fraction+ composition data method; "C" stands for composition data method; "Br" stands for estimates from Brar et al. (1992) The symbols are experimental data.

6.2.3. Conclusion

Triad fraction data describe the polymer chain's structure. It can provide better estimation of reactivity ratios than composition because they contain more information. At the same time, the model is not as sensitive to perturbations in the experimental data. Furthermore, using the instantaneous composition data, as an additional response for model estimation, improves the estimates by only a small degree.

6.3. Cumulative composition model

The largest advantage of the cumulative composition model is that the experiment is not constrained by the low conversion requirement to get reliable estimation of reactivity ratios. However, this does not mean that any conversion experimental data will result in precise estimation. A good experimental design is essential to obtain reliable estimation results.

Because Non-linear least squares (NLLS) is used to optimize reactivity ratios, a D-optimal design is used to find the suitable experimental data points. As mentioned in chapter 4, the D-optimal design can be easily visualized due to the simplicity of the derivative space. The design points are selected such that the area formed by connecting the origin and the two support points is the largest possible.

A copolymer system with or without azeotropic point will show great difference in kinetics. STY/ AN system and MMA/VAc are the case studies discussed in the following sections. This work is mainly focused on the numerical integrated cumulative composition model (see Chapter 2), overall mole conversion x and monomer feed ratio f_{10} as independent variables and cumulative composition $\overline{F_1}$ or residual monomer ratio f_1 as response used for estimation.

6.3.1. System with azeotropic point (STY/AN)

6.3.1.1. D-optimal design for cumulative composition $\overline{F_1}$ as response

Here the STY/AN system copolymerization in bulk at 60°C is simulated as an example. The initial reactivity ratio 0.36(r_1) and 0.078 (r_2) are obtained from Garcia-Rubio's paper (1985). The objective function for NLLS can be written as

$$S(r) = \sum \left(\hat{\overline{F}}_1 - \overline{F}_1 \right)^2 \tag{6.8}$$

The design locus is shown in Figure 6.16. Each circle in the plot represents the change in derivative with different conversions at certain monomer feed ratio. The arrows indicate the direction of increase of conversion and monomer feed ratios. This figure shows that the trace of the derivative varying with conversion is along small circles. If the optimal experimental points will be obtained at different feed ratios, it would be possible to form a large area. That means that combining the experimental data of different monomer feed ratios will improve the precision of the reactivity ratio estimation in a larger degree as compared to using experimental data of one monomer feed ratio at different conversions. This proves the observation of Plaumann et al. (1989) that for integrated models, the experiment should start at different initial monomer feed ratios because otherwise, the error will be large.

This design locus plot also shows that the optimal points are obtained in two directions parallel to the two axes respectively. This character is to make the design nearly orthogonal. Also the derivative in the r_2 direction is higher than the one in the r_1 direction. Thus, the estimation of r_2 may be more precise.

Furthermore, from the design locus plot, we can find that when the cumulative variable is used as a response, low conversion data can supply more information.

The above conclusion will be shown on the following case studies.

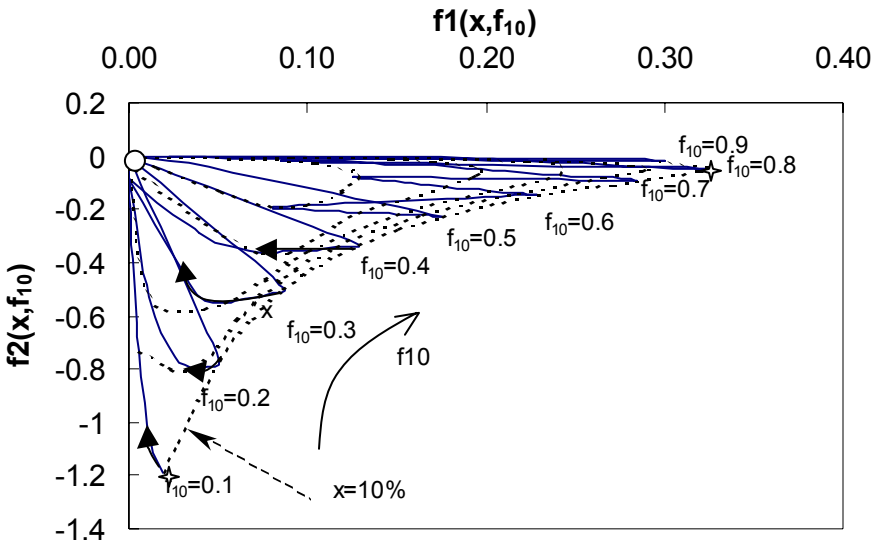

Figure 6.16 Design locus for model 1, conversion x increases in the direction indicated by the arrows: Low conversion is at farther point, high conversion is close to the origin. $f1(x, f_{10}) = \partial \overline{F}_1 / \partial r_1$, $f2(x, f_{10}) = \partial \overline{F}_1 / \partial r_2$ **The solid arrows show the direction of conversion increasing. The dashed lines are the conversion contours. The interval of the conversion between two lines is 0.2. Two stars are the two optimal points.**

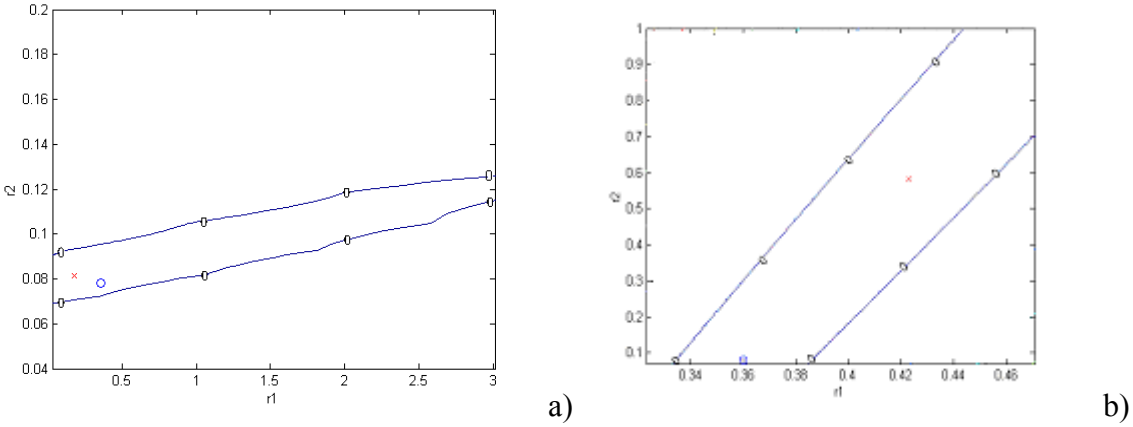

a) b)

Figure 6.17 a)f10=0.1, STY/AN b)f10=0.8, STY/AN contour at 0 level is 95% joint confidence region. Both simulations have 9 points

From figure 6.16, the optimal design points correspond to monomer feed ratios of 0.1 and 0.8 and low conversion (10%). The first case uses experimental data at a monomer feed ratio of 0.1 and 0.8, respectively. The simulation shows that using experimental data at one feed ratio result in very poor estimation (Figure 6.17). High acrylonitrile feed ratio experiments result in good estimation of r_2, whereas high styrene feed ratio experiments result in good estimation of r_1. So the combination of experimental data at different feed ratios will give good estimates for this system (Figure 6.18). This simulation results agree well with the results from the D-optimal design.

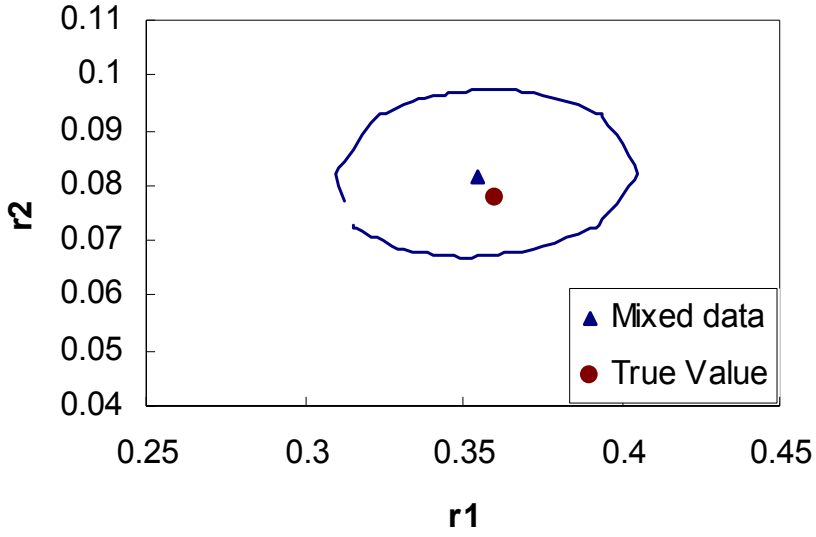

Figure 6.18 95% JCR with mixed experimental data at f10=0.1 and 0.8

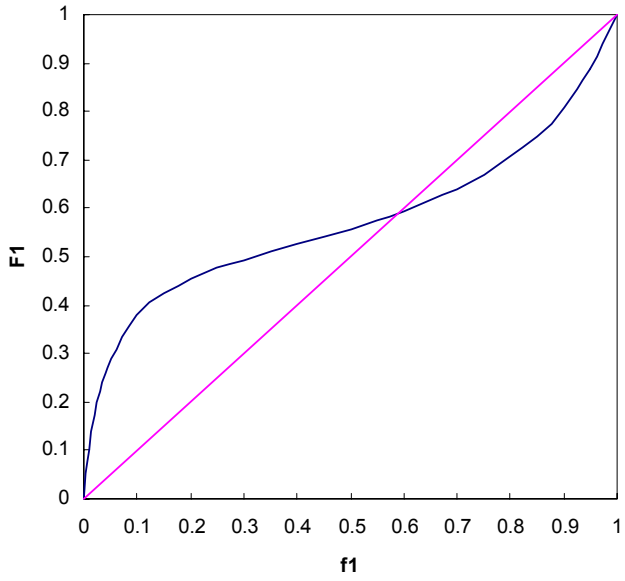

Figure 6.19 Composition curve for STY/ AN, r_1=0.36,r_2=0.078

Monomer feed ratios of 0.1 and 0.8 correspond to the largest composition drift on either side of the azeotropic point. The composition curve is shown as Figure 6.19.

To improve the estimation, besides replicating experiments, more data along the evolution of the conversion at two monomer feed ratios can be chosen. The following case1a uses four replicate experiments on each optimal point; cases 1b and 1c use more data near the optimal conversion at feed ratios of 0.1 and 0.8. In case 1b, there are four sampling points at different conversions on each optimal feed experiment. In case 1c, there are three sampling data on each optimal feed experiment. To make sure the extra sampling points can form large area in the design locus, the conversion does not exceed 30%.

The selected extra experimental data can suggest a point at two feed ratios respectively. These points also should maximize the derivative space. That means that the area formed by the extra points and the origin should be as large as possible in the design loci plot. If only one extra point is added, the point with the large norm of the Jacobian matrix may bring more information for estimation. This is shown in cases 1a and 1b. From Figure 6.20, although case 1b has the same experimental data points as case 1a, the estimates are poorer because the added points have less information in case 1b than in case 1a. Case 1c has the poorest precision due to the less sampling points.

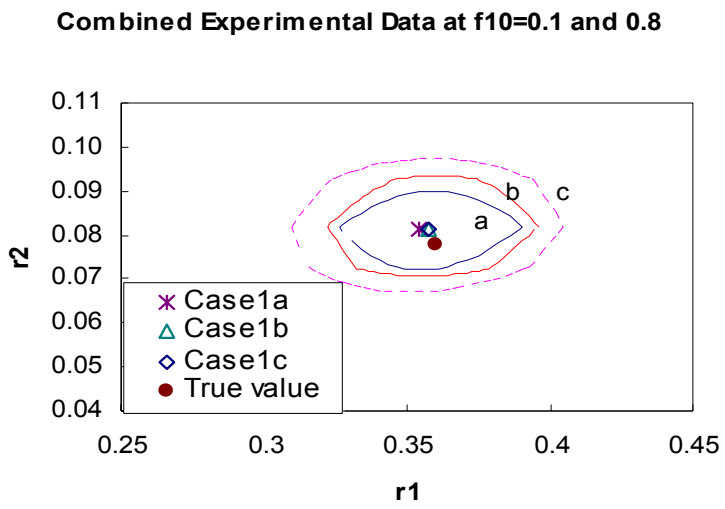

Figure 6.20 95% JCR with combined experimental data: Case 1a: 4 replicates at two monomer feed ratios; Case 1b: 4 data points at different conversions at 2 monomer feed ratios; Case 1c: 3 data points at 2 monomer feed ratios

However, if one monomer has been consumed up at certain conversion, the instantaneous polymer composition at that time does not correlate with the reactivity ratios. The cumulative polymer composition has lost the reactivity ratio information at this conversion. So these extra data has no benefit for estimation.

In conclusion, for $r_1<1$ and $r_2<1$, the two optimal feed ratios are located on either side of the azeotropic point.

Generally, with cumulative composition $\overline{F_1}$ as the response, the most informative data will occur at low conversion. For polymer composition of STY/AN system, when feed ratio is between 0.2-0.4, the high acrylonitrile ratio region, the most sensitive points to r_2 will reach when f_1 move to 0.11, where the composition drift is the largest. For these feed ratios, the corresponding optimal point may move to the conversion about 60%.

For a system with an azeotropic point the almost orthogonal design may result in the precise estimation.

6.3.1.2. D-optimal design for monomer residual mole fraction f_1 as the response

The monomer residual mole fraction can be the response, because it can be conveniently obtained with the conversion from gas chromatography (Garcia-Rubio et al., 1985). The objective function is given by:

$$S(r) = \sum \left(\hat{f}_1 - f_1 \right)^2 \qquad (6.9)$$

In this study the focus is on the effect of experimental design on the estimation accuracy. To simplify the discussion, in our simulation, conversion is assumed to have no error and f_1 has the same error as $\overline{F}_1$.

The D-optimal design locus is shown in Figure 6.21. Similar to the previous case, the information from one feed ratio is not enough to get good estimates. The combination of experimental data from different monomer feed ratio is necessary. However, the design in this case shows large differences compared to the design based on the cumulative composition response. Generally, high conversion is more informative in this case. However, the farthest point from the origin is not on the highest conversion line. The conversion at that point is close to 90% from a feed ratio of 0.5-0.7, 80% at a feed ratio of 0.4, and 40%-60% at other feed ratios. Furthermore, the optimal points of STY/AN system are located on f_{10}=0.5 and f_{10}=0.6 at high conversion, where it is near the azeotropic point. Both of these points contain similar information in the derivative in the r_1 and r_2 direction. That means that the estimates have similar precision and have high correlation between them.

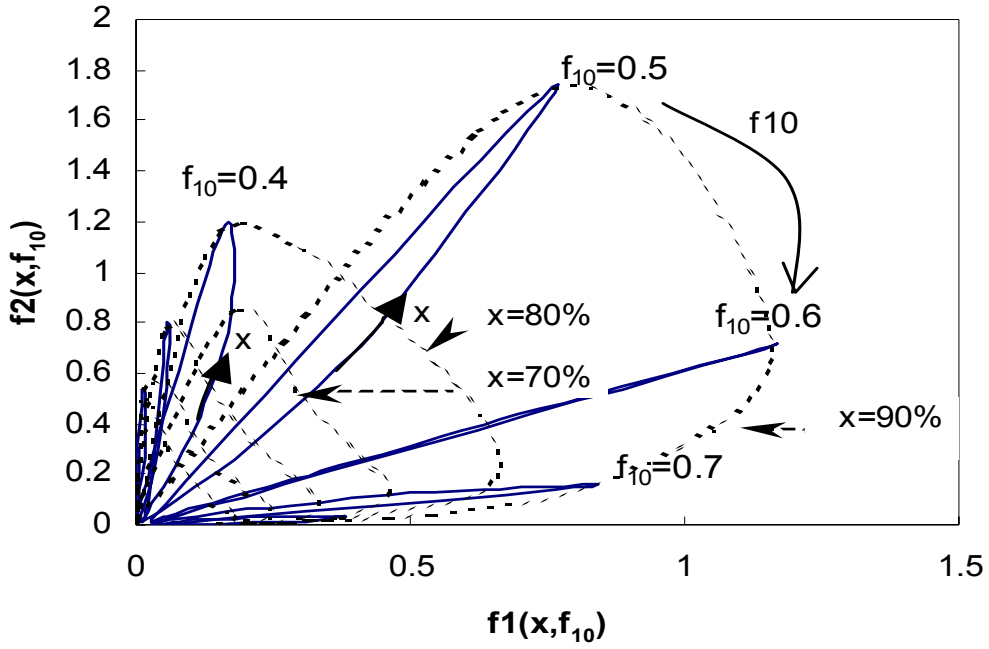

Figure 6.21 Design locus for the response of the instantaneous monomer residuals, $f1(x, f_{10}) = -\partial f_1/\partial r_1$, $f2(x, f_{10}) = \partial f_1/\partial r_2$ **. The symbols are the same as in Figure 6.16.**

The following case 2_a (Figure 6.22) shows the estimation results at the optimal design. Although the uncertainty of estimation is similar to the $\overline{F_1}$ response, there is higher correlation between parameters.

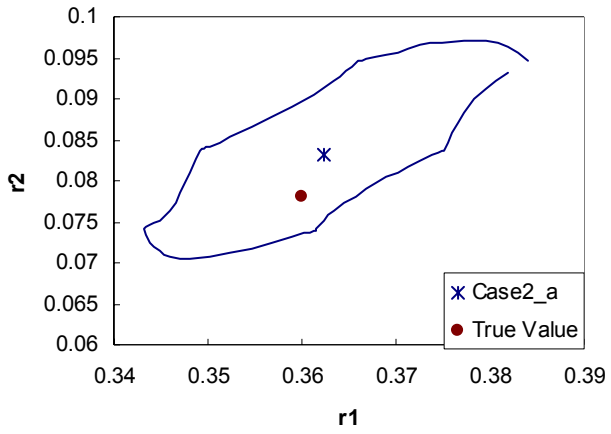

Figure 6.22 Case 2_a, combined data at feed ratio f10=0.5, 0.6. Each feed ratio has three replicated data points.

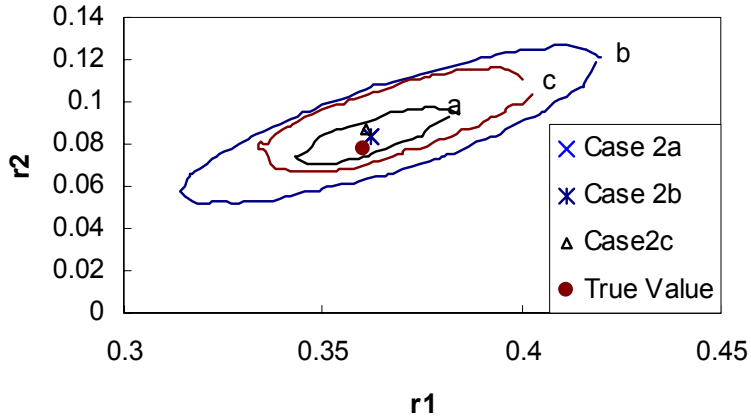

Figure 6.23 95% JCR of combined experimental data at f_{10}=0.5 and f_{10}=0.6. Case 2a is Case 2_a in Figure 6.22; Case 2b uses two arbitrary points in information-rich region at each feed ratio; Case 2c, two typical points at each feed ratio on response curve in Figure 6.24.

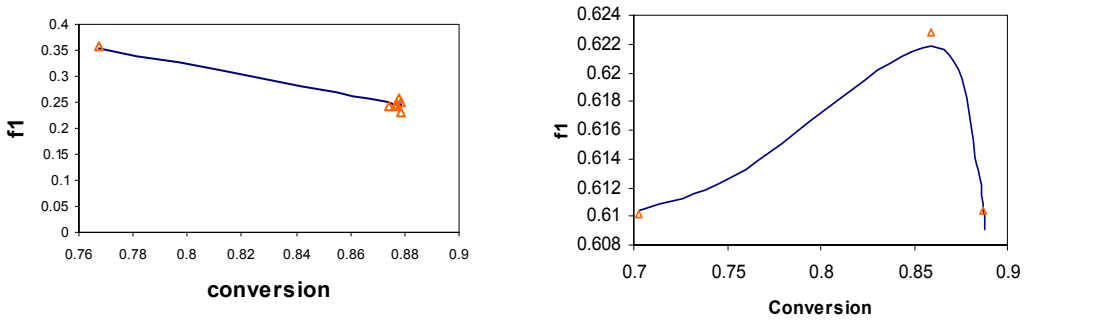

a) b)

Figure 6.24 The response curve for model 4 at fixed monomer feed ratio. a) f10=0.5; b) f10=0.6

From Figures 6.23 and 6.24, choosing the typical points along the evolution of the monomer residual over the conversion also can decrease the impact of measurement error to some extent.

- Remarks

1. $\overline{F_1}$ or f_1 as response:

The support point when monomer residual data are used is usually located in the high conversion region. On the other hand the best support point when the cumulative polymer composition data are used is located in the low conversion region. That is more convenient for experimentation.

2. Azeotropic point and the region near it.

Monomer residual experimental data are obtained as instantaneous quantities. The monomer residual mole fraction is very sensitive to the reactivity ratios at the azeotropic point and the support region near it at high conversion, whereas the polymer cumulative composition is sensitive to the reactivity ratios at the high composition drift region.

3. Before the azeotropic point, the polymer composition response is sensitive to r_2, whereas after the azeotropic point, the polymer composition response is sensitive

to r_1(Figure 6.16). Thus combining data from the two regions results in better estimation of reactivity ratios and reduces the parameters' correlation.

6.3.2. System without an azeotropic point (MMA/VAc)

6.3.2.1. D-optimal design for cumulative composition $\overline{F_1}$ as response

The MMA/VAc system, copolymerizing in bulk at 60°C, is an example of a system without an azeotropic point. The reactivity ratio used is based on the results of Dube and Penlidis (1995), r_1=24.0254 and r_2=0.02611 (MMA is monomer 1 and VAc is monomer 2). For r_1>1, r_2<1, there is only one region with large composition drift. The design locus (shown in Figure 6.25) is similar to the system with azeotropic point in the sense that using the response of cumulative average composition, the high conversion data contain very little information about reactivity ratios. The locus of high VAc feed ratio almost enclose that of MMA high feed ratio, which covers a very small region. It indicates that the high MMA (the faster monomer) experiment cannot supply much information on reactivity ratio estimation. On the other hand, the high VAc (the slower monomer) experiment can supply more information on reactivity ratios. Even at the same feed ratio, the cumulative composition data at different conversions can supply more information than high MMA concentration data. This is very different from the system having an azeotropic point. It is due to the large composition drift resulting from the great difference of the reactivity ratios of this system. Because $r_1 >> r_2$, MMA incorporates into the copolymer much faster than VAc, so the high MMA concentration region behavior is like a homopolymerization. This character is to be useful in using online detection techniques to obtain some priori knowledge of reactivity ratios. It indicates that several points in one experiment at different conversions may result in reasonable estimation (Figure 6.26). If the reactivity ratios are not very different, this phenomenon may not be so obvious. However, the region corresponding to this situation is only from low to mid high conversion. From the design locus (Figure 6.25), when conversion increases, the point moves to the origin quickly (arrows in Figure 6.25). The conversion of point A at feed ratio 0.2 is only 30%; Point B at feed ratio 0.4 is only 50%. The experimental points at different feed ratios are still a better choice. The plot also indicates that when the

monomer feed ratio is less than 0.1, the derivative decreases greatly in the r_1 direction and increase greatly in the r_2 direction. That means the information of r_2 contained in the response of polymer position increases and the information of r_1 decreases. The experimental data in this region may help to decrease the correlation of parameters. For this system, one optimal point is located around a feed ratio of f_{10}=0.01. The other point is approximately f_{10}=0.2. Both of the conversions are around 10%. Figure 6.27 shows the 95% JCR of estimation at monomer 1 (MMA) feed ratio 0.1, 0.2 and 0.01, 0.2 respectively. It is obviously that the latter combination decreases the correlation between parameter r_1 and r_2.

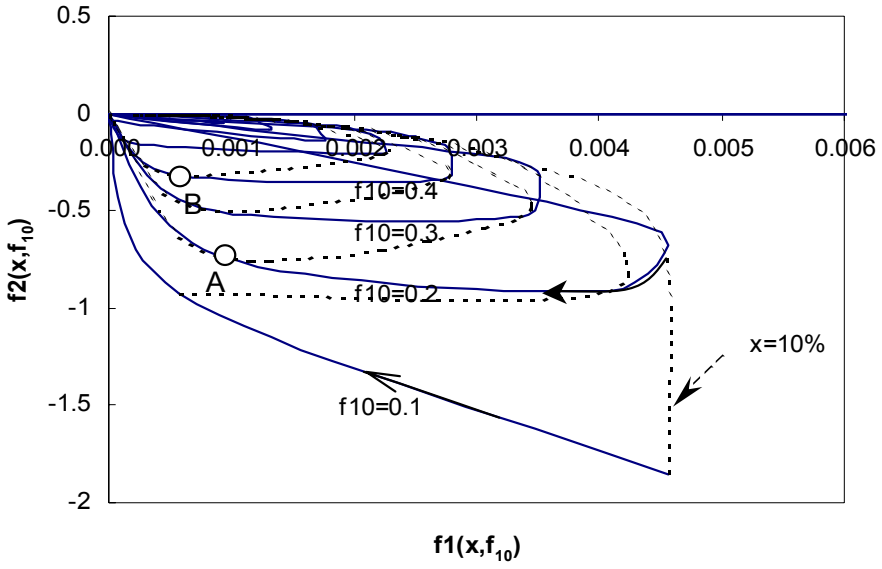

Figure 6.25 Design locus for cumulative composition model of MMA/VAc system. The cumulative polymer composition is a response.

$f1(x, f_{10}) = \partial \overline{F}_1 / \partial r_1$, $f2(x, f_{10}) = \partial \overline{F}_1 / \partial r_2$ **Symbols are the same as in Figure 6.16. The interval of conversion contours is 0.1**

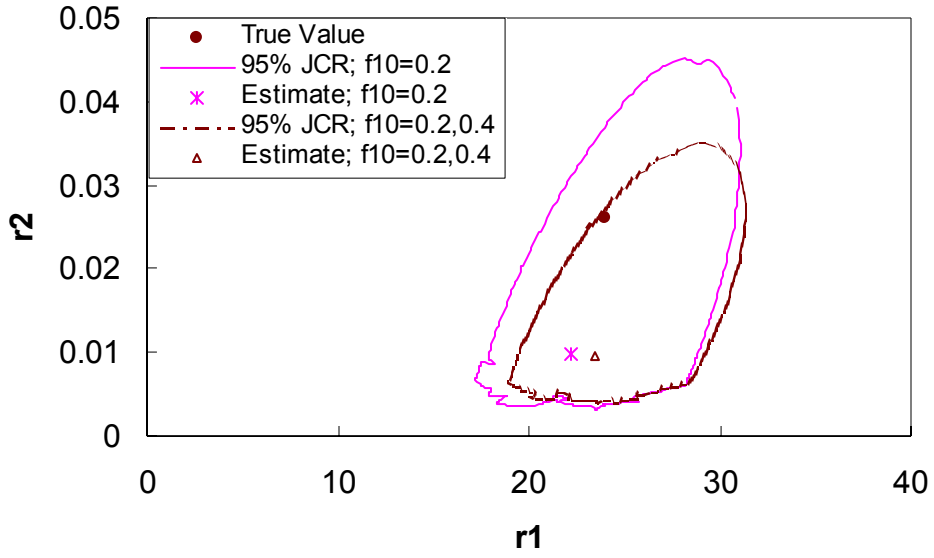

Figure 6.26 Comparison estimation with experimental data at one feed ratio f_{10}=0.2 and at two monomer feed ratio f_{10}=0.2 and 0.4

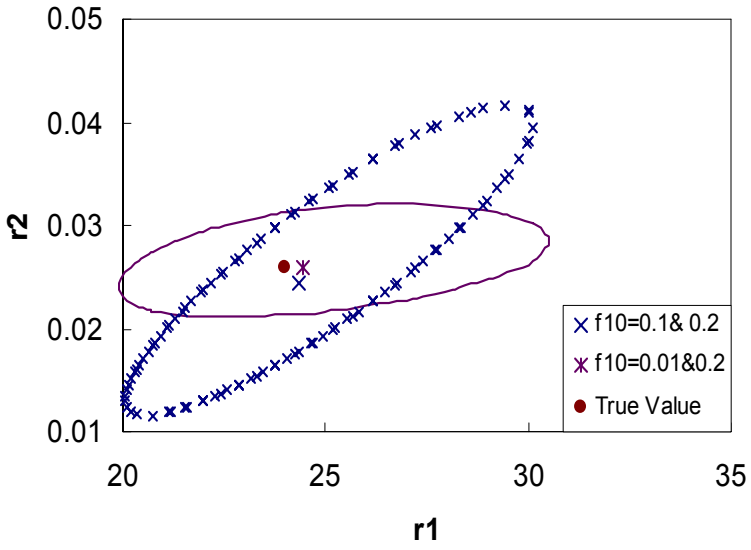

Figure 6.27 95% joint confidence region for reactivity ratio estimation of MMA/VAc system. Comparison of two combinations of monomer feed ratios.

6.3.2.2. D-optimal design for monomer residual mole fraction f_1 as the response

From the MMA/VAc design locus (Figure 6.28), for the response of instantaneous residual monomer mole fraction, the optimal region for the reactivity ratio estimation moves to high conversion. In the slower-monomer-rich mixture, the optimal region usually occurs before the faster monomer is consumed. In the faster-monomer-rich mixture, the optimal region is usually located at high conversion. Usually the steepest part of the composition curve includes substantial information about the reactivity ratios (Figure 6.29). Furthermore, if the slower monomer (VAc) has high concentration in the feed, even the experimental points at the same feed ratio may form the large area (Figure 6.28), i.e. they contain substantial information for the estimation of reactivity ratios. In the MMA/VAc system, the monomer feed ratio of 0.5 is a typical case. The experimental data at conversion of 60% and 50%, corresponding to A and B may supply more information than some combinations of experiment data at other feed ratios (see Figures 6.28 and 6.30). The estimate of r_1 has larger uncertainty than r_2, because in the derivative space f_1 is not sensitive in the r_1 direction. Finally, the approximate optimal design is at monomer feed ratios of 0.25 and 0.75 at conversions of 30% and 70% respectively.

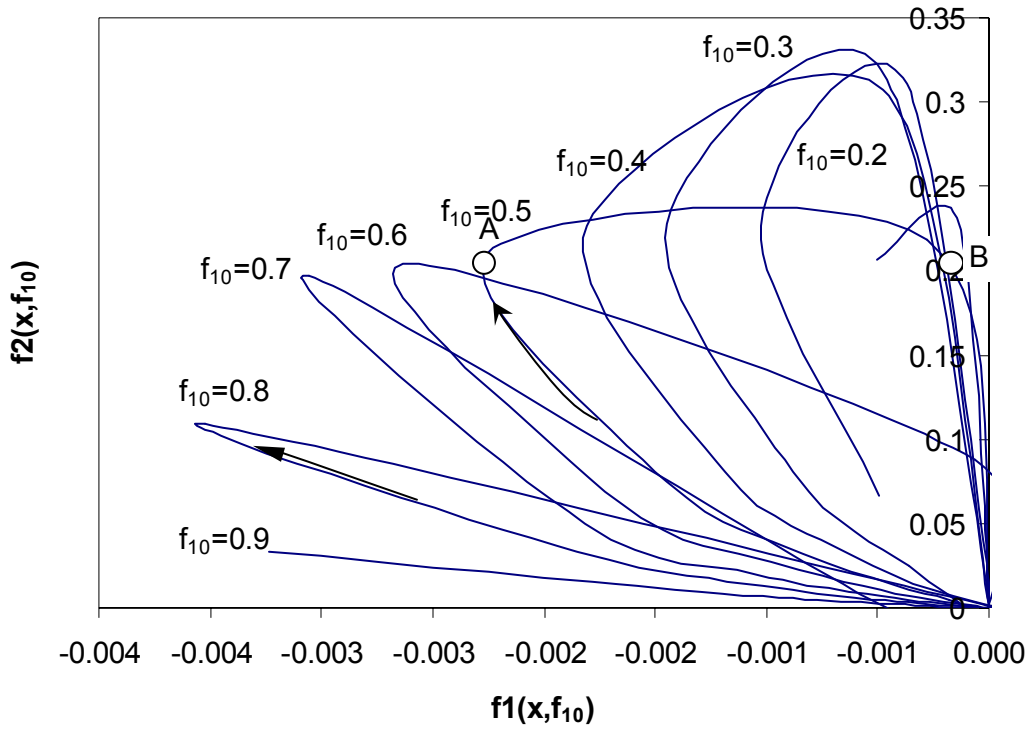

Figure 6.28 Design loci for cumulative composition model of MMA/VAc system. Monomer residual mole fraction as a response

$f1(x, f_{10}) = \partial f_1 / \partial r_1$, $f2(x, f_{10}) = \partial f_1 / \partial r_2$

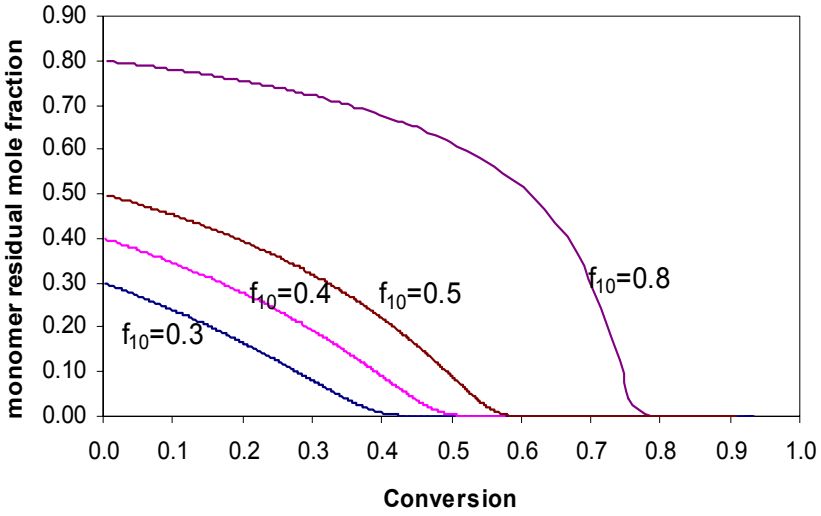

Figure 6.29 Instantaneous monomer residual vs. conversion at different monomer feed ratio. MMA/VAc copolymer. Initiator is AIBN. $[I]_0$=0.01M

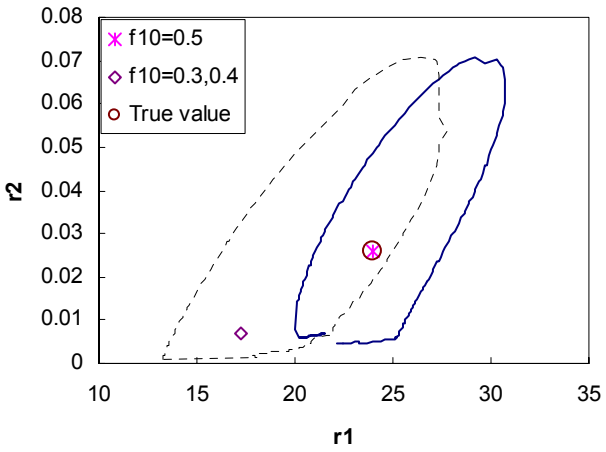

Figure 6.30 Comparison of estimation for experimental data at one monomer feed ratio 0.5 and the combination data of monomer feed ratios 0.3 and 0.4.

- Remarks

Comparing the responses of the cumulative polymer composition and instantaneous monomer residual shows that the cumulative polymer composition is stable for estimation. Because the optimal points usually are located on the high conversion region for instantaneous monomer residual where it is usually very low and easy perturbed by noise, the precision of estimation from the instantaneous monomer residual response is not as good as that from the cumulative polymer composition response. That also means that if instantaneous monomer residual is used as a response, high accuracy of measurement is necessary.

6.3.3. Alternative models: time as the independent variable

In dynamic systems, time as independent variable is easier to measure and control than conversion. Conversion itself becomes a response varying between 0-1.

6.3.3.1. Independent variables are time and f_{10}; dependent variables are conversion x and residual monomer ratio f_1

The objective function for estimation is given by

$$S(r) = \sum \left(\hat{x} - x\right)^2 + \sum \left(\hat{f}_1 - f_1\right)^2 \tag{6.10}$$

$$\frac{df_1}{dt} = -\frac{k_{11}k_{22}\left(r_1 f_1^{\,2} + 2f_1 f_2 + r_2 f_2^{\,2}\right)}{k_{22}r_1 f_1 + k_{11}r_2 f_2} \cdot \left(F_1 - f_1\right)[R\cdot] \tag{6.11}$$

$$\frac{dx}{dt} = \frac{k_{11}k_{22}\left(r_1 f_1^{\,2} + 2f_1 f_2 + r_2 f_2^{\,2}\right)}{k_{22}r_1 f_1 + k_{11}r_2 f_2} \cdot \left(1 - x\right)[R\cdot] \tag{6.12}$$

Here the conversion is also considered as a response. Because the overall conversion contains information from both monomers, the parameter estimates are highly correlated (Figure 6.31). Furthermore, because $r_1 > r_2$, the conversion is more sensitive to r_1 than r_2. The composition data as the second response can compensate for this defect to some extent (Figure 6.32). When the total polymerization rate increases, the sensitivity of conversion to the reactivity ratios also increases. Thus conversion data used to estimate reactivity ratios is usually in the medium to high range.

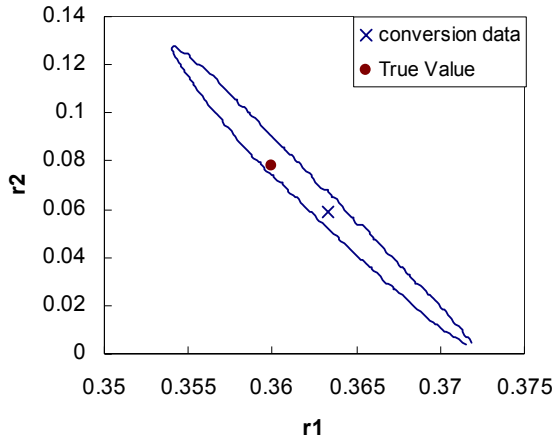

Figure 6.31 95% JCR of estimation with conversion data, f10=0.4,0.3

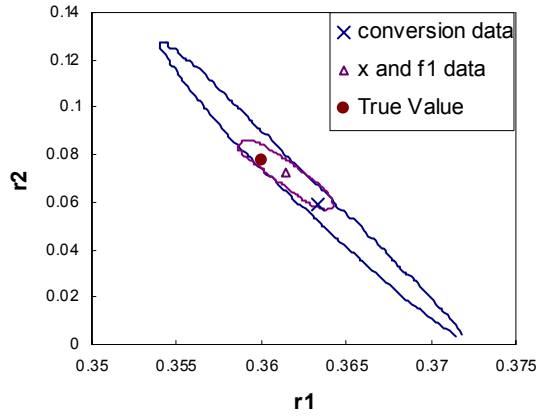

Figure 6.32 Comparison of 95% JCR of data set with monomer residual mole fraction as the second response

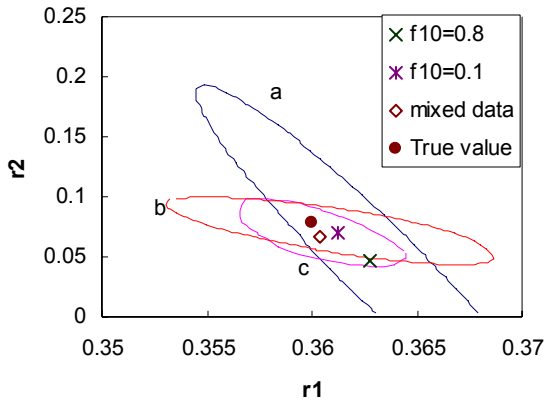

Figure 6.33 The effect of mixed data at different feed ratio. Contour a, f10=0.8; Contour b, f10=0.1; Contour c, combined data at f10=0.8 and f10=0.1

Because the reaction speed and monomer residual mole fraction varies with monomer feed ratio significantly, using the experimental data at different feed ratios can decrease the impact of the measurement error in the single feed ratio experimental data. In Figure 6.33, when using 9 data points at f_{10}=0.8 and f_{10}=0.1 respectively, the estimation is poor. But by picking 4 points from each data set and combining them together, the accuracy of the estimation is improved greatly.

According to a D-optimal design, f_{10}=0.4, time=300min and f_{10}=0.6 time=480min are the two best points. But at f_{10}=0.4 and time=300min, the instantaneous monomer fraction f_1 is lower than the measurement error, so it is not suitable for estimation. An alternative choice is choosing the points near the best point. Both of these two points are at high conversion where the reaction speed starts decreasing. Here the conversion data have larger influence on the estimation.

The next case shows the combination of three feed ratio data. It does not improve the estimation greatly (Figure 6.34 and 6.35)

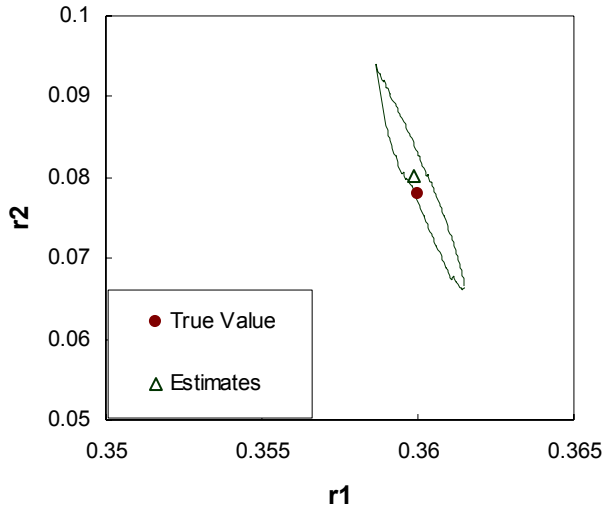

Figure 6.34 Combined data at f_{10}=0.4, 0.6

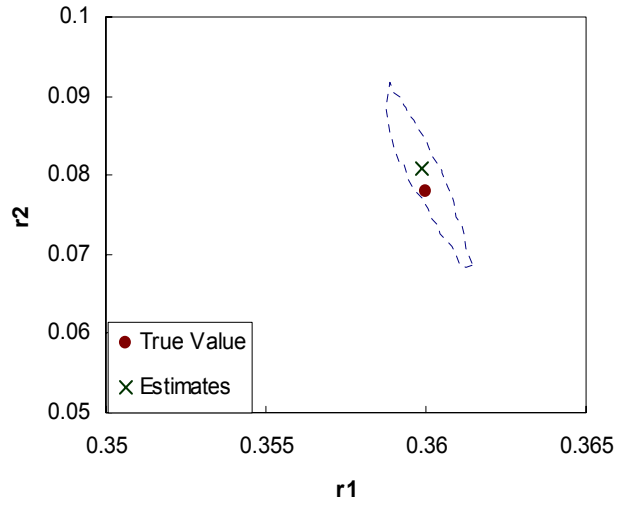

Figure 6.35 Combined data at three feed ratios. f_{10}=0.3, 0.4, 0.6

Remarks:

- Using time as the independent variable the experiments can be easily determined using the experimental design approach.
- Conversion data can be taken as a response to estimate the reactivity ratios, because it can supply sufficient information for reactivity ratio estimation and it can be obtained precisely. Composition data as a second response can reduce the high correlation of the parameters. In multiresponse estimation using conversion and composition data, conversion data dominates the estimation results. The improvement from composition data is very limited. But because the experimental point is usually located on mid high conversion, a suitable kinetics model describing high conversion behavior is very important.

6.3.3.2. Independent variables are time t and f_{10}; dependent variables are monomer residual quantity N1, N2

$$S(r) = \sum \left(\hat{N}_1 - N_1\right)^2 + \sum \left(\hat{N}_2 - N_2\right)^2 \tag{6.13}$$

$$\frac{dN_1}{dt} = -\frac{k_{11}k_{22}\left(r_1 N_1 + N_2\right)}{k_{22}r_1 N_1 + k_{11}r_2 N_2} \cdot N_1[R\cdot] \tag{6.14}$$

$$\frac{dN_2}{dt} = -\frac{k_{11}k_{22}\left(r_2 N_2 + N_1\right)}{k_{22}r_1 N_1 + k_{11}r_2 N_2} \cdot N_2[R\cdot] \tag{6.15}$$

The absolute quantities of monomers (Equation 6.13-6.15) are used as responses in this model. According to D-optimal design, for STY/AN system at 60°C, the optimal points are located on the monomer feed ratio 0.5 and time 300, 360 minutes corresponding conversion 60% and 77%. This mid-high conversion is where the quantity of monomer starts to change its reaction speed. In Figure 6.36, this design is compared to a design based on evenly distributed experimental data from low conversion (20minutes) to high conversion (420 minutes) at the same feed ratio. Although only three data points in optimal design are picked, the estimation result is similar to 9-points evenly distributed case (base case). The data at low conversion have little contribution for the estimation.

An improvement can be achieved by adding extra data at the different feed ratios. The following examples combine the data at feed ratio 0.5 and 0.3 or 0.5 and 0.6. The results

of two combinations are similar (Figure 6.37). Compared with Figure 6.36, the uncertainty of r_2 decreases, especially for data with feed ratio 0.3. Thus, the high acrylonitrile (monomer 2) concentration region contains more information on r_2. Overall, all of above cases for this model have high correlation between the parameters in the estimation.

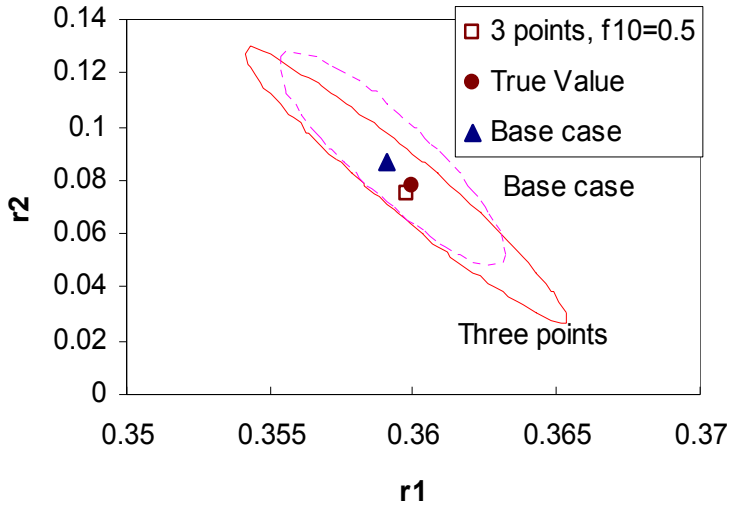

Figure 6.36 Comparison of 95% JCR contour, f10=0.5, 3 data points at information rich region. Base case, 9 points evenly distributed from 20min to 340 min.

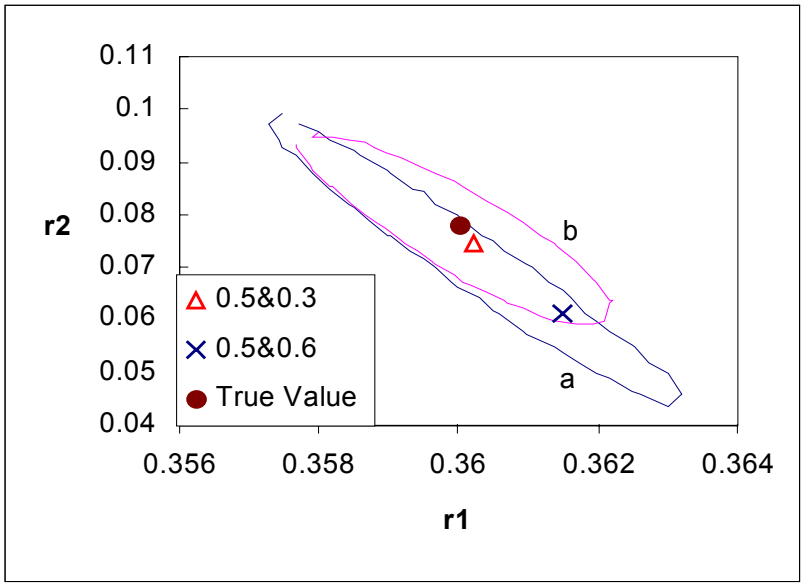

Figure 6.37 Comparison of combined data at different feed ratios. a) 95% JCR contour of mixed data at feed ratio 0.5 and 0.6; b) 95% JCR contour of combined data at feed ratio 0.5 and 0.3

6.3.4. Some discussions for Meyer-Lowry equation

6.3.4.1. Special region for Meyer-Lowry equation

Meyer-Lowry equation (Equation.2.27) is the analytical solution of Mayo-Lewis equation. Hautus et al. (1985) pointed out that when applying this model, there could be some problems. There exists singularity when $r_1 \rightarrow 1$ or $r_2 \rightarrow 1$. Hautus et al. (1985) gave some transformations to avoid the singular region for the analytical integrated equation. If both r_1 and r_2 approach to 1, other methods have to be used to avoid this situation.

Giz (1998) gave a transformation of the Meyer-Lowry equation to avoid the singularity as follows:

$$(1-x)^{(1-r_1)(1-r_2)} = Q^{(1-r_1)(1-r_2)} \qquad (6.16)$$

where Q in equation 6.16 is equal to the right side of equation 2.27. The modified model reduces the singularity point, and converges easier than the Meyer-Lowry equation. We checked Giz's data (1998) with Burke's method (1994) based on Meyer-Lowry equation. The results are listed in Table 6.12. It shows that the reactivity ratio estimates from

equation 6.16 highly depend on the initial guesses. This may be due to the modified equation becoming more nonlinear. Therefore it is difficult to converge to the global minimum point. Incidentally, from Table 6.12, the EKT method shows poor result when the reactivity ratios are close to 1.

The other two singularities at $r_1+r_2=2$ and at azeotropic point ($f1=\delta$) should also be paid more attention.

In addition to the above problem, the Meyer-Lowry equation may exhibit an unfeasible region for the independent variable. From a mathematical point, the base of exponent function must be positive, i.e., $(f_{1,0}-\delta)(f_1-\delta)>0$. But during the optimization process, the function may not always satisfy this condition, which causes numerical difficulties. Hautus et al. (1985) suggested a so-called "penalty value" to overcome the difficulties.

Table 6.12 Test of Giz's EVM. Comparison with Burke's M-L method

0.40%error forConversion,1.20% error for Composition

True value		EKT (initial guess)		EVM from Giz		Burke's M-L	
r1	r2	r1	r2	r1	r2	r1	r2
0.90	0.90	0.89	0.88	0.88	0.92	0.88	0.92
0.90	0.90	0.91	0.90	0.87	0.86	0.88	0.92
0.90	1.05	0.97	1.07	0.96	1.06	0.94	1.02
0.90	1.05	0.90	1.04	0.94	1.09	0.94	1.02

1.00% error for Conversion, 5.00% error for Composition.

True value		EKT (initial guess)		EVM from Giz		Burke's M-L	
r1	r2	r1		r1	r2	r1	r2
0.90	0.90	0.75	0.78	0.85	0.86	1.05	1.08
0.90	0.90	0.87	0.80	0.73	0.74	1.05	1.08
0.90	1.05	0.67	0.85	0.72	0.92	0.92	0.98
0.90	1.05	0.85	0.88	0.90	0.97	0.92	0.98

Compared with the analytical integrated model-Meyer-Lowry equation, the numerical integrated model is less constrained. Moreover, the numerical cumulative composition model Equation 2.31 still has one singularity at x=1. It is better to use data before the conversion reaches1. Giz (1998) has checked some special conditions in estimating the reactivity ratios using the Meyer-Lowry equation. Those conditions are either near the singularities of the Meyer-Lowry equation (ie. r_1-> 1 or r_2->1), or with extremely high composition drift. The simulated composition data were generated following Giz's rules (1998). They were obtained with initial monomer 1 fraction between 20% and 80%, and by numerically integrating Equation 2.8 up to a randomly selected conversion between 25%-50%. Random errors were added to the conversion and the copolymer composition data. The initial monomer composition is assumed to be error free. The simulated data with three levels of error, low, medium and high, are revisited here to evaluate the differential model. The initial guesses come from the EKT method and are given in Giz's article. The estimates are listed in Tables 6.13-6.15. At low and medium error levels (Tables 6.13-6.14), the point estimates from the two models are close to the true values. A better comparison can be made by comparing joint confidence regions at the high error level, as shown in Figure 6.38. The joint confidence regions (JCR) are centered at the point estimates from the differential model. The plots of JCR show that there is no significant difference between the true values and the point estimates from the differential model. The point estimates from the integrated model also have no significant difference with that from the differential model except in the case of Figure 6.38 d. In that plot, both reactivity ratios are greater than unity, and the point estimates from the integrated model are located on the edge of the 95% joint confidence region, which means the difference between two estimates may be significant. Comparing the distances between true values and point estimates, the differential model gives more accurate results. Furthermore, there are two additional findings. When the reactivity ratios are near unity, the differential model shows better point estimates than the analytical integrated model (Figure 6.38 a, b, c). When the true reactivity ratios are greatly different from each other, which implies large composition drift, the differential model does not give better estimates than the analytical integrated model (Figure 6.38 e).

Table 6.13 Comparison of the model estimates. 0.40% error added for Conversion, 1.20% error added for composition

True values		Initial guess		Differential composition model		Analytical integrated model	
r1	r2	r1	r2	r1	r2	r1	r2
0.90	0.50	0.93	0.54	0.90	0.50	0.98	0.53
0.90	0.90	0.89	0.88	0.87	0.89	0.94	0.93
0.90	1.05	0.97	1.07	0.89	1.04	0.93	1.07
10.00	5.00	3.37	1.61	10.84	5.39	10.53	5.24
10.00	0.05	9.93	0.07	10.01	0.04	10.17	0.05

Table 6.14 Comparison of the model estimates. 0.50% error added for Conversion, 2.00% error added for composition

True values		Initial guess		Differential composition model		Analytical integrated model	
r1	r2	r1	r2	r1	r2	r1	r2
0.90	0.50	0.97	0.50	0.87	0.49	0.88	0.49
0.90	0.90	0.88	0.91	0.90	0.87	0.94	0.90
0.90	1.05	0.86	1.00	0.88	1.04	0.87	1.04
10.00	5.00	3.09	0.80	10.50	5.31	9.40	4.75
10.00	0.05	9.93	0.07	11.24	0.06	11.12	0.06

Table 6.15 Comparison of the model estimates. 1.00% error added for Conversion, 5.00% error added for composition

True values		Initial guess		Differential composition model		Analytical integrated model	
r1	r2	r1	r2	r1	r2	r1	r2
0.90	0.50	0.90	0.52	1.05	0.59	0.94	0.55
0.90	0.90	0.75	0.78	0.84	0.83	1.01	0.93
0.90	1.05	0.67	0.85	0.90	1.04	0.94	1.07
10.00	5.00	3.37	1.61	8.27	4.27	14.19	7.12
10.00	0.05	9.93	0.07	9.39	0.03	9.26	0.03

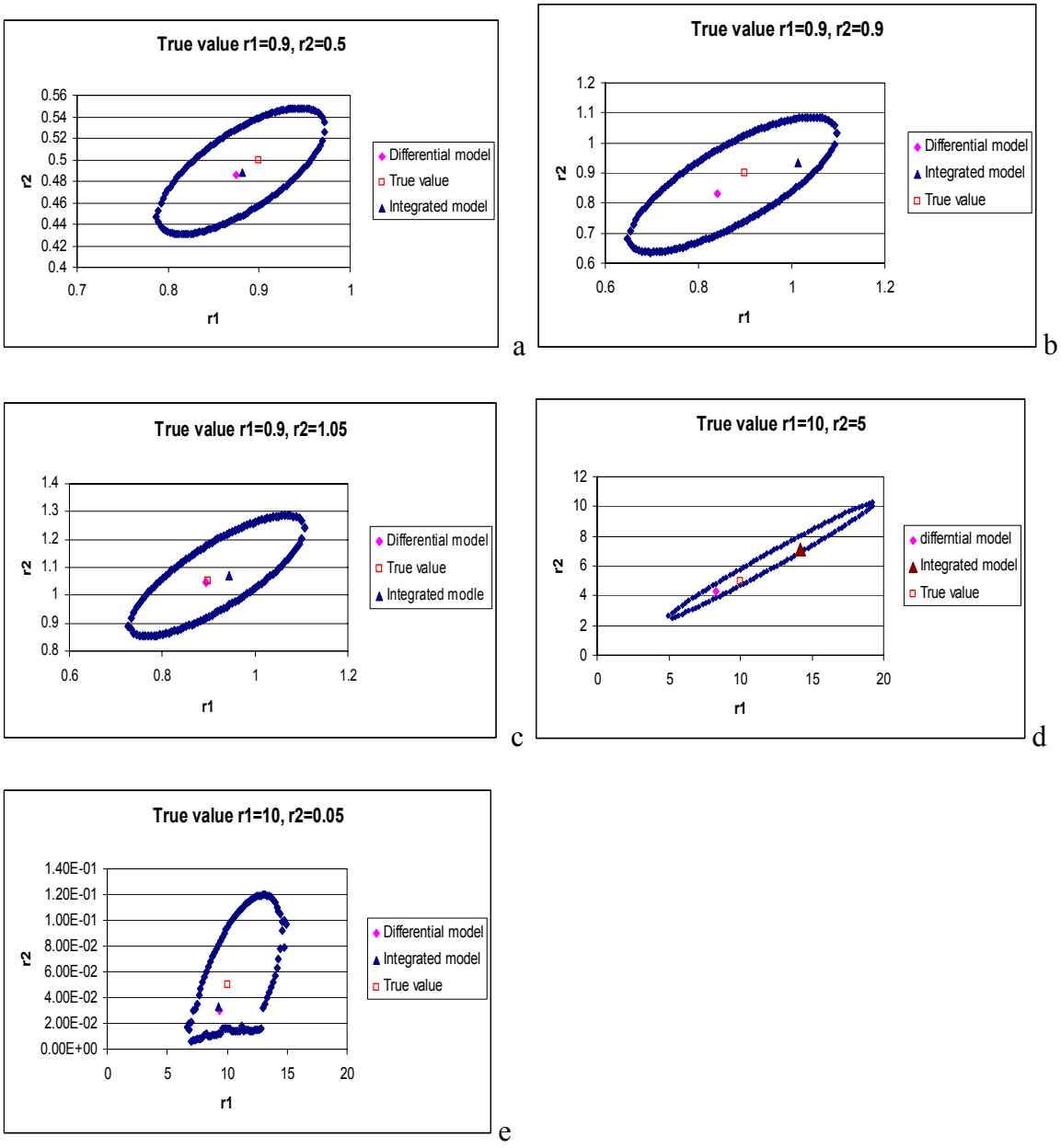

Figure 6.38 95% exact joint confidence region. The error for polymer composition is 5%

6.3.4.2. Performance of Meyer-Lowry equation at high conversion

The objective function is

$$SS = \sum \left[\overline{F}_1, i(calc) - \overline{F}_1, i(\exp) \right]^2 \qquad (6.17)$$

At high conversion, in the glass transition region, polymerization rate constant kp_{ij} decreases, which result in the reactivity ratios changing. There are four critical free volume mole fractions corresponding four kp_{ij} (i, j=1,2). When the free volume mole fraction reaches the largest of the four critical volume mole fractions, the reactivity ratios start to change. Then, when the free volume mole fraction reaches the minimum of the four critical free volume mole fractions, the reactivity ratios become constant again. Of course their values are different from those at low conversion. For the analytical cumulative model, i.e. the Meyer-Lowry equation, there exists an assumption that the reactivity ratios do not change. So before the glass transition region, it has the same estimation as model 1(numerical integrated composition model). After kp changes, the wrong assumption of constant reactivity ratios will affect on the estimation accuracy.

This case still uses the STY/AN system with combined data at feed ratio 0.8 and 0.1. The last conversion data at each feed ratio is close to 90%. The estimations from two methods are almost same (Figure 6.39). One reason is that the glass transition occurs at high conversion and it has small impact on the cumulative polymer composition. The other reason is for this STY/ AN system, when f_{10}=0.1, monomer 1 has consumed up at mid high conversion, and later the reactivity ratios do not affect the polymer composition. Therefore, the analytical Meyer-Lowry does not show an obvious difference. When the data at feed ratio 0.5 are selected instead of the data at f_{10}=0.1, for which the monomer has not been used up before glass transition, the uncertainty of the Meyer-Lowry equation increases (Figure 6.40).

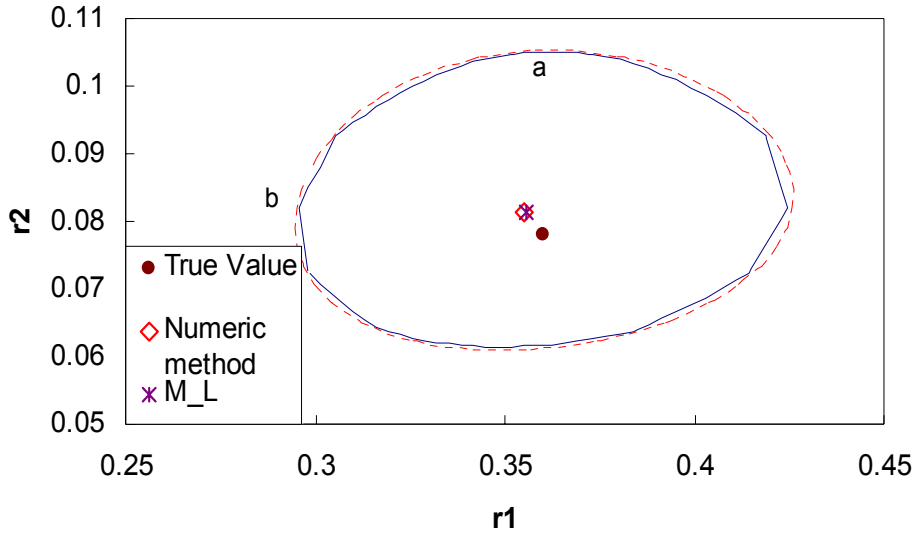

Figure 6.39 95% JCR of estimation from Meyer-Lowry equation and numerical method. Contour a is 95% JCR of numerical method; contour b is 95% JCR of Meyer-Lowry equation

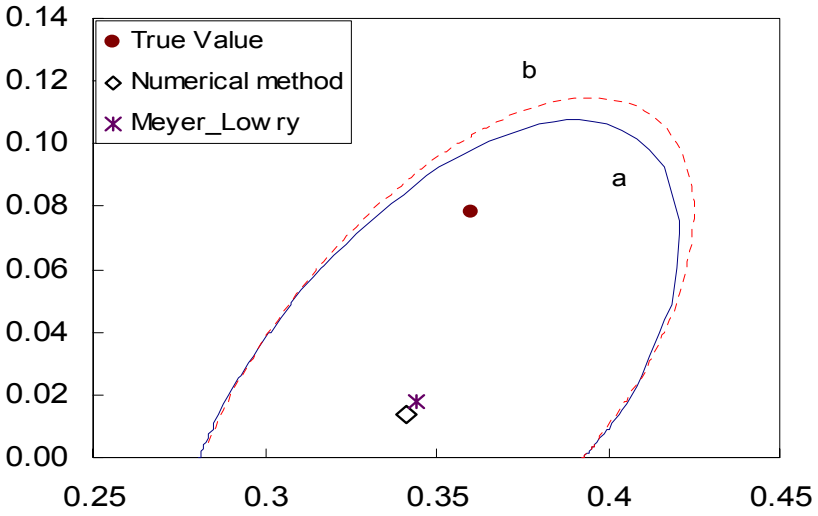

Figure 6.40 95% JCR of estimation from Meyer-Lowry equation and numerical method. Contour a is 95% JCR of numerical method; contour b is 95% JCR of Meyer-Lowry equation

Table 6.16 comparison of estimation between the Meyer-Lowry equation and the numerical integrated equation (Model 1), with no error data

	r_1	r_2	residual	
			r_1	r_2
Model #1	0.36795	0.07377	0.00795	-0.00423
Meyer_Lowry	0.38285	0.08130	0.02285	0.00330
True Value	0.36	0.078		

An extreme example is choosing all data at glass transition region without measurement error. The estimation of r_1 from Meyer-Lowry equation is not so good.

The above discussion shows that although the reactivity ratios change at glass transition region and decrease the estimation precision obtained with the Meyer-Lowry equation, the impact is small

6.3.5. Experimental data verification

6.3.5.1. MMA/VAc, BA/MMA (Dube and Penlidis, 1995)

To compare the estimates between the cumulative model and the instantaneous model at low conversion, the experimental data reported by Dube and Penlidis (1995) are used. The estimates from the differential model agree well with the reactivity ratios estimated by the integrated model. They are also close to the estimates made by RREVM (Table 6.17). The last column of Table 6.17 has estimates from Burke (1994) using the Meyer-Lowry equation. The agreement with the rest of the estimates is satisfactory. It can be seen from Figure 6.41, that the 95% joint confidence region (JCR) of the estimates obtained from the differential model includes that of RREVM; the point estimates from these two models almost overlap. That indicates that the estimates for BA/MMA at low conversion (<10%) from the differential model are acceptable. But for the BA/VAc and

MMA/VAc systems, the confidence regions of these two methods shown in Figures 6.42 and 6.43 do not overlap at all. Although the conversions are very low in these two systems (<5%), it is likely that the estimates from the differential model are more reliable at the high composition drift exhibited by these systems (Figure 6.44). Potential problems can arise in using the instantaneous model (such as RREVM) for systems with high composition drift.

Table 6.17 Experimental data from Dube and Penlidis (1995)

		RREVM (Dube et al.)	Integrated Eq (Dube et al.)	Differential Eq.	Burke's M-L*
BA/MMA	r1	0.2976	0.2936	0.2924	0.2926
	r2	1.7894	1.7773	1.7758	1.7776
BA/VAc	r1	5.9388	5.9582	5.9561	5.95643
	r2	0.02622	0.01443	0.0144	0.01437
MMA/VAc	r1	24.0254	26.1975	25.8235	25.8211
	r2	0.02611	0.01526	0.0158	0.01577

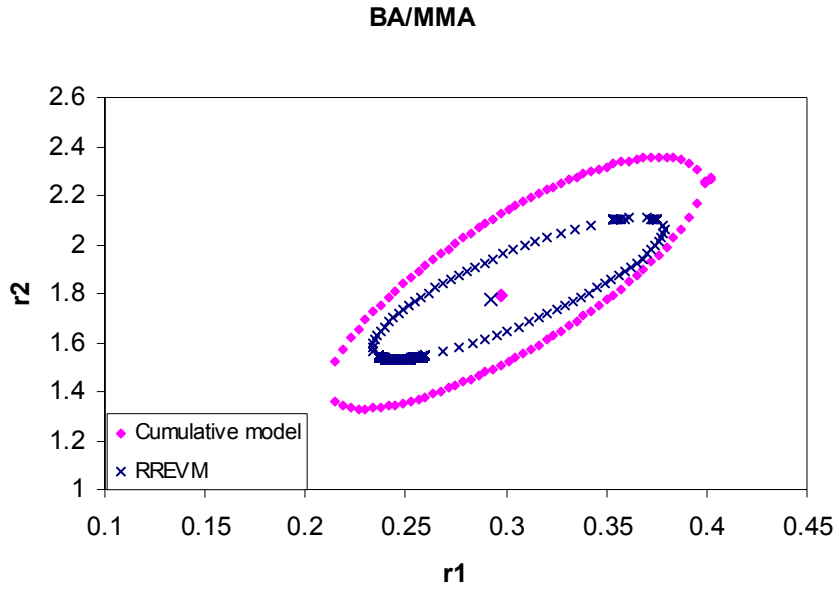

Figure 6.41 95% confidence region for BA/MMA system

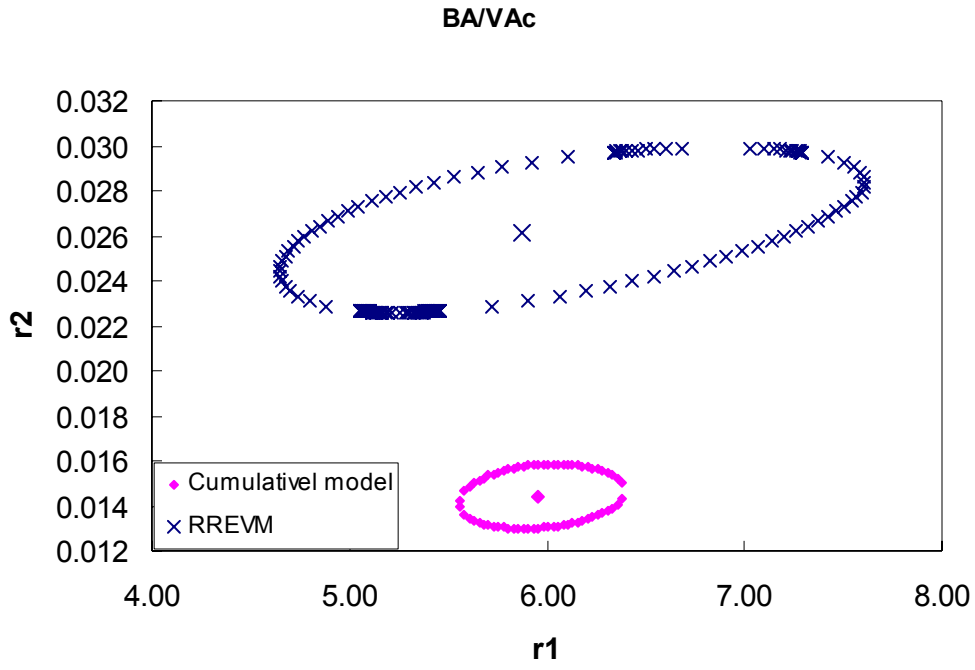

Figure 6.42 95% joint confidence region for BA/VAc

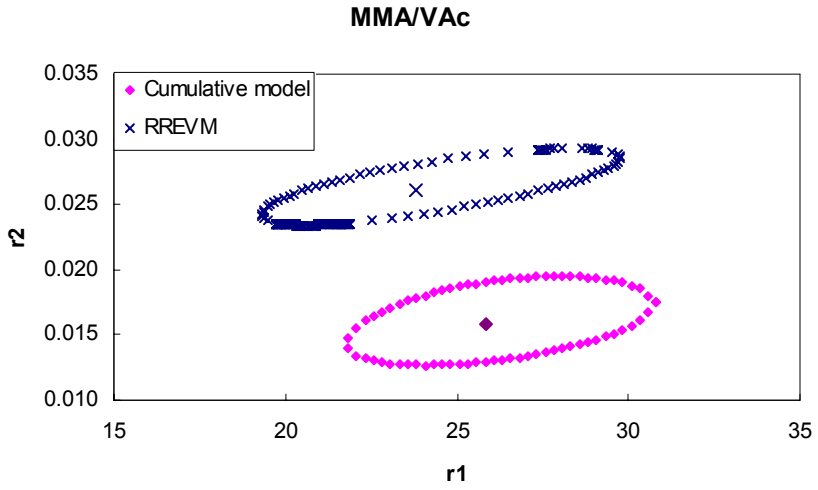

Figure 6.43 95% joint confidence region for MMA/VAc

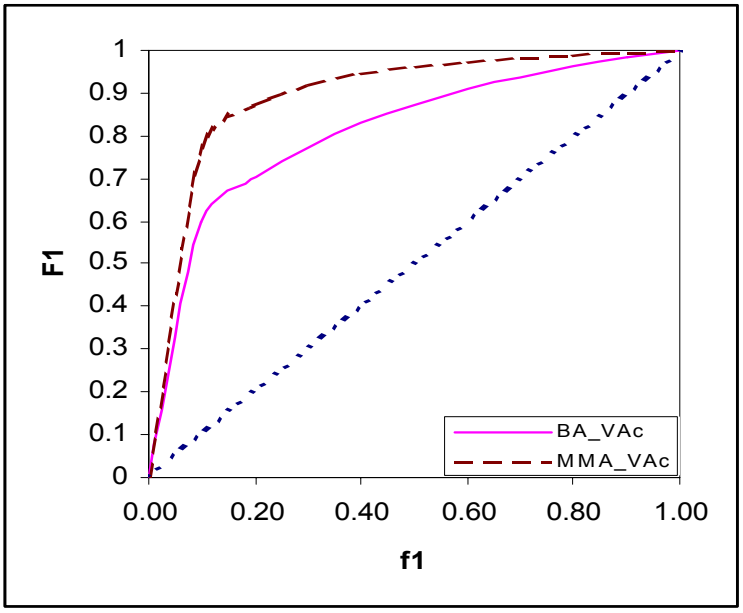

Figure 6.44 Composition curve of BA/VAc and MMA/VAc system

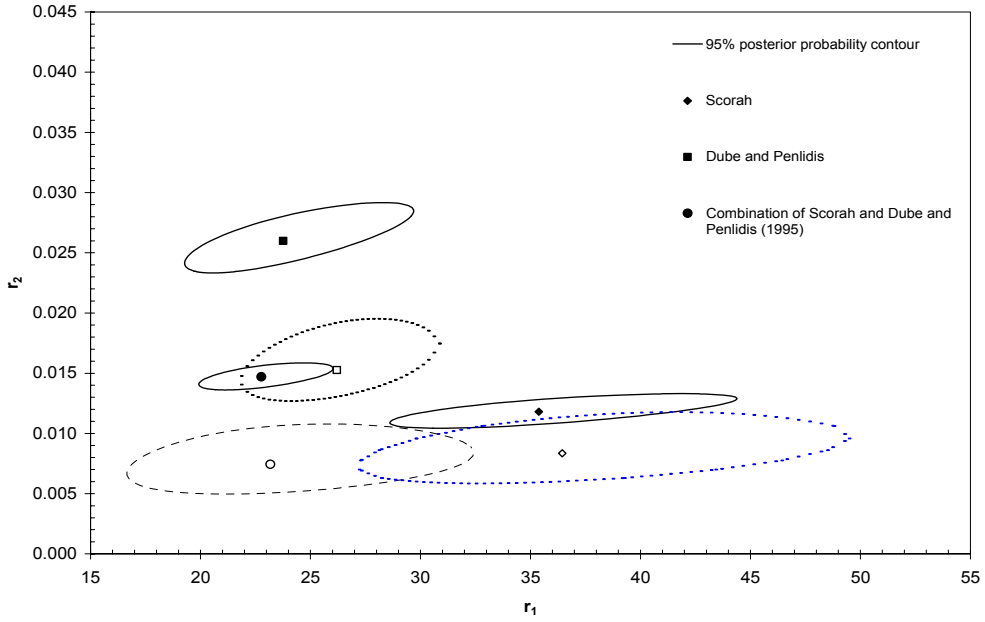

Figure 6.45 Comparison of estimation from Scorah et al. (2001) and Dube and Penlidis (1995). The solid line and symbol are obtained from instantaneous model. The dashed lines and the corresponding open symbols are obtained from cumulative model.

6.3.5.2. MMA/VAc

Dube and Penlidis (1995) did a series of experiments of MMA/VAc in bulk copolymerization at 60°C to estimate the reactivity ratios. The initiator was AIBN, and its concentration was 0.01 mol/L. The overall weight conversion was controlled about 3-4% or so. Monomer feed ratios were 0.0126 and 0.103. Each feed ratio had four replicated experiments, which gave eight experiment runs in total for estimation.

Scorah et al. (2001) did a series of experiments of MMA/VAc in bulk copolymerization at 60°C to estimate the reactivity ratios too. The initiator, AIBN, was adjusted to 0.05 mol/L. The overall weight conversion was controlled at 1%. Monomer feed ratios were 0.00758 and 0.0709. Each feed ratio had four replicated experiments. Totally eight experiment runs for estimation.

In the above experiments, conversion was determined gravimetrically and the copolymer composition was determined by H^1 NMR.

From Figure 6.45, even though the conversion is controlled at a very low level, the estimation from the instantaneous model has shown significant difference with that from the cumulative composition model. Using the cumulative composition model, the difference between the two sets of experimental data decreases. This also implies that the measurements from the two different sources still involve some potential differences.

6.4. Cumulative triad fractions

In the triad fraction model, the standard deviations of different triad sequences are similar. Therefore, the triad fraction variances/ covariances need not be considered in the design. So the design criterion can be approximated by:

$$\left|\mathbf{M}\right|^{-1} = \left|\sum_{i=1}^{r}\sum_{j=1}^{r}\mathbf{J}_i'\mathbf{J}_j\right| \qquad (6.18)$$

Because the expression of responses has no correlation between two reactivity ratios, i.e. the monomer-1-centered triad fraction has no relation with reactivity ratio of radical 2, Equation 6.18 can be simplified further as:

$$\left|\mathbf{M}\right|^{-1} = \left|\sum_{i=1}^{r}\sum_{j=1}^{r}\mathbf{J}_i'\mathbf{J}_j\right| = \left|\mathbf{G}_i'\mathbf{G}_j\right| \tag{6.19}$$

$$\mathbf{g}_i = \sum_{k=1}^{r}\mathbf{j}_{k,i} \tag{6.20}$$

where $\mathbf{j}_{k,i}$ is the derivative of k response to parameter θ_i. As before, the analysis of D-optimal design of triad fraction can be visualized as a univariate D-optimal design.

Cumulative triad fractions are similar with cumulative composition. They change greatly at different monomer feed ratio more than at different conversion. The support points are located on both sides of the azeotropic points at low conversion (<10%) when the composition drift is the largest. The best choice is to do the replicated experiments as well as the cumulative composition D-optimal design. If on line detection is available, the experimental data along the evolution of the reaction can be chosen to avoid new system error to be introduced into the replicated experiment. STY/AN is used as the case study for simulation. In order to compare with cumulative composition model, the true reactivity ratios are based on Garcia-Rubio's result (1985), r_1=0.36 and r_2=0.078. Their design points are similar to the ones obtained with the cumulative composition model. The estimates and 95% joint confidence contour at different error level are shown in Figure 6.46. The experimental data at different error level result in consistent estimation. Compare this Figure with 95% joint confidence region of cumulative composition model (Figure 6.11), the uncertainty of estimates at high error level of the cumulative triad fraction model is less than the uncertainty of estimate at medium error level of the cumulative composition model. The multiresponses of triad fraction contribute to the improvement of estimation. However, this improvement is not as large as the instantaneous triad fraction model vs. the instantaneous composition model. It also implies that the cumulative composition model estimates provides higher precision than the instantaneous composition model.

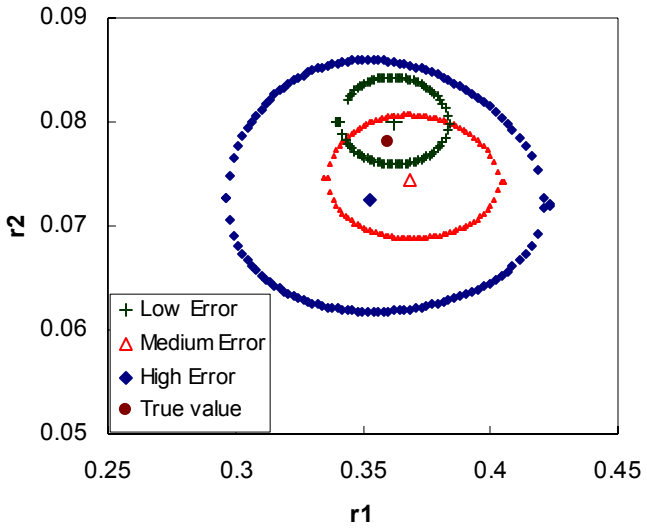

Figure 6.46 95% joint confidence region at different error level. True reactivity ratio is r_1=0.36, r_2=0.078 (Garcia-Rubio et al., 1985)

6.5. Instantaneous composition model for terpolymer

Although many researchers using the reactivity ratios obtained from the constituent copolymer in stead of the terpolymer system directly, it has been proved that estimating reactivity ratios from terpolymer directly is more accurate than from the corresponding copolymers. So here the instantaneous composition model for terpolymer is discussed for estimation. The reactivity ratio from copolymer can be used as prior knowledge for the experimental design for the terpolymer system.

The experimental design is a random design. Each set of data contains three independent observations over a random variable uniformly distributed in the range 0-1 and normalized by the sum of three observations.

The examples from Koenig (1980) are used to simulate the experimental data and the estimation (Table 6.18) indicating that the random experimental design is suitable here.

The Alfrey-Goldfinger equation describing the terpolymer system is much more complicated than Mayo-Lewis equation, so the Jacobian matrix is not easy to obtain. Duever et al. (1983) transferred the form of Alfrey-Goldfinger equation into

multiplicative form. It is relatively easy to obtain the Jacobian matrix and obtained estimation with EVM method. But for the purpose of NLLS use, the error structure changes and it is not easy to evaluate the error.

Here to improve the precision, two methods are used for estimation. One is using the every two polymer composition ratio as responses and the analytical Jacobian matrix. The other is to use each polymer composition as a response and a finite difference approximate the Jacobian matrix. The estimation results of these two methods based on the case of Duever et al. (1983) are listed in Table 6.20 and 6.21.

Table 6.18 The estimates of Koenig's data

	Koenig's work (1980)	This work
r12	0.50±0.02	0.4981
r13	0.41±0.08	0.3013
r21	0.50±0.02	0.5077
r23	1.20±0.14	1.0393
r31	0.04±0.04	0.0561
r32	0.15±0.07	0.1988

Table 6.19 Point estimation comparison

	True value used in Duever et al. (1983)	No error	Low error	Medium error
r12	0.6965	0.7017	0.7265	1.0107
r13	0.1093	0.1095	0.1065	0.1478
r21	0.1359	0.1378	0.1522	0.2425
r23	0.35	0.3565	0.5913	0.2009
r31	0.3135	0.3136	0.3148	0.3212
r32	1.31	1.3052	1.3208	1.3211

Table 6.20 Terpolymer reactivity ratio estimation with response of composition ratio

	True value	Objective function		
		$(y-F1/F3)^2+(y-F2/F3)^2$	$(y-F2/F1)^2+(y-F3/F1)^2$	$(y-F1/F2)^2+(y-F3/F2)^2$
r12	0.6965	0.5268	0.7569	-
r13	0.1093	0.1340	0.1647	-
r21	0.1359	0.1024	0.1794	-
r23	0.35	0.1463	0.1367	-
r31	0.3135	0.3389	0.3357	-
r32	1.31	1.8602	1.4085	-

*In the last column, the estimation did not converge.

Table 6.21 Terpolymer reactivity ratio estimation with the response of polymer composition

	True value	Objective function		
		$(y-F1)^2+(y-F2)^2$	$(y-F2)^2+(y-F3)^2$	$(y-F1)^2+(y-F3)^2$
r12	0.6965	0.771	0.7467	0.6664
r13	0.1093	0.1608	0.1556	0.1547
r21	0.1359	0.1878	0.2303	0.1328
r23	0.35	0.1862	0.2058	0.1244
r31	0.3135	0.3377	0.3373	0.3361
r32	1.31	1.3939	1.5282	1.5184

From the above two tables, it is obviously that when using the composition ratio, the estimation is sensitive to which composition as denominator of the ratio, while the composition as response, the model is symmetric. Any two of three polymer compositions can provide similar precise estimation.

Because the summary of three components equals unit, which means those compositions are linear dependent, how to choose the response will affect the accuracy of the estimation. The following discussion focuses on the effect of different methods to avoid the linear dependence problem. One is to obtain the each composition independently; the other is just to choose two of three compositions.

The true reactivity ratios for simulation are chosen from Duever et al. (1983), Koenig's book (1980) and Dube and Penlidis (1995) respectively. All of estimation results show that at each error level, estimation from three independent measurements is better than that from two of three measurements of polymer composition.

Those estimates also indicate that if the reactivity ratios of a pair of monomer are very different, the estimation of those reactivity ratios is lacking.

In Duever's case, the difference between r_{23} and r_{32} are a bit large. When the error level increases, the estimation of r_{23} becomes worse than others (Table 6.22-6.23). In Koenig's case (Table 6.24), r_{13} and r_{31}, r_{23} and r_{32} have great difference. When the error level increases the estimation r_{31} and r_{32} become worse. In the Dube's case (Table 6.25-6.26), this becomes very inaccurate. r_{23} and r_{32} are different with 3 orders. Even at low error level, r_{32} is estimated one order's larger than its true value. At medium error level, the estimate of r_{23} is also unreasonable. At high error level, the estimation does not converge.

This is not a surprising phenomenon. If the two reactivity ratios of a pair of monomers are different greatly, there must be one monomer that has low probability to be converted into the polymer and not easy to obtain the accurate measurement.

Under this condition, random experiment design cannot give the precise estimation because each component does not contain the same information for reactivity ratio. Here D-optimal design is used to get six experiment points, and then do replicate experiment at

each point. There are a total twelve experiment points. The design points are listed in Table 6.27. Reasonable estimation is obtained from low error level to high error level.

Table 6.22 The estimation of reactivity ratios using the simulated data with different error level and three component compositions (F1, F2, F3). True reactivity ratios are from Duever et al. (1983)

	True Value	No error	Low error	Medium error	High error
r12	0.6965	0.6967	0.7372	0.7684	0.6316
r13	0.1093	0.1093	0.1110	0.1178	0.1066
r21	0.1359	0.1359	0.1421	0.1320	0.1458
r23	0.3500	0.3501	0.3836	0.4250	0.5010
r31	0.3135	0.3135	0.3240	0.3205	0.3323
r32	1.3100	1.3094	1.3000	1.3370	1.6527

Table 6.23 The estimation of reactivity ratios using the simulated data with different error level and two component compositions (F1, F2). True reactivity ratios are from Duever et al. (1983)

	True Value	No error	Low error	Medium error	High error
r12	0.6965	0.6967	0.7561	0.7763	0.6555
r13	0.1093	0.1093	0.1076	0.1147	0.1166
r21	0.1359	0.1359	0.1436	0.1359	0.1558
r23	0.3500	0.3501	0.3822	0.4742	0.5384
r31	0.3135	0.3135	0.3241	0.3416	0.3570
r32	1.3100	1.3094	1.2751	1.4324	1.9164

Table 6.24 The estimation of the simulated data with different error level and three component compositions (F1, F2, F3). True reactivity ratios are from Koenig's book (1980)

	True Value	No error	Low error	Medium error	High error
r12	0.5	0.4998	0.5022	0.4788	0.4879
r13	0.41	0.4100	0.4220	0.3754	0.3621
r21	0.5	0.4997	0.4943	0.4471	0.4194
r23	1.2	1.1998	1.1537	1.1441	1.3904
r31	0.04	0.0400	0.0457	0.0491	0.0620
r32	0.15	0.1501	0.1690	0.1660	0.1852

Table 6.25 The estimation of the simulated data with different error level and three component compositions (F1, F2, F3). True reactivity ratios are BA/MMA/VAc system (Dube and Penlidis, 1995)

	True Value	No error	Low error	Medium error
r12	0.298	0.2981	0.2986	0.2752
r13	5.939	5.9265	6.7811	6.3973
r21	1.789	1.7895	1.8039	1.7548
r23	24.025	23.9411	26.9046	43.8529
r31	0.0262	0.0222	0.3693	0.4157
r32	0.0261	0.022	0.3129	0.7817

Table 6.26 The estimation of the simulated data with different error level and two component compositions (F1, F2). True reactivity ratios are BA/MMA/VAc system (Dube and Penlidis, 1995)

	True Value	No error	Low error	Medium error
r12	0.298	0.2981	0.2978	0.2869
r13	5.939	5.9265	5.7096	9.4004
r21	1.789	1.7895	1.8058	1.7758
r23	24.025	23.9411	27.4153	111.6173
r31	0.0262	0.0222	0.3232	2.1709
r32	0.0261	0.022	0.2720	5.2250

Table 6.27 Design point for BA/MMA/VAc system (Dube and Penlidis, 1995)

f1	f2	f3
0.0129	0.0769	0.9102
0.0129	0.0129	0.9742
0.2882	0.0129	0.6989
0.0200	0.0200	0.9600
0.2882	0.0769	0.6349
0.3000	0.1000	0.6000

Table 6.28 The estimation of the simulated data with different error level and three component compositions (F1, F2, F3). True reactivity ratios are from Dube and Penlidis (1995)

	True Value	Low error	Medium error	High error
r12	0.298	0.2814	0.3029	0.2956
r13	5.939	5.8798	6.0618	5.6159
r21	1.789	1.7035	1.7901	1.8725
r23	24.025	24.3838	23.2441	21.8634
r31	0.0262	0.0263	0.0243	0.0214
r32	0.0261	0.0263	0.0245	0.0218

From the above discussion, some conclusions are obtained. Firstly, a good experimental design is the premise to get precise estimation, especially for those systems with reactivity ratios having large difference. Secondly, measuring all the component compositions independently is better than using two of three compositions to overcome the colinearity problem. Some problems occurring during the estimation of copolymer also exist in the estimation of terpolymer. The instantaneous terpolymer model is also only suitable for small composition drift system. Visualized composition drift of terpolymer will be discussed in a section dealing with azeotropic points for these systems.

6.6. Instantaneous composition model for multicomponent systems

Walling-Briggs (1945) gave the generic formula describing a multicomponent polymerization using determinants. It was used to calculate the composition from a list of reactivity ratios. Because of its complexity, it is not widely used. Hocking and Klimchuk (1996) rewrote the composition equation trying to obtain a simpler form. For terpolymer, their transformed equation is similar to the Alfrey-Goldfinger equation, which can be regarded as a special instance of Walling-Briggs equation. But for tetrapolymer, the composition prediction result is not as stable as that of Walling-Briggs equation. The comparison is shown in the Tables 6.29 and 6.30. All reactivity ratios and experimental data are from Hocking and Klimchuk (1996). Obviously the predictions of Walling-Briggs equation are closer to the experimental results. Hence, although the Walling-

Briggs equation is very complicated, because of its symmetry, it can give reliable predictions for multicomponent systems. So in this work, the Walling-Briggs equation is used to estimate reactivity ratios directly.

Table 6.29 Example from Hocking and Klimchuk (1996). Prediction of polymer composition compared with experimental results

Monomer		Monomer feed fraction	Polymer composition		
			Experiment	Hocking and Klimchuk(1996)	This work
1	Acrylonitrile	0.30	0.3090	0.3878	0.3080
2	Butyl acrylate	0.30	0.2186	0.1283	0.1897
3	Vinylidene dichloride	0.30	0.1231	0.1352	0.1302
4	Styrene	0.10	0.3491	0.3487	0.3721
1	Acrylonitrile	0.40	0.3832	0.4534	0.3615
2	Butyl acrylate	0.30	0.2083	0.1113	0.1728
3	Vinylidene dichloride	0.20	0.0708	0.0855	0.0806
4	Styrene	0.10	0.3377	0.3498	0.3851

Table 6.30 Reactivity ratios of the tetrapolymer system of Table 6.29

r_{ij}	M1	M2	M3	M4
M1		1.003	0.91	0.04
M2	1.005		0.83	0.15
M3	0.37	0.85		0.14
M4	0.41	0.76	2.00	

The rules of estimation with the terpolymer equation can also be extended to the Walling-Briggs equation. This generic model can be reduced to a terpolymer and copolymer system. The following case estimates reactivity ratios for a terpolymer system using the Walling-Briggs equation.

The estimation example uses simulated data with a random experimental design. The measurement error levels are according to Burke's thesis (1994). Compared with the true values (see Table 6.31), the estimation at different error levels is acceptable. And it gives the same results as the Alfrey-Goldfinger equation.

Table 6.31 The estimation of reactivity ratios using simulated data with different error level and three component compositions (F1, F2, F3). True reactivity ratios are from Duever et al. (1983)

	True Value	No error	Low error	Medium error	High error
r12	0.6965	0.6967	0.7372	0.7684	0.6316
r13	0.1093	0.1093	0.1110	0.1178	0.1066
r21	0.1359	0.1359	0.1421	0.1320	0.1458
r23	0.3500	0.3501	0.3836	0.4250	0.5010
r31	0.3135	0.3135	0.3240	0.3205	0.3323
r32	1.3100	1.3094	1.3000	1.3370	1.6527

6.7. Azeotropic point investigation

Definition of azeotropic point comes from the copolymer composition plot, where the monomer unit fraction in the copolymer equals the monomer feed fraction. It is used to classify the different trends of copolymer composition versus conversion at the two sides of the azeotropic point. This is important for the design of a copolymerization process.

6.7.1. Copolymer system

Azeotropic point exists in a system when $r_1<1$ and $r_2<1$. When $r_1>1$ and $r_2>1$, the system also has a mathematical azeotropic point, however the system has not been observed in practice as yet. Therefore our discussion focuses on the system with $r_1<1$ and $r_2<1$. In such a system, the azeotropic point is not a stable point. Small monomer concentration fluctuations will cause the operating point to move away from the azeotrope.

6.7.1.1. Analytical solution

The analytical solution for azeotropic point of a copolymer system is easy to obtain:

$$F_1 = f_1 = \frac{1-r_2}{2-r_1-r_2} \tag{6.21}$$

There also exist two trivial solutions for $f_1=0$ and 1. If the monomer feed fraction is located between the azeotropic point and 1, the copolymer composition fraction will tend to 1 with increase in conversion, whereas if the monomer feed fraction is located between the azeotropic point and 0, the copolymer composition fraction will tend to 0 with increase of conversion.

6.7.1.2. Numerical solution

The objective is seeking a zero point for the following:

$$\varphi(f_1) = F_1 - f_1 = \frac{(r_1-1)f_1^{\,2} + f_1}{(r_1+r_2-2)f_1^{\,2} + 2(1-r_2)f_1 + r_2} - f_1 \tag{6.22}$$

This can be transformed to:

$$\varphi(f_1) = (1-f_1)f_1\left(-(r_1+r_2-2)f_1 + r_2 - 1\right) \tag{6.23}$$

Table 6.32 shows solutions for the azeotropic point of three different copolymer systems. The results from the numerical method agree well with the analytical results, no matter what the reactivity ratio values are.

Table 6.32 Azeotropic point for copolymer

Reactivity ratio		Azeotropic point (f_1)	
r_1	r_2	Analytical	Numerical
0.5	0.41	0.5412844	0.5412844
0.9	0.03	0.9065421	0.9065420
1.5	50	0.9898990	0.9898990

6.7.2. Terpolymer system

6.7.2.1. Analytical solution

The composition equation is described by the Alfrey-Goldfinger equation. It is more complicated than the copolymer composition equation and its analytical solution is not easy to obtain. However, it is still meaningful to try because it can be used to evaluate the numerical results. Here we resort to MAPLE to obtain the analytical solution (see Appendix). There are seven roots. One is the true solution of azeotropic point, in which none of the monomer fractions is zero. The other six roots are trivial solutions. Among these solutions, three are the azeotropic points of the constituent copolymer systems and the other three correspond to the homopolymers. This indicates that if all the constituent copolymers of the terpolymer have azeotropic points, then the terpolymerization may have an azeotropic point.

6.7.2.2. Numerical solution

Alfrey-Goldfinger equation is rewritten as Equation 6.24. This equation with the constraint equation $f_1+f_2+f_3=1$ is used to obtain the azeotropic point.

$$\begin{aligned}&\left(f_1 r_{32} r_{23} + f_2 r_{31} r_{23} + f_3 r_{32} r_{21}\right)\left(f_1 r_{13} r_{12} + f_2 r_{13} + f_3 r_{12}\right)\\&= \left(f_1 r_{32} r_{13} + f_2 r_{31} r_{13} + f_3 r_{12} r_{31}\right)\left(f_1 r_{23} + f_2 r_{23} r_{21} + f_3 r_{21}\right)\\&= \left(f_1 r_{12} r_{23} + f_2 r_{13} r_{21} + f_3 r_{12} r_{21}\right)\left(f_1 r_{32} + f_2 r_{31} + f_3 r_{32} r_{31}\right)\end{aligned} \tag{6.24}$$

Several cases are used to check the azeotropic point (see Table 6.33). All reactivity ratios are less than 1 in "General" system 1 (Duever et al., 1983) and greater than 1 in "General" system 2. Both of these two systems have azeotropic points. Some of the constituent copolymers in STY/MMA/AN system (Koenig, 1980) and BA/MMA/VAc (Dube and Penlidis, 1995) have no azeotropic point. Neither do these two terpolymer systems have an azeotropic point. The non-zero solution is not valid because the mole fraction should be between 0-1.The corresponding composition plots (Figures 6.47 and 6.48) clearly show each composition of terpolymer at different feed monomer fraction. Because polymer composition is not determined by one monomer fraction, at each monomer fraction the corresponding polymer composition varies over a range. In the STY/MMA/AN system, although there is no azeotropic point, each component has the region where $f_i=F_i$ (i= 1, 2 or 3) for some monomer fraction. In BA/MMA/VAc system, only component BA contains the region where $f_1=F_1$, so it is impossible for the whole system to have an azeotropic point.

Table 6.33 Case study of azeotropic point for terpolymerization

	analytical solution	numerical solution	result
General 1(Duever, 1983) r12=0.6965 r13=0.1093 r21=0.1359 r23=0.35 r31=0.3135 r32=0.31	f1 = 0.4220, f2 = 0.0321, f3 = 0.5458	f1 = 0.4220, f2 = 0.0321, f3 = 0.5458	F1 = 0.4221, F2 = 0.0321, F3 = 0.5458
General 2 r12= 1.5 r13=1.41 r21=1.5 r23=1.2 r31=1.04 r32=1.15	f1 = 0.2268, f2 = 0.3588, f3 = 0.4143	f1 = 0.2268, f2 = 0.3588, f3 = 0.4143	F1 = 0.2268, F2 = 0.3588, F3 = 0.4143
STY=1 MMA=2 AN=3 r12=0.52 r21=0.47 r13=0.31 r31=0.04 r23=1.45 r32=0.17	f1=0.022660, f2=1.856990, f3=-0.879650;	f1=0.0227, f2=1.8570, f3=-0.8797;	No azeotropic point
BA=1 MMA=2 VAC=3 r12=0.298 r21=1.789 r13=5.939 r31=0.0262 r23=24.025 r32=0.0261	f1=0.033678, f2=-0.061641, f3=1.027962;	f1 = 0.033678, f2 = -0.061641, f3 = 1.027962;	No azeotropic point

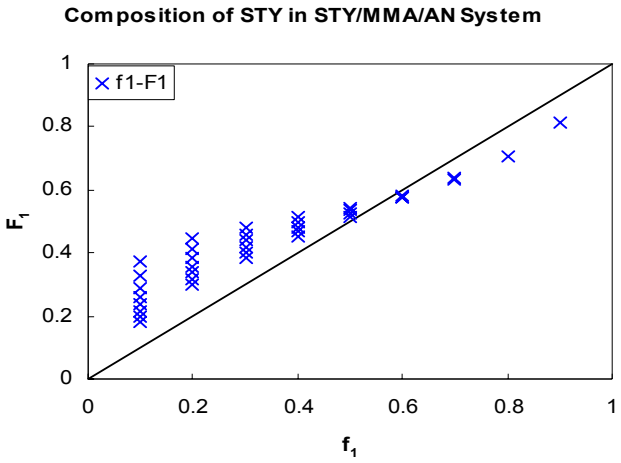

a)

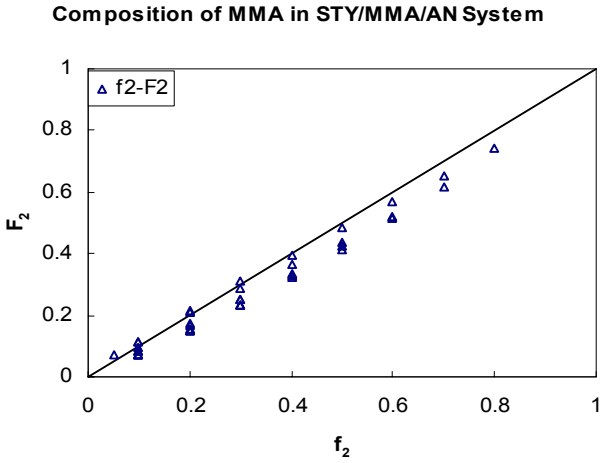

b)

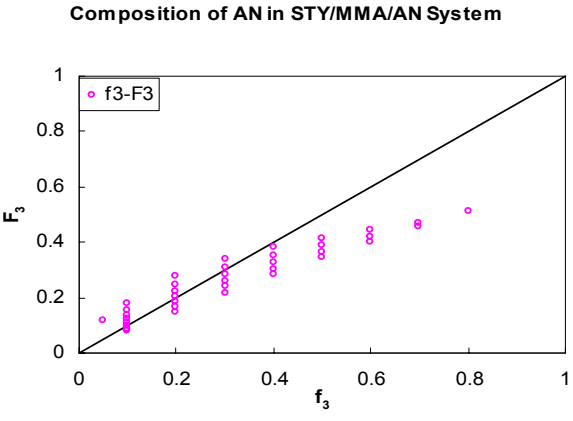

c)

Figure 6.47 Composition change with monomer feed fraction for each component of STY/MMA/AN system

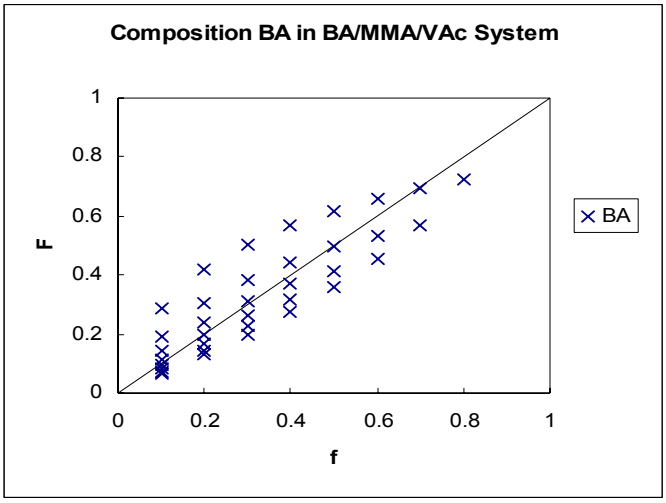

a)

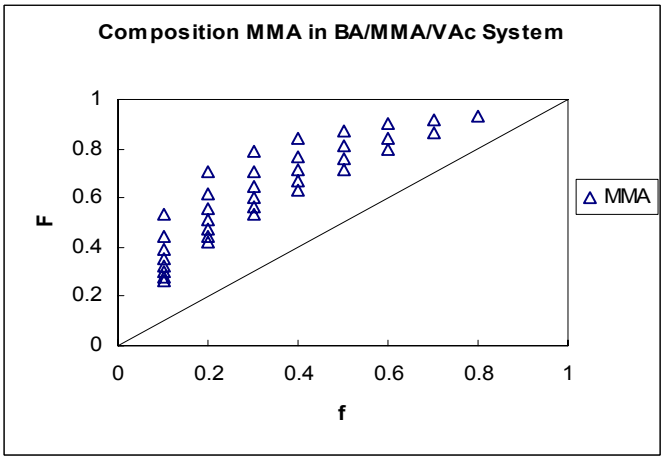

b)

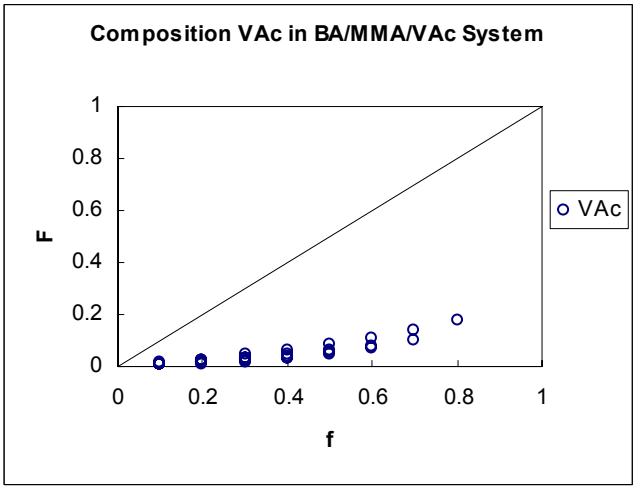

c)

Figure 6.48 Composition change with monomer feed fraction for each component of BA/MMA/VAc system

6.7.2.3. Graphical solution

The copolymer composition curve shows how the instantaneous copolymer composition varies with monomer fraction. It visualizes the composition drift and the effect of the azeotropic point on the system. For a terpolymer the phase plot is used to visualize the instantaneous composition change in terpolymerization. In the phase plot of "General 1" system (see Figure 6.49), the solid curves are the paths where $f_i=F_i$ (i=1,2 or 3). For example, along the path AE and BF, $f_2=F_2$; along the path CDB, $f_1=F_1$; along the path ADC, $f_3=F_3$. The dot lines are the corresponding polymer composition. The composition drift is shown between the solid curve and its corresponding dot curve. The crossing point of two paths is the azeotropic point of this system. A, B and C are three crossing points on the border of the plot. They correspond to the three trivial analytical solutions, which are the azeotropic points of the constituent copolymers. Obviously the only inner crossing point D is the true azeotropic point of this system. This agrees well with the analytical solution.

The graphical solution can supply additional information as follows. All the operating points on the paths will move in the opposite direction of composition drift which is parallel to either of the component axes (see the arrows on the paths, Figure 6.49). In fact the paths built up the direction field of the system (see Figure 6.49). According to the plot, the azeotropic point D is not a stable point. Any deviation of monomer fraction will cause the operating point to move away from this point. This property is similar to the azeotropic point in copolymer systems. Also, the plot is separated into three parts by the paths. On the left side of path AC, the operating point will move towards f_3=1. On the right side of path CB, the operating point will move towards f_1=1. In the region between AC and CB, the operating point will move towards f_2=1. The azeotropic points C and D are very close, which makes the composition drift in the circle region (Figure 6.49) very small. That makes difficult to determine the azeotropic point accurately by experiment.

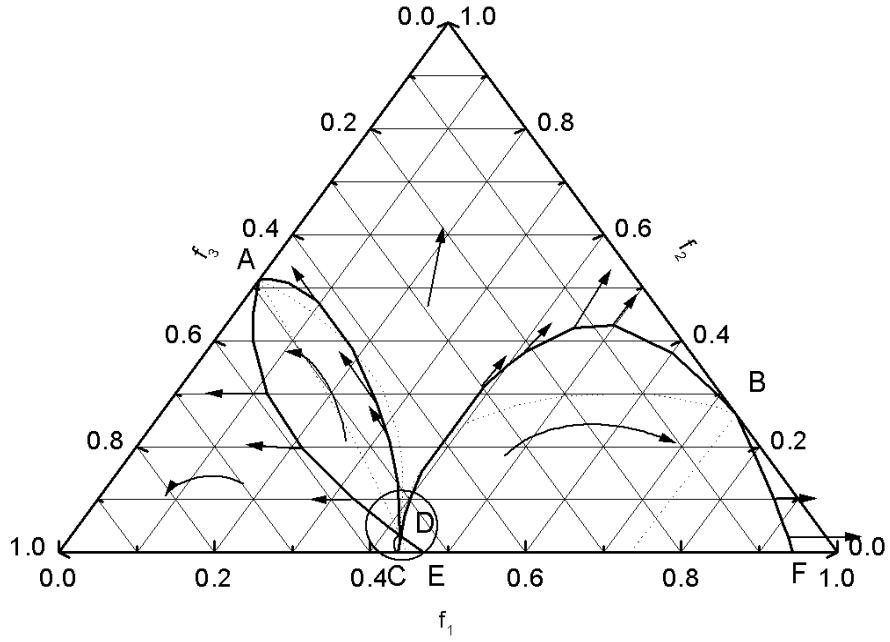

Figure 6.49 General system 1 with azeotropic point. On the path CB, $f_1=F_1$; on the path AE and BF, $f_2=F_2$; on the path AC, $f_3=F_3$. The dot lines are corresponding polymer composition curve.

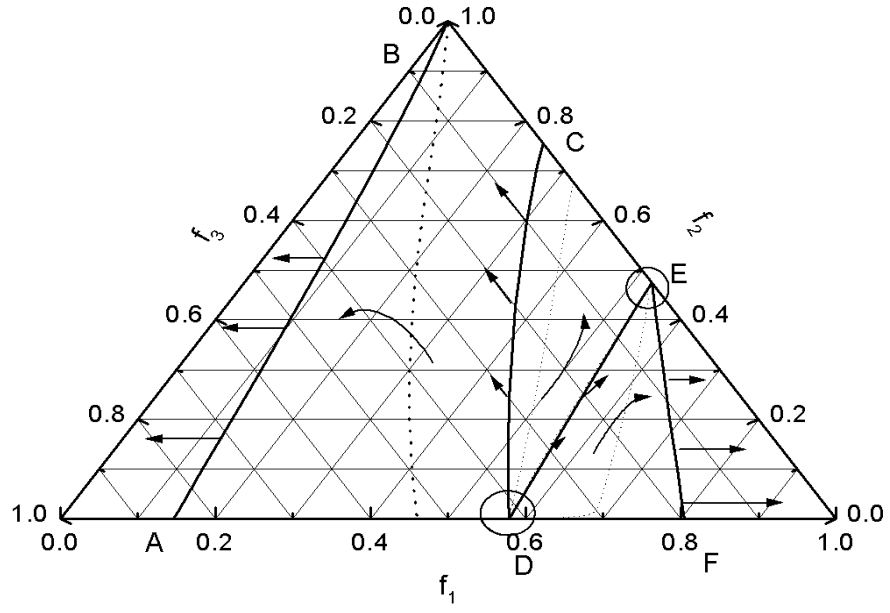

Figure 6.50 Phase plot for STY/MMA/AN system On the path DE, $f_1=F_1$; on the path AB and EF, $f_2=F_2$; on the path CD, $f_3=F_3$

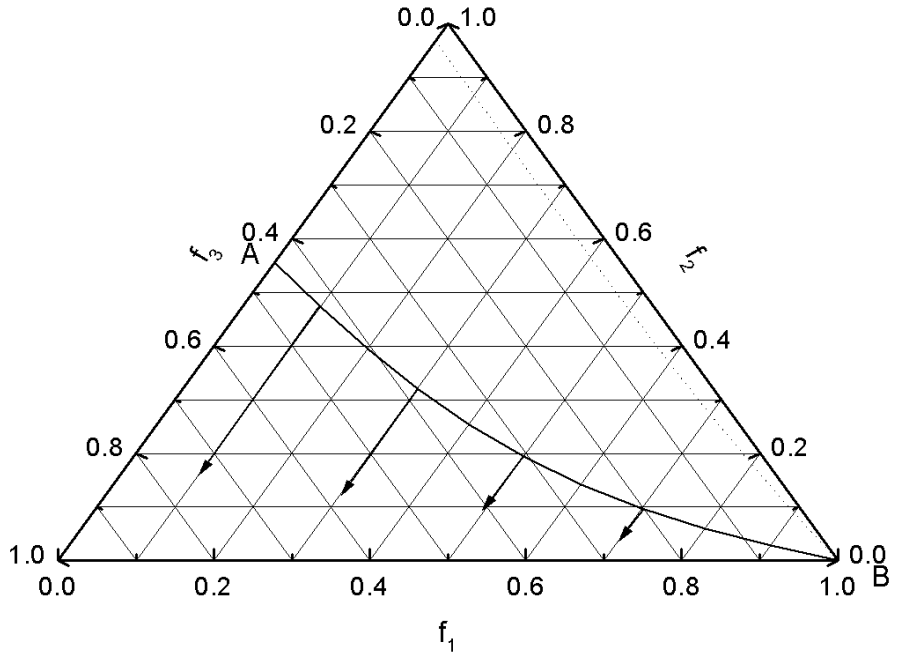

Figure 6.51 Phase plot BA/MMA/VAc. On the path AB, $f_1=F_1$.

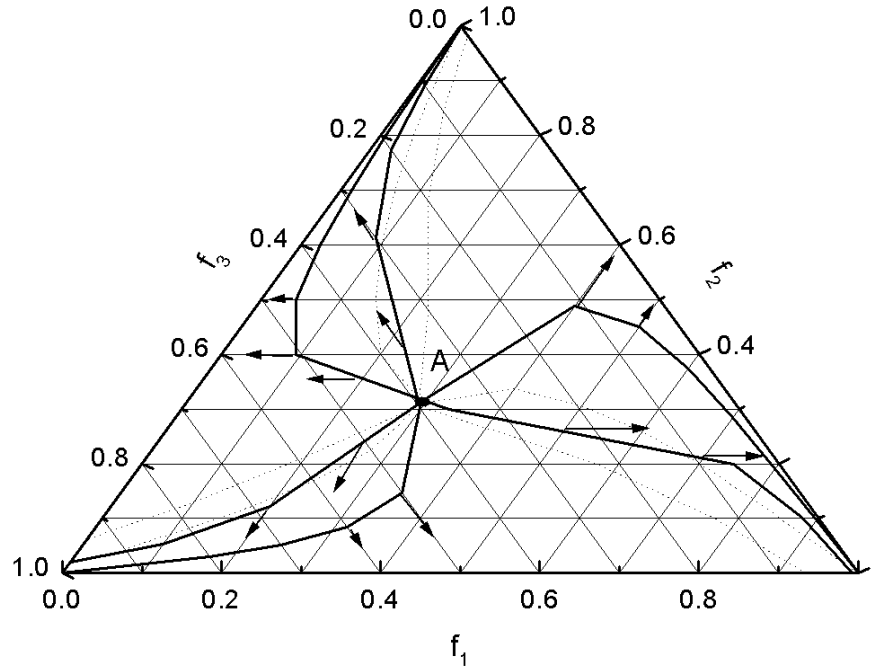

Figure 6.52 General system: $r_{12}=1.6965$, $r_{13}=0.1093$, $r_{21}=0.1359$, $r_{23}=1.35$, $r_{31}=2.3135$, $r_{32}=0.31$. The azeotropic point is $f_1=0.2950$, $f_2=0.3070$, $f_3=0.3980$

Similarly, the phase plots of STY/MMA/AN and BA/MMA/VAc system are shown (Figures 6.50 and 6.51). In STY/MMA/AN system phase plot (Figure 6.50), along the path AB and EF, $f_2=F_2$; path DE, $f_1=F_1$, path CD, $f_3=F_3$. Although there are two crossing points of EF/DE and DE/CD respectively, both of these two points are located on the border of the plot. There is no true azeotropic point in this system. But in the regions near the two points D, E and the region between DE, the composition drift is very small. DE path separates the plot into two parts. On the right side of DE, the operating point will move to $f_1=1$. On the right side of DE, the operating point will move to $f_3=1$. In BA/MMA/VAc system (Figure 6.51), there is only one path where $f_1=F_1$, and the composition drift is very large. The operating point finally will move to $f_3=1$, because VAc is the slowest monomer to be incorporated into the polymer.

Usually, if all the constituent copolymers have an azeotropic point, the terpolymer system also has an azeotropic point. There is a special case. If none of the constituent copolymers has an azeotropic point, there are two kinds of terpolymers that have an azeotropic point. One kind is like in Figure 6.52 ($r_{12}>1$, $r_{13}<1$, $r_{21}<1$, $r_{23}>1$, $r_{31}>1$, $r_{32}<1$). The other system is $r_{12}<1$, $r_{13}>1$, $r_{21}>1$, $r_{23}<1$, $r_{31}<1$, $r_{32}>1$. It has a similar phase plot to Figure 6.52, but the direction of the curves is counterclockwise.

6.7.3. Tetrapolymer system

Tetrapolymer system is more complicated than terpoplymer system. The equation is hard to solve analytically. Here we just develop the numerical algorithm. The general equations for azeotropic point are derived from the Walling-Briggs equation (2.39):

$$\begin{aligned} D_1\left\{f_1+\frac{f_2}{r_{12}}+\frac{f_3}{r_{13}}+\cdots+\frac{f_n}{r_{1n}}\right\} &= D_2\left\{\frac{f_1}{r_{21}}+f_2+\frac{f_3}{r_{23}}+\cdots+\frac{f_n}{r_{2n}}\right\} \\ &\vdots \\ &= D_n\left\{\frac{f_1}{r_{n1}}+\frac{f_2}{r_{n2}}+\frac{f_3}{r_{n3}}+\cdots+f_n\right\} \end{aligned} \tag{6.25}$$

Here D_1 to D_n have the same meaning as in Equation 2.39. When n=4, the tetrapolymer composition is described. These equations are used to recalculate the copolymer and

terpolymer systems mentioned above. The same results are obtained. This gives more confidence in the reliability of this algorithm.

Two general tetrapolymer systems are analyzed with Equation 6. 25. According to the experience with terpolymer systems, it follows that when not all the constituent copolymers have an azeotropic point, the tetrapolymer system may not have an azeotropic point, whereas when all the constituent copolymers have an azeotropic point, the tetrapolymer system may have an azeotropic point. In Table 6.34, comonomers 2 and 3, 4 and 3 and 2 and 4 have no azeotropic point, so this tetrapolymer system has no azeotropic point. In Table 6.35, all of the constituent copolymers have an azeotropic point. An azeotropic point of this tetrapolymer is found as expected. But this is not so simple in the tetrapolymer case. The third case (Table 6.36) shows that the constituent copolymer formed by comonomers 1 and 3 has no azeotropic point, but the tetrapolymer system still contains one azeotropic point. Recalculating the polymer composition at monomer feed ratio at the azeotropic point, the result satisfies the condition of azeotropic point. This indicates that the kinetics in the multicomponent system is more complicated.

Table 6.34 Reactivity ratios of a general tetrapolymer

	M1	M2	M3	M4
M1		0.5	0.41	2
M2	0.5		1.2	2.53
M3	0.04	0.15		0.91
M4	0.14	0.24	0.37	
	No azeotropic point!			

Table 6.35 Reactivity ratios of the tetrapolymer are less than 1; including its azeotropic point and verification by recalculating the polymer composition

	M1	M2	M3	M4
M1		0.5	0.41	0.2
M2	0.5		0.2	0.53
M3	0.4	0.15		0.91
M4	0.14	0.24	0.37	
	The numerical solusion is f1= 0.3901 f2=0.1601 f3=0.1082 f4=0.3415			
	f1	f2	f3	f4
	0.3901	0.1601	0.1082	0.3415
	F1	F2	F3	F4
	0.3901	0.1601	0.1082	0.3416

Table 6.36 Reactivity ratios with r_{31} >1

	M1	M2	M3	M4
M1		0.5	0.41	0.02
M2	0.5		0.2	0.53
M3	1.4	0.15		0.91
M4	0.14	0.24	0.37	

	The numerical solution is f1=0.4100 f2=0.1381 f3=0.0600 f4=0.3919			
	f1	f2	f3	f4
	0.4100	0.1381	0.0600	0.3919
	F1	F2	F3	F4
	0.4100	0.1381	0.0600	0.3919

7. Concluding remarks and recommendations

7.1. Concluding remarks

1) Instantaneous triad fraction model

Instantaneous triad fraction model has four independent responses corresponding to four out of six triad fractions in the copolymer. Both additive and multiplicative error structures give consistent estimation results at different error levels. For a correlated error structure, estimation methods such as the Box-Draper technique, which take into account the variance-covariance structure, will yield more precise reactivity ratio estimates.

2) Combination of instantaneous composition and triad fraction models

Instantaneous composition model is widely used to estimate reactivity ratios. Then the monomer feed ratio and polymer composition can be obtained precisely. Triad fraction model is a multiresponse model that is more robust to measurement error as compared to the composition model. The combination did not offer any remarkable improvements over the simpler counterparts.

3) The character of experimental design with cumulative models

For cumulative models, there are two independent variables, conversion x and monomer feed fraction. According to the experimental design, the combination of data at different monomer feed fractions can get reliable reactivity ratio estimation. When the cumulative polymer composition is the response, for systems with azeotropic point, the optimal monomer feed fractions are located on both sides of the azeotropic point where the composition drift is the largest. For systems without azeotropic point, the optimal monomer feed fractions are located on the slow monomer rich region. When the instantaneous monomer residual is the response, for systems with azeotropic point, the optimal points are close to the azeotropic point at high conversion.

Using the response of cumulative copolymer composition has its advantages. The optimal experiment runs are usually at low conversion and the parameter estimates have lower correlation compared with the instantaneous monomer residual fraction as response.

For cumulative triad fraction model, the optimal points are similar with these of the cumulative composition model. This gives the possibility to combine the two kinds of measurements at the same polymerization experiment to improve the precision of reactivity ratio estimation.

Furthermore, due to the little information contained in high conversion data (when k_p starts to decrease), there is no great impact on the estimation with the analytical cumulative model (Meyer-Lowry model), when using full conversion data.

4) Improvement of estimation of the cumulative model

The cumulative model decreases the uncertainty of estimation compared with the instantaneous model. For large composition drift systems, the instantaneous composition model cannot provide correct estimates.

5) Time as independent variable in cumulative model

When time is an independent variable in cumulative model, the uncertainty of estimation decreases obviously, but the correlation between parameters is serious due to the conversion dependency with respect to the independent variables. Experimental data at different feed ratios give better estimates than those at one feed ratio. Precise reactivity ratio estimation highly depends on the accuracy of other kinetics parameters. The lack of fit is a problem if the critical parameters in the kinetics are not accurate.

6) Azeotropic point

Numerical results agree well with the analytical results for copolymer and terpolymer. The result for tetrapolymer is verified by its prediction.

The analytical solution of the terpolymer equation proved that there is only one azeotropic point for a terpolymer system.

7.2. Recommendations for future work

1) Combine the measurements of cumulative composition and triad fractions

The estimation accuracy of the cumulative composition model is better than that for the instantaneous composition model. Since the optimal points of the cumulative composition and triad fraction models are similar, combining these two kinds of

measurements is expected to produce better estimation without extra polymerization experiments.

2) Using optimization algorithm considering the variance –covariance structure

NLLS is widely used, because it does not take into account the variance-covariance of the error in objective function.

But if some measurements such as triad fractions have correlated error, this violates the assumption of NLLS. If the error of the dependent variable and independent variable is of the same order such as with the instantaneous monomer mole fraction and conversion in the cumulative composition model, this violates another NLLS assumption. Because the error should be constant and normally distributed, the objective function cannot be transformed flexibly in order to avoid destroying the error structure.

To solve the above problems, the variance-covariance structure has to be taken into account, such as with the EVM framework.

3) Cumulative model with time as independent variable

The estimation of time as independent variable is highly constrained by other kinetic parameters of the model. They are mainly the critical parameters in copolymerization such as the critical free volume fractions. If these kinetic parameters can be estimated together with reactivity ratios, this problem may be solved.

4) Improve the optimal design

So far, D-optimality has been used exclusively. Other optimal designs can be tried and their results compared with D-optimal designs.

Bibliography

Aguilar MR, Gallardo A, Fernández MdM, Román JS. In situ quantitive H^1 NMR monitoring of monomer consumption: a simple and fast way of estimating reactivity ratios. Macromolecules 2002;35:2036-41.

Atkinson AC, Donev AN. Optimum experimental designs. New York: Oxford University Press, 1992.

Batz HG, Fanzman GF, Ringsdorf H. Pharmalogically active polymers 3: Model reactions for synthesis of pharmalogiclly active polymers by way of monomeric and polymeric reactive esters. Macromol Chem 2004;1973:172-6.

Belleney J, Hélary G, Migonney V. Terpolymerization of methyl methacrylate, poly(ethylene glycol) methyl ether methacrylate or poly(ethylene glycol) ethyl ether methacrylate with methacrylic acid and sodium styrenesulfonate: determination of the reactivity ratios. European Polymer Journal 2002;38.

Bernhardt S, Glöckner P, Ritter H. Cyclodextrins in polymer synthesis: influence of methylated β-cyclodextrin as host on the free radical copolymerization reactivity ratios of hydrophobic acrylates as guest monomers in aqueous medium. Polymer Bulletin (Berlin, Germany) 2001;46:153-7.

Box GEP, Draper NR. The Bayesian estimation of common parameters from several responses. Biometrika 1965;52:355-65.

Brar AS, Charan S. Reactivity ratios and Microstructure determination of (Vinyl Acetate)-(Methyl methacrylate) copolymers. European Polymer Journal 1993;29:755-9.

Brar AS, Dutta K. Reactivity ratios and sequence determination of acrylonitrile/hexyl methacrylate copolymers by one and two dimensional NMR spectroscopy. Macromolecular Chemistry and Physics 1998;199:2005-16.

Brar AS, Hekmatyar SK. Microstructure determination of the acrylonitrile-styrene-methyl methacrylate terpolymers by NMR spectroscopy. J Appl Polym Sci 1999;74:3026-32.

Brar AS, Yadav A. Glycidyl meththacrylate and vinylidene chloride copolymers. Nuclear magnetic resonance characterisation. Polym J 2003;35:37-43.

Buback M, Wittkowski L, Lehmann SA, Mähling F-O. High-pressure free-radical copolymerization of ethene-methacrylic acid and of ethene-acrylic acid, 1. (Meth)acrylic acid reactivity ratios. Macromolecular Chemistry and Physics 1999;200:1935-41.

Buback M, Wittkowski L. High-pressure free-radical copolymerization of ethene with methacrylic acid and ethene with acrylic acid. 2 Ethene reactivity ratios. Macromolecular Chemistry and Physics 2000;201:419-26.

Burke, A. L. Model discrimination techniques for the modelling of copolymerization reactions. 1994. University of Waterloo, PhD Thesis

Camail M, Essaoudi H, Gedoux B, et al. Radical terpolymerization of acrylamide, acrylic acid and N-(1,1-dimethyl-3-oxobutyl)acrylamide. European Polymer Journal 1998;34:1007-12.

Catalgil-Giz H, Giz A, Alb AM, et al. Online Monitoring of Composition, Sequence Length, and Molecular Weight Distributions during Free Radical Copolymerization, and Subsequent Determination of Reactivity Ratios. Macromolecules 2002;35:6557-71.

Chambard G, Klumperman B, German AL. Dependence of chemical composition of styrene/butyl acrylate copolymers on temperature and molecular weight. Polymer 1999;40:4459-63.

Cheetham PF, Huckerby TN, Tabner BJ. A High-Field ^{13}C-NMR Study of the Aqueous Copolymerisation of Acrylonitrile and Vinyl Acetate. Determination of Comonomer Reactivity Ratios. European Polymer Journal 1994;30:581-7.

Coskun MF, Demirelli K, Güzel D, Coskun M. Free-radical copolymerization of 3-phthalimido-2-hydroxypropyl methacrylate with styrene: the determination of monomer reactivity ratios and thermal analysis studies. Journal of Polymer Science, Part A: Polymer Chemistry 2002;40:650-8.

Coskun M, Ilter Z. Copolymerization of (2-phenyl-1,3-dioxolane-4-yl)methyl methacrylate with alkyl methacrylates: reactivity ratios and copolymer characterization. Journal of Polymer Science, Part A: Polymer Chemistry 2002;40:1184-91.

Coote ML, Johnston LPM, Davis TP. Copolymerization Propagation Kinetics of Styrene and Methyl Methacrylate-Revisited. 2. Kinetic Analysis . Macromolecules 1997;30:8191-204.

Czerwinski WK. Copolymerization at moderate to high conversion levels:1. New evaluation procedure of the relative reactivity ratios in terms of the terminal model. Polymer 1998;39:183-7.

Czerwinski WK. Copolymerization at moderate to high conversion levels: 2. Estimation of relative reactivity ratios in terms of the penultimate model for systems r2 = 0. Polymer 1998;39:189-92.

De P, Sathyanarayana DN. High-pressure kinetics of oxidative copolymerization of styrene with a-methylstyrene. Macromolecular Chemistry and Physics 2002a;203:2218-24.

De P, Sathyanarayana DN. Oxidative copolymerization of indene with p-tert-butylstyrene: synthesis, characterization, thermal analysis, and reactivity ratios. Journal of Polymer Science, Part A: Polymer Chemistry 2002b;40:9-18

De P, Sathyanarayana DN. Reactivity ratios for the terpolymerization of methyl methacrylate, vinyl acetate, and molecular oxygen. Journal of Polymer Science, Part A: Polymer Chemistry 2002c;40:564-72.

Demirelli K, Kaya I, Coskun M. 3,4-Dichlorobenzyl methacrylate and ethyl methacrylate system: monomer reactivity ratios and determination of thermodynamic properties at infinite dilution by using inverse gas chromatography. Polymer 2001;42:5181-8.

Draper NR, Hunter WG. Design of experiments for prameter estimation in multiresponse situations. Biometrika 1966;53:525.

Dube MA, Penlidis A. A systematic approach to the study of multicomponent polymerization kinetics-the butyl acrylate/methyl methacrylate/vinyl acette example:1. Bulk copolymerization. Polymer 1995;36:587-97.

Duever TA, O'Driscoll KF, Reilly PM. The use of the Error-in-Variables model in terpolymerization. J Polym Sci , Part A: Polym Chem 1983;21:2003-10.

Erbil C, Ozdemir S, Uyanik N. Determination of the monomer reactivity ratios for copolymerization of itaconic acid and acrylamide by conductometric titration method. Polymer 2000;41:1391-4.

Erol I, Soykan C. Copolymerization of methyl methacrylate with 2-methylbenzyl methacrylate and 4-methylbenzyl methacrylate: synthesis, characterization, and monomer reactivity ratios. Journal of Macromolecular Science, Pure and Applied Chemistry 2002;A39:953-68.

Fernández-García M, Torrado F, Martínez, et al. Free radical copolymerization of 2-hydroxyethyl methacrylate with butyl methacrylate: determination of monomer reactivity ratios and glass transition temperatures. Polymer 2000;41:8001-8.

Fernández-García M, Fernández-sanz M, Madruga EL, et al. Solvent Effects on the Free-Radical Copolymerization of Styrene with Butyl Acrylate. I. Monomer Reactivity Ratios. J Polym Sci , Part A: Polym Chem 2000;38:60-7.

Fernández-Monreal C, Sánchez-Chaves M, Martínez G, Madruga EL. Stereochemical configuration of 2-hydroxyethyl methacrylate/styrene copolymers obtained in N,N-dimethylformamide solution over a whole range of conversion. Acta Polymerica 1999;50:408-12.

Filley J, McKinnon JT, Wu DT, Ko GH. Theoretical Study of Ethylene-Vinyl Acetate Free-Radical Copolymerization: Reactivity Ratios, Penultimate Effects, and Relative Rates of Chain Transfer to Polymer. Macromolecules 2002;35:3731-8.

Galimberti M, Piemontesi F, Fusco O, et al. Ethene/Propene Copolymerization with High Product of Reactivity Ratios from a Single Center, Metallocene-Based Catalytic System. Macromolecules 1998;31:3409-16.

Galimberti M, Piemontesi F, Mascellani N, et al. Metallocenes for Ethene/Propene Copolymerizations with High Product of Reactivity Ratios. Macromolecules 1999;32:7968-76.

Garcia-Rubio LH, Lord MG, MacGregor JF, Hamielec AE. Bulk copolymerization of styrene and acrylonitrile: Experimental kinetics and mathematical modelling. Polymer 1985;26:2001-13.

Gauthier M, Carrozzella T, Penlidis A. Sulfobetaine Zwitterionomers Based on n-Butyl Acrylate and 2-Ethoxyethyl Acrylate: Monomer Synthesis ans Copolymerization Behavior. J Polym Sci , Part A: Polym Chem 2002;40:511-23.

Gendy TS, Barakat Y, Mohammad AI, Youssef AM. Polymeric surfactants for enhanced oil recovery part V. Production model for the effect of temperature and length of polyoxythlene chain or HLB on surface dynamic properties of some ethoxylated polymeric monomer. Polym Int 1991;24:234-40.

Giz A. An erroor-in-variables method for use when the reactivity ratios in copolymerization are close to one. Macromol Theory Simul 1998;7:391-7.

Glockner P, Ritter H. Cyclodextrins in polymer chemistry. Influence of methylated b-cyclodextrin as host on the free radical copolymerization reactivity ratios of isobornyl acrylate and butyl acrylate as guest monomers in aqueous medium. Macromolecular Rapid Communications 1999;20:602-5.

Habibi A, Vasheghani-Farahani E, Semsarzadeh MA, Sadaghiani K. A Generalized Least Square Model for the Determination of Monomer Reactivity Ratios in Free Radical Copolymerization Systems . Macromolecular Theory and Simulations 2003a;12:184-95.

Habibi A, Vasheghani-Farahani E, Semsarzadeh M, Sadaghiani K. Monomer reactivity ratios for lauryl methacrylate–isobutyl methacrylate in bulk free radical copolymerization . Polymer International 2003b;52:1434-43.

Haddleton DM, Crossman MC, Hunt KHr, et al. Identifying the Nature of the Active Species in the Polymerization of Methacrylates: Inhibition of Methyl Methacrylate Homopolymerizations and Reactivity Ratios for Copolymerization of Methyl Methacrylate/n-Butyl Methacrylate in Classical Anionic, Alkyllithium/Trialkylaluminum-Initiated, Group Transfer Polymerization, Atom Transfer Radical Polymerization, Catalytic Chain Transfer, and Classical Free Radical Polymerization. Macromolecules 1997;30:3992-8.

Hagiopol C, Frangu O, Dumitru L. A nonlinear method for the estimation of reactivity ratios in copolymerization processes. J Macromol Sci -CHEM 1989;A26:1363-79.

Hakim M, Verhoeven V, Mcmanus NT, Dube MA, Penlidis A. High-temperature Solution Polymerization of Butyl Acrylate/Methyl Methacrylate: Reactivity Ratio Estimation. Journal of Applied Polymer Science 2000;77:602-9.

Hautus FLM, German AL, Linssen HN. On Numerical Problems When Reactivity Ratios are Computed Using the Integrated Copolymer Equation. J Polym Sci :Polym Lett Ed 1985;23:311-5.

Hill DJT, Lang AP, O'Donnell JH, O'Sullivan PW. Determination of Reactivity Ratios From Analysis of Triad Fraction-Analysis of the copolymerization of Styrene and Acrylonitrile as Evidence for the Penultimate Model. App Polym J 1989;25:911-5.

Hill DJT, O'Donnell JH, O'Sullivan PW. Analysis of the mechanism of copolymerization of styrene and acrylonitrile. Macromolecules 1982;15:960-6.

Hocking MB, Klimchuk KA. A refinement of the terpolymer equation and its simple extension to two- and four-component systems. J Polym Sci , Part A: Polym Chem 1996;34:2481-97.

Ichimura K, Nishio Y. Photocrosslinkable polymers p-phenylene diacrylate group in the side chain: Argon laser photoresists. J Polym Sci , Part A: Polym Chem 1987;25:1590.

Ito H, Dalby C, Pomerantz A, et al. Monomer Reactivities and Kinetics in Radical Copolymerization of Hydroxystyrene Derivatives and tert-Butyl (Meth)acrylate. Macromolecules 2000;33:5080-9.

Jo WH, Lee YU. Off-Lattice Monte Carlo Simulation of Hyperbranched Polymers,2: Effect of the Reactivity Ratio of linear to Terminal Unit on the Microstructure of Hyperbranched Polymers Based on AB_2 Monomers. Macromol Theory Simul 2001;10:225-31.

Johncka M, Mullera L, Neyera A, Hofstratba JW. Copolymer of halogenated acrylates and methacrylates for the optical telecommunication, optical properties thermal analysis and determination of unsaturation by quantitative F-T Raman and FT-IR spectrocopy. European Polymer Journal 2000;36:1251-64.

Kaim A. Application of the Monomer Reactivity Ratios to the Kinetic-Model Discrimination and the Solvent-Effect Determination for the Styrene/Acrylonitrile Monomer System. J Polym Sci , Part A: Polym Chem 2000;38:846-54.

Kaim A. True reactivity ratios for styrene-methyl methacrylate copolymerization in bulk. Macromol Theory Simul 1998;7:97-103.

Kaim A, Oracz P. Solvent effects on true terminal reactivity ratios for styrene-methyl methacrylate copolymerization system. Polymer 1999;40:6925-32.

Kaim A, Oracz P. Terminal and penultimate models of copolymerization in the styrene-acrylonitrile system in bulk according to UNIFAC. Polymer 1998;39:3901-4.

Kelen T, Tudos F. Analysis of the linear methods for Determining copolymerization reactivity ratios.I A new improved linear graphic method. J Macromol Sci -CHEM 1975;A9:1-27.

Koenig JL. Chemical Microstructure of Polymer Chains. John Wiley & Sons, 1980.

Kucharski M, Lubczak R. Copolymerization of hydroxyalkyl methacrylates with acrylamide and methacrylamide I. Determination of reactivity ratios. J Appl Polym Sci 1997;64:1259-65.

Lousenberg RD, Shoichet MS. Radical copolymerization of novel trifluorovinyl ethers with ethyl vinyl ether and vinyl acetate: Estimating reactivity ratios and understanding reactivity behavior of the propagating radical. J Polym Sci , Part A: Polym Chem 2000;38:1344-54.

Manders BG, Smulders W, Aerdts AM, Van Herk AM. Determination of Reactivity Ratios for the System Methyl Methacrylate-n-Butyl Methacrylate. Macromolecules 1997;30:322-3.

Marten CR. Technology of paints, varnishes and lacquers. New York: Reinhod, 1968.

Mcmanus NT, Dube MA, Penlidis A. High Tempreture Bulk Copolymerization of Butyl Acrylate/Methyl Methacrylate: Reactivity ratio estimation. Polym React Eng J 1999.

McManus NT, Penlidis A, Rempel GL. A kinetic investigation of the copolymerization of acrylonitrile and vinyl acetate in bulk. Dev. Chem. Eng. Mineral Process., 1998a,6(3/4), 153-170

Mcmanus NT, Kim J.D., Penlidis A. Observations on styrene-hydroxyethyl acrylate and styrene-hydroxyethyl acrylate-ethyl acrylate polymerizations. Polymer Bulletin (Berlin) 1998b;41:661-8.

Mcmanus NT, Penlidis A, Dube MA. Copolymerization of alpha-methyl styrene with butyl acrylate in bulk. Polymer 2002;43:1607-14.

Mao R, Huglin MB. A new linear method to calculate monomer reactivity ratios by using high conversion copolymerization data: terminal model. Polymer 1993;34:1709-15.

Maxwell IA, Aerdts AM, German AL. Free radical copolymerization: an NMR Investigatioj of current kinetic models. Macromolecules 1993;26:1956-64.

Mohammed S, Daniels ES, Klein A, El-Aasser MS. Bulk copolymerization of dimethyl meta-isopropenyl benzyl isocyanate (TMI®): Determination of reactivity ratios. J Appl Polym Sci 1998;67:559-68.

Monett D, Méndez JA, Abraham GA, et al. An evolutionary approach to the estimation of reactivity ratios. Macromolecular Theory and Simulations 2002;11:525-32.

Murray DL, Harwood HJ, Shendy SMM, Piirma I. The use of sequence distributions to determine monomer feed compositions in the emulsion copolymerization of chlorotrifluoroethylene with vinyl acetate and vinyl propionate. Polymer 1995;36:3841-8.

Ni H, Hunkeler D. Prediction of copolymer composition drift using artificial neural networks: copolymerization of acrylamide with quaternary ammonium cationic monomers. Polymer 1997;38:667-75.

O'Driscoll KF. Computation of Reactivity Ratios from Sequence Distribution Information. J Polym Sci :Polym Lett Ed 1980;18:2747-9.

Oliva L, Longo P, Izzo L, Di Serio M. Zirconocene-Based Catalysts for the Ethylene-Styrene Copolymerization: Reactivity Ratios and Reaction Mechanism . Macromolecules 1997;30:5616-9.

Oracz P, Kaim A. Use of the Maximum Likelihood Method for Composition Data Analysis in the Radical Copolymerization Terminal Model. Macromol Theory Simul 2001;10:374-80.

Otsu T, Ito T, Imoto M. Vinyl polymerization CXL V.III, relative reaction of alkyl methacrylates in radicl copolymerization. Kogyo Kagu Ku Zasshi 1966;69:996.

Palmer DE, Mcmanus NT, Penlidis A. Copolymerization with depropagation: a study of a-methylstyrene/methyl methacrylate in solution at elevated temperatures. J Polym Sci , Part A: Polym Chem 2001;39:1753-63.

Palmer DE, Mcmanus NT, Penlidis A. Polymerization with Depropagation: A Study of α-Methyl Styrene/Methyl methyacrylate in Bulk at Elevated Temperatuatures. J Polym Sci , Part A: Polym Chem 2000;38:1981-90.

Pandeya SC, Rather N, Singh A. Synthesis and characterization of biologicl active barium containing polymer films. J Polym Materials 1999;16:253-8.

Patino-Leal H, Reilly PM, O'Driscoll KF. On the estimation of reactivity ratios**.** J Polym Sci :Polym Lett Ed 1980;18:219-27.

Payne AF. Organic coating technology. 1st ed. New York: 1964.

Plaumann HP, Branston RE. On Estimating Reactivity Ratios Using the Integrated Mayo-Lewis Equation. J Polym Sci , Part A: Polym Chem 1989;27:2819-22.

Polic AL, Duever TA, Penlidis A. Case Studies and Literature Review on the Estimation of Copolymerization Reactivity Ratios. J Polym Sci , Part A: Polym Chem 1998;36:813-22.

Prevost V, Petit A, Pla F. Studies on chemical oxidative copolymerization of aniline and o-alkoxysulfonated anilines II. Mechanistic approach and monomer reactivity ratios. European Polymer Journal 1999;35:1229-36.

Rainaldi I, Cristallini C, Ciardelli G, Giusti P. Copolymerization of acrylic acid and 2-hydroxyethyl methacrylate onto poly(N-vinylpyrrolidone): template influence on comonomer reactivity. Macromolecular Chemistry and Physics 2000;201:2424-31.

Roos SG, Mueller AHE, Matyjaszewski K. Copolymerization of n-Butyl Acrylate with Methyl Methacrylate and PMMA Macromonomers: Comparison of Reactivity Ratios in Conventional and Atom Transfer Radical Copolymerization. Macromolecules 1999;32:8331-5.

Rossignoli PJ, Duever TA. the Estimation of Copolymer ReactivityRatios: A Review and Case Studies Using the Error-In-Variables Model and Nonlinear Least Squares. Polymer Reaction Engineering J. 1995;3:361-95.

Rudin A, O'Driscoll KF, Rumack MS. Use of n.m.r. Data to calculate Copolymer reactivity ratios. Polymer 1981;22:740-7.

Ryttel A. Copolymerization of ethyl methacrylate with N-(3- or 4-halophenyl)maleimides: The monomer reactivity ratios. J Appl Polym Sci 1999;74:2924-30.

Sanghvi PG, Patel AC, Gopalkrishnan KS, Devi S. Reactivity ratios and sequence distribution of styrene-acrylonitrile copolymers synthesized in microemulsion medium. European Polymer Journal 2000;36:2275-83.

Sarzotti DM, Soares JBP, Penlidis A. Ethylene/1-hexene copolymers synthesized with a single-site catalyst: Crystallization analysis fractionation, modeling, and reactivity ratio estimation. Journal of Polymer Science: Part B: Polymer Physics 2002;40:2595-611.

Scorah MJ, Hua H, Dube MA. Bulk and Solution Copolymerization of Methyl Methacrylate and Vinyl Acetate. J Appl Polym Sci 2001;82:1238-55.

Senthilkumar U, Balaji R, Nanjundan S. Copolymerization of 2-(N-phthalimido)ethyl methacrylate with glycidyl methacrylate: synthesis, characterization, and monomer reactivity ratios. J Appl Polym Sci 2001;81:96-103.

Shan G-R, Weng Z-X, Huang Z-M, Pan Z-R. Reactivity ratios for copolymerization with the participation of a charge-transfer complex. Chinese Journal of Polymer Science 2000;18:423-30.

Smith BL, Klier J. Determination of monomer reactivity ratios for copolymerizations of methacrylic acid with poly(ethylene glycol) monomethacrylate. J Appl Polym Sci 1998;68:1019-25.

Shawki SM, Hamielec AE. Estimation of the Reactivity Ratios in the Copolymerization of Acrylic Acid and Acrylamide from Composition-Conversion Measurements by an Improved Nolinear Least-Squares Method. J Appl Polym Sci 1979;23:3155-66.

Stergiou G, Dousikos P, Pitsikalis M. Radical copolymerization of styrene and alkyl methacrylates: monomer reactivity ratios and thermal properties. European Polymer Journal 2002;38:1963-70.

Tamizharasi S, Srinivas G, Sulochana N, Reddy BSR. cpolymerization of 4-chlorophenyl acrylate with methyl acrylate: synthesis, characterization reactivity ratios and their application in the leather industry. J Appl Polym Sci 2004;1999:1153-60.

Thamizharasi S, Gnanasundaram P, Balasubramanian S. Copolymerization of 4-nitrophenyl acrylate (NPA) with methyl methacrylate (MMA): synthesis, characterization and reactivity ratios. Journal of Macromolecular Science, Pure and Applied Chemistry 1999a;A36:1949-66.

Thamizharasi S, Gnanasundaram P, Reddy BSR. Copolymerization of 4-acetylphenyl acrylate with methyl methacrylate and butyl methacrylate: synthesis, characterization and reactivity ratios. European Polymer Journal 1997a;33:1487-94.

Thamizharasi S, Srinivas G, Sulochana N, Reddy BSR. Copolymerization of 4-chlorophenyl acrylate with methyl acrylate: synthesis, characterization, reactivity ratios, and their applications in the leather industry. J Appl Polym Sci 1999b;73:1153-60.

Thamizharasi S, Gnanasundaram P, Reddy BSR. Copolymerization of 4-nitrophenyl acrylate with glycidyl methacrylate: Synthesis, characterization, and reactivity ratios. J Appl Polym Sci 1997b;65:1285-91.

Tidwell PW, Mortimer GA. An Improved Method of Caculating Copolymerization Reactivity Ratios. J Polym Sci , Part A: Polym Chem 1965;3:369-87.

Van Den Brink M, Van Herk AM, German AL. Nonlinear regression by visualization of the sum of residual space applied to the integrated copolymerization equation with errors in all variables. I. Introduction of the model, simulations and design of experiments. J Polym Sci , Part A: Polym Chem 1999;37:3793-803.

Van Den Brink M, Smulders W, Van Herk AM, German AL. Nonlinear regression by visualization of the sum of residual space applied to the integrated copolymerization equation with errors in all variables. II. Application to the system methyl methacrylate-α-methylene-γ-butyrolactone using on-line Raman spectroscopy. J Polym Sci , Part A: Polym Chem 1999;37:3804-16.

Van Herk AM, Dröge T. Nonlinear least squares fitting applied to copolymerization modeling. Macromol Theory Simul 1997;6:1263-76.

Vijayanand PS, Penlidis A, Nanjundan S. Copolymerization of 4-benzyloxycarbonylphenyl acrylate with methyl methacrylate: Synthesis, characterization, and determination of reactivity ratios. Journal of Macromolecular Science, Pure and Applied Chemistry 2003;A40:125-40.

Vijayanand PS, Penlidis A, Radhakrishnan S, Nanjundan S. Copolymers of 3,5-dimethylphenyl methacrylate and methyl methacrylate: Synthesis, characterization, and determination of reactivity ratios. Journal of Macromolecular Science, Pure and Applied Chemistry 2002;A39:591-608.

Vijayaraghavan PG, Reddy BSR. Copolymerization of 4-methyl and 4-methoxyphenyl acrylates with glycidyl methatlate:synthesis,characterization,reactivity ratios and application as adhesive for leather industry. J Appl Polym Sci 1996;61:943.

Yamada K, Nakano T, Okamoto Y. Free-radical copolymerization of vinyl esters using fluoroalcohols as solvents: The solvent effect on the monomer reactivity ratio. J Polym Sci , Part A: Polym Chem 2000;38:220-8.

Warson H. The application of synthetic resin emulsions. London: Ernest Benn, 1972.

Zaldivar C, del Sol O, Gerardo D.lglesias. On the preparation of acrylic acid/vinyl acetate copolymers with constant composition-1.copolymerization reactivity ratios. Polymer 1997;39:1997-245.

Zerroukhi A, Cincu C, Montheard JP. Substituted styrenes-maleic anhydride copolymers - Measurements of the reactivity ratios with high conversions and relations between molecular masses and viscosity. J Appl Polym Sci 1999;71:1447-54.

Zhao Y, Li H, Liu P, et al. Reactivity ratios of free monomers and their charge-transfer complex in the copolymerization of N-butyl maleimide and styrene. J Appl Polym Sci 2002;83:3007-12.

Ziaee F, Nekoomanesh M. Monomer reactivity ratios of styrene-butyl acrylate copolymers at low and high conversions. Polymer 1997;39:203-7.

Appendix

The analytical solution of azeotropic point of terpolymer

Let $f_i=F_i=X_i$ (i=1,2,3), r={r_{11}, r_{12}, r_{21}, r_{23}, r_{31}, r_{32}}. Six trivial roots are:

$\{X_1=1, X_2=0, X_3=0\}, \{X_1=0, X_2=1, X_3=0\}, \{X_1=0, X_2=0, X_3=1\}$

$$\left\{X_1=0,\ X_2=\frac{1-r_6}{2-r_4-r_6},\ X_3=\frac{1-r_4}{2-r_4-r_6}\right\}$$

$$\left\{X_1=\frac{1-r_5}{2-r_2-r_5},\ X_2=0,\ X_3=\frac{1-r_2}{2-r_2-r_5}\right\}$$

$$\left\{X_1=\frac{1-r_3}{2-r_1-r_3},\ X_2=\frac{1-r_1}{2-r_1-r_3},\ X_3=0\right\}$$

The non-trivial root is:

$$\begin{aligned}X_1 = (&-r_6^2 r_3^2 r_4 r_2^2 - r_3^2 r_5^2 r_6^2 r_4 r_2^2 - r_3^2 r_1^2 r_5^2 r_2 r_4 - r_6 r_3^2 r_1^2 r_5 r_4 + r_6^2 r_1 r_2 r_5^2 r_4^2\\
&- r_5^2 r_1^2 r_3^2 r_4^2 r_6 + 2 r_3 r_1^2 r_5^2 r_4^2 r_6 + r_6 r_3 r_1^2 r_5 r_4 - r_6 r_3^2 r_5 r_1^2 r_2 + r_6 r_3^2 r_1 r_5 r_2\\
&- r_6 r_3^2 r_2^2 r_1 r_5^2 + r_6^2 r_3^2 r_1 r_2^2 r_5 + r_3^2 r_1^2 r_5^2 r_2 r_4^2 r_6 + r_6^2 r_3^2 r_1 r_2 r_5 r_4\\
&- 2 r_6^2 r_3 r_1 r_2 r_5^2 r_4^2 - r_6^2 r_3 r_1 r_2 r_5 r_4 - r_6^2 r_3 r_1 r_2^2 r_5^2 r_4 + r_6^2 r_3^2 r_1 r_2 r_5^2 r_4^2\\
&+ r_6 r_3 r_2 r_1^2 r_5^2 r_4 - r_3^2 r_1 r_5^2 r_2^2 r_4 r_6 - r_3^2 r_1^2 r_5^2 r_2 r_6 r_4 + r_3^2 r_1 r_5^2 r_6^2 r_4 r_2^2\\
&+ r_5^2 r_1^2 r_4^2 + r_6^2 r_3^2 r_2^2 + r_3^2 r_2^2 r_1 r_5^2 - r_3 r_1^2 r_5^2 r_4 + r_3^2 r_2 r_1^2 r_5^2 - r_3^2 r_2 r_1 r_5^2\\
&- r_6 r_1^2 r_4^2 r_5^2 - r_6^2 r_3^2 r_1 r_2 r_4 - 2 r_6^2 r_3^2 r_1 r_2 r_5 r_4^2 + 2 r_3^2 r_5 r_4 r_6^2 r_2^2\\
&+ r_3^2 r_5^2 r_1^2 r_4 + r_6 r_3^2 r_2^2 r_5^2 + 2 r_6 r_3 r_1 r_5^2 r_2^2 r_4 - r_6 r_3 r_1^2 r_5 r_4^2 - r_6 r_3^2 r_5 r_1 r_2^2\\
&+ r_6 r_3^2 r_5 r_1^2 r_4^2 + r_6 r_3^2 r_1 r_5 r_4 r_2^2 - r_6^2 r_3 r_2^2 r_5 r_4 + 2 r_6 r_3^2 r_1^2 r_5 r_2 r_4\\
&+ r_6 r_3 r_5^2 r_1 r_2 r_4^2 - r_6 r_3 r_2^2 r_5^2 r_4 - r_6 r_3^2 r_1^2 r_5 r_2 r_4^2 - r_3 r_1^2 r_5^2 r_2 r_4^2 r_6\\
&+ 2 r_6^2 r_3 r_1 r_2 r_5 r_4^2 - r_3^2 r_1 r_5 r_4 r_6^2 r_2^2 + r_6^2 r_3^2 r_1 r_2 r_4^2 - r_3 r_1^2 r_5^2 r_4^2\\
&- r_3 r_1^2 r_5^2 r_2 r_4 + r_3 r_1^2 r_5^2 r_2 r_4^2 + r_3 r_5^2 r_1 r_2 r_4 - r_6 r_5^2 r_1 r_2 r_4^2 - r_6^2 r_3^2 r_2^2 r_5\end{aligned}$$

$$+r_6^2 r_3 r_2^2 r_5^2 r_4 - r_6 r_2^2 r_3^2 r_5 + r_6 r_2^2 r_4 r_5 r_3 - r_5^2 r_4 r_1 r_2^2 r_3 - r_6 r_2 r_3 r_4^2 r_5 r_1)$$
$$/\ (-2 r_6^2 r_3^2 r_4 r_2^2 - r_3^2 r_5^2 r_6^2 r_4 r_2^2 - r_3^2 r_1^2 r_5^2 r_2 r_4 - r_6^2 r_1^2 r_2 r_5^2 r_4^2$$
$$-2 r_6 r_3^2 r_1^2 r_5 r_4 + 2 r_6^2 r_1 r_2 r_5^2 r_4^2 - r_3^2 r_1^2 r_6^2 r_2 r_4 - r_5^2 r_1^2 r_3^2 r_4^2 r_6$$
$$-r_3 r_1^2 r_5 r_6^2 r_4^2 + 3 r_3 r_1^2 r_5^2 r_4^2 r_6 + 2 r_6 r_3 r_1^2 r_5 r_4 - 2 r_6 r_3^2 r_5 r_1^2 r_2$$
$$+2 r_6 r_3^2 r_1 r_5 r_2 - r_6 r_3^2 r_2^2 r_1 r_5^2 + 3 r_6^2 r_3^2 r_1 r_2^2 r_5 - r_6^2 r_3^2 r_2^2 r_1^2 r_5$$
$$+r_3^2 r_1^2 r_5^2 r_2 r_4^2 r_6 + r_3 r_1^2 r_5^2 r_6^2 r_2 r_4^2 - r_3 r_1^2 r_5 r_6^2 r_2 r_4^2 - r_6 r_3 r_2 r_5^2 r_1 r_4$$
$$+2 r_6^2 r_3^2 r_1 r_2 r_5 r_4 + r_6^2 r_3 r_1^2 r_2^2 r_5^2 r_4 - 3 r_6^2 r_3 r_1 r_2 r_5^2 r_4^2 - r_6^2 r_3 r_1 r_2 r_5 r_4$$
$$-3 r_6^2 r_3 r_1 r_2^2 r_5^2 r_4 + r_6^2 r_3^2 r_1 r_2 r_5^2 r_4^2 - r_6 r_1^2 r_5 r_4^2 + 2 r_6 r_3 r_2 r_1^2 r_5^2 r_4$$
$$-r_3^2 r_1 r_5^2 r_2^2 r_4 r_6 - r_3^2 r_1^2 r_5 r_6^2 r_2 r_4 + r_3^2 r_1^2 r_5 r_4 r_6^2 r_2^2 - r_3^2 r_1^2 r_5^2 r_2 r_6 r_4$$
$$+r_3^2 r_1 r_5^2 r_6^2 r_4 r_2^2 + 3 r_5^2 r_1^2 r_4^2 + 3 r_6^2 r_3^2 r_2^2 + r_3^2 r_2^2 r_1 r_5^2 - r_3 r_1^2 r_5^2 r_4$$
$$+r_3^2 r_2 r_1^2 r_5^2 - r_3^2 r_2 r_1 r_5^2 - 2 r_6 r_1^2 r_4^2 r_5^2 + r_6^2 r_3^2 r_1^2 r_2 - r_6^2 r_3 r_1^2 r_4$$
$$-r_6^2 r_3^2 r_1 r_2 + r_6^2 r_3 r_1^2 r_4^2 + r_6^2 r_3^2 r_1^2 r_4 - 3 r_6^2 r_3^2 r_1 r_2 r_4 - 3 r_6^2 r_3^2 r_1 r_2 r_5 r_4^2$$
$$+3 r_3^2 r_5 r_4 r_6^2 r_2^2 - r_3 r_5 r_2^2 r_6^2 r_4^2 + r_3^2 r_5^2 r_1^2 r_4 + r_6 r_3^2 r_2^2 r_5^2 + r_6^2 r_1^2 r_5 r_4^2$$
$$+6 r_6 r_3 r_1 r_5^2 r_2^2 r_4 - r_6 r_1 r_2^2 r_4^2 r_5^2 - 3 r_6 r_3 r_1^2 r_5 r_4^2 - 3 r_6 r_3^2 r_5 r_1 r_2^2$$
$$+2 r_6 r_3 r_1^2 r_5 r_2 r_4^2 - r_6 r_3^2 r_5 r_1 r_2 r_4 - 3 r_6 r_3 r_1^2 r_5^2 r_2^2 r_4 + 2 r_6 r_3^2 r_5 r_1^2 r_4^2$$
$$+2 r_6 r_3^2 r_1 r_5 r_4 r_2^2 + 3 r_6 r_1^2 r_5^2 r_2 r_4^2 + r_6 r_3^2 r_1^2 r_5 r_2^2 r_4^2 - 3 r_6^2 r_3 r_2^2 r_5 r_4$$
$$+6 r_6 r_3^2 r_1^2 r_5 r_2 r_4 - r_6 r_3 r_1^2 r_5 r_2 r_4 + 2 r_6 r_3 r_5^2 r_1 r_2 r_4^2 - 2 r_6 r_3 r_2^2 r_5^2 r_4$$
$$-3 r_6 r_3^2 r_1^2 r_5 r_2 r_4^2 + 2 r_6 r_3^2 r_1^2 r_5 r_2^2 - 3 r_3 r_1^2 r_5^2 r_2 r_4^2 r_6 - 2 r_6^2 r_1 r_2 r_5 r_4^2$$
$$-r_3 r_1 r_5 r_2^2 r_6^2 r_4^2 - r_3 r_1 r_5^2 r_2^2 r_6 r_4^2 + 2 r_6^2 r_3 r_1 r_4 r_2 + 6 r_6^2 r_3 r_1 r_2 r_5 r_4^2$$
$$+2 r_6^2 r_3 r_1 r_2^2 r_5 r_4 - 3 r_3^2 r_1 r_5 r_4 r_6^2 r_2^2 + 2 r_6^2 r_3^2 r_1 r_2 r_4^2 + r_3^2 r_1 r_5 r_2^2 r_6^2 r_4^2$$
$$+r_1 r_2^2 r_4^2 r_5^2 - 2 r_3 r_1^2 r_5^2 r_4^2 - 2 r_1^2 r_5^2 r_2 r_4^2 + r_5^2 r_2^2 r_6 r_4^2 + r_5 r_2^2 r_6^2 r_4^2$$

$$
\begin{aligned}
&- 3\,r_3 r_1^{\,2} r_5^{\,2} r_2 r_4 + 3\,r_3 r_1^{\,2} r_5^{\,2} r_2 r_4^{\,2} + 2\,r_3 r_5^{\,2} r_1 r_2 r_4 + r_6^{\,2} r_3 r_4^{\,2} r_2^{\,2} \\
&+ 2\,r_3 r_1^{\,2} r_5^{\,2} r_2^{\,2} r_4 - r_3^{\,2} r_1 r_2^{\,2} r_6^{\,2} r_4^{\,2} - 2\,r_6^{\,2} r_3^{\,2} r_1 r_2^{\,2} - r_3 r_1^{\,2} r_5^{\,2} r_2^{\,2} r_4^{\,2} \\
&+ r_3 r_1^{\,2} r_5^{\,2} r_2^{\,2} r_6 r_4^{\,2} - 3\,r_6 r_5^{\,2} r_1 r_2 r_4^{\,2} - 3\,r_6 r_3^{\,2} r_1^{\,2} r_5 r_4 r_2^{\,2} + 3\,r_3^{\,2} r_1 r_4 r_6^{\,2} r_2^{\,2} \\
&- r_6 r_2^{\,2} r_4^{\,2} r_5 - r_6^{\,2} r_2^{\,2} r_4 r_3 - 2\,r_6^{\,2} r_3^{\,2} r_2^{\,2} r_5 + 2\,r_6^{\,2} r_3 r_2^{\,2} r_5^{\,2} r_4 - r_6 r_2^{\,2} r_3^{\,2} r_5 \\
&+ 2\,r_6 r_2^{\,2} r_4 r_5 r_3 + 2\,r_6 r_2 r_4^{\,2} r_5 r_1 - r_6 r_4 r_1 r_2^{\,2} r_5 r_3 - 2\,r_5^{\,2} r_4 r_1 r_2^{\,2} r_3 - r_5^{\,2} r_4^{\,2} r_2 r_1 \\
&- r_6 r_2 r_3 r_4^{\,2} r_5 r_1 - 2\,r_6^{\,2} r_2 r_3 r_4^{\,2} r_1)
\end{aligned}
$$

$$
\begin{aligned}
X_2 = (&-r_6^{\,2} r_1^{\,2} r_2 r_5^{\,2} r_4^{\,2} - r_6 r_3^{\,2} r_1^{\,2} r_5 r_4 + r_6^{\,2} r_1 r_2 r_5^{\,2} r_4^{\,2} - r_3^{\,2} r_1^{\,2} r_6^{\,2} r_2 r_4 \\
&- r_3 r_1^{\,2} r_5 r_6^{\,2} r_4^{\,2} + r_3 r_1^{\,2} r_5^{\,2} r_4^{\,2} r_6 + r_6 r_3 r_1^{\,2} r_5 r_4 - r_6 r_3^{\,2} r_5 r_1^{\,2} r_2 + r_6 r_3^{\,2} r_1 r_5 r_2 \\
&+ 2\,r_6^{\,2} r_3^{\,2} r_1 r_2^{\,2} r_5 - r_6^{\,2} r_3^{\,2} r_2^{\,2} r_1^{\,2} r_5 + r_3 r_1^{\,2} r_5^{\,2} r_6^{\,2} r_2 r_4^{\,2} - r_3 r_1^{\,2} r_5 r_6^{\,2} r_2 r_4^{\,2} \\
&- r_6 r_3 r_2 r_5^{\,2} r_1 r_4 + r_6^{\,2} r_3^{\,2} r_1 r_2 r_5 r_4 + r_6^{\,2} r_3 r_1^{\,2} r_2^{\,2} r_5^{\,2} r_4 - r_6^{\,2} r_3 r_1 r_2 r_5^{\,2} r_4^{\,2} \\
&- 2\,r_6^{\,2} r_3 r_1 r_2^{\,2} r_5^{\,2} r_4 - r_6 r_1^{\,2} r_5 r_4^{\,2} + r_6 r_3 r_2 r_1^{\,2} r_5^{\,2} r_4 - r_3^{\,2} r_1^{\,2} r_5 r_6^{\,2} r_2 r_4 \\
&+ r_3^{\,2} r_1^{\,2} r_5 r_4 r_6^{\,2} r_2^{\,2} + r_5^{\,2} r_1^{\,2} r_4^{\,2} + r_6^{\,2} r_3^{\,2} r_2^{\,2} - r_6 r_1^{\,2} r_4^{\,2} r_5^{\,2} + r_6^{\,2} r_3^{\,2} r_1^{\,2} r_2 \\
&- r_6^{\,2} r_3 r_1^{\,2} r_4 - r_6^{\,2} r_3^{\,2} r_1 r_2 + r_6^{\,2} r_3 r_1^{\,2} r_4^{\,2} + r_6^{\,2} r_3^{\,2} r_1^{\,2} r_4 - r_6^{\,2} r_3^{\,2} r_1 r_2 r_4 \\
&+ r_6^{\,2} r_1^{\,2} r_5 r_4^{\,2} + 2\,r_6 r_3 r_1 r_5^{\,2} r_2^{\,2} r_4 - r_6 r_3 r_1^{\,2} r_5 r_4^{\,2} - r_6 r_3^{\,2} r_5 r_1 r_2^{\,2} \\
&+ r_6 r_3 r_1^{\,2} r_5 r_2 r_4^{\,2} - 2\,r_6 r_3 r_1^{\,2} r_5^{\,2} r_2^{\,2} r_4 + 2\,r_6 r_1^{\,2} r_5^{\,2} r_2 r_4^{\,2} - r_6^{\,2} r_3 r_2^{\,2} r_5 r_4 \\
&+ 2\,r_6 r_3^{\,2} r_1^{\,2} r_5 r_2 r_4 + r_6 r_3^{\,2} r_1^{\,2} r_5 r_2^{\,2} - r_3 r_1^{\,2} r_5^{\,2} r_2 r_4^{\,2} r_6 - r_6^{\,2} r_1 r_2 r_5 r_4^{\,2} \\
&+ r_6^{\,2} r_3 r_1 r_4 r_2 + 2\,r_6^{\,2} r_3 r_1 r_2 r_5 r_4^{\,2} + r_6^{\,2} r_3 r_1 r_2^{\,2} r_5 r_4 - r_3^{\,2} r_1 r_5 r_4 r_6^{\,2} r_2^{\,2} \\
&- r_1^{\,2} r_5^{\,2} r_2 r_4^{\,2} - r_3 r_1^{\,2} r_5^{\,2} r_2 r_4 + r_3 r_1^{\,2} r_5^{\,2} r_2^{\,2} r_4 - r_6^{\,2} r_3^{\,2} r_1 r_2^{\,2} - r_6 r_5^{\,2} r_1 r_2 r_4^{\,2} \\
&- r_6 r_3^{\,2} r_1^{\,2} r_5 r_4 r_2^{\,2} + r_3^{\,2} r_1 r_4 r_6^{\,2} r_2^{\,2} - r_6^{\,2} r_3^{\,2} r_2^{\,2} r_5 + r_6^{\,2} r_3 r_2^{\,2} r_5^{\,2} r_4 + r_6 r_2 r_4^{\,2} r_5 r_1 \\
&- r_6 r_4 r_1 r_2^{\,2} r_5 r_3 - r_6^{\,2} r_2 r_3 r_4^{\,2} r_1) \Big/ (-2\,r_6^{\,2} r_3^{\,2} r_4 r_2^{\,2} - r_3^{\,2} r_5^{\,2} r_6^{\,2} r_4 r_2^{\,2} \\
&- r_3^{\,2} r_1^{\,2} r_5^{\,2} r_2 r_4 - r_6^{\,2} r_1^{\,2} r_2 r_5^{\,2} r_4^{\,2} - 2\,r_6 r_3^{\,2} r_1^{\,2} r_5 r_4 + 2\,r_6^{\,2} r_1 r_2 r_5^{\,2} r_4^{\,2} \\
&- r_3^{\,2} r_1^{\,2} r_6^{\,2} r_2 r_4 - r_5^{\,2} r_1^{\,2} r_3^{\,2} r_4^{\,2} r_6 - r_3 r_1^{\,2} r_5 r_6^{\,2} r_4^{\,2} + 3\,r_3 r_1^{\,2} r_5^{\,2} r_4^{\,2} r_6 \\
&+ 2\,r_6 r_3 r_1^{\,2} r_5 r_4 - 2\,r_6 r_3^{\,2} r_5 r_1^{\,2} r_2 + 2\,r_6 r_3^{\,2} r_1 r_5 r_2 - r_6 r_3^{\,2} r_2^{\,2} r_1 r_5^{\,2} \\
&+ 3\,r_6^{\,2} r_3^{\,2} r_1 r_2^{\,2} r_5 - r_6^{\,2} r_3^{\,2} r_2^{\,2} r_1^{\,2} r_5 + r_3^{\,2} r_1^{\,2} r_5^{\,2} r_2 r_4^{\,2} r_6 + r_3 r_1^{\,2} r_5^{\,2} r_6^{\,2} r_2 r_4^{\,2}
\end{aligned}
$$

$$
\begin{aligned}
&- r_3 r_1^2 r_5 r_6^2 r_2 r_4^2 - r_6 r_3 r_2 r_5^2 r_1 r_4 + 2 r_6^2 r_3^2 r_1 r_2 r_5 r_4 + r_6^2 r_3 r_1^2 r_2^2 r_5^2 r_4 \\
&- 3 r_6^2 r_3 r_1 r_2 r_5^2 r_4^2 - r_6^2 r_3 r_1 r_2 r_5 r_4 - 3 r_6^2 r_3 r_1 r_2^2 r_5^2 r_4 + r_6^2 r_3^2 r_1 r_2 r_5^2 r_4^2 \\
&- r_6 r_1^2 r_5 r_4^2 + 2 r_6 r_3 r_2 r_1^2 r_5^2 r_4 - r_3^2 r_1 r_5^2 r_2^2 r_4 r_6 - r_3^2 r_1^2 r_5 r_6^2 r_2 r_4 \\
&+ r_3^2 r_1^2 r_5 r_4 r_6^2 r_2^2 - r_3^2 r_1^2 r_5^2 r_2 r_6 r_4 + r_3^2 r_1 r_5^2 r_6^2 r_4 r_2^2 + 3 r_5^2 r_1^2 r_4^2 \\
&+ 3 r_6^2 r_3^2 r_2^2 + r_3^2 r_2^2 r_1 r_5^2 - r_3 r_1^2 r_5^2 r_4 + r_3^2 r_2 r_1^2 r_5^2 - r_3^2 r_2 r_1 r_5^2 \\
&- 2 r_6 r_1^2 r_4^2 r_5^2 + r_6^2 r_3^2 r_1^2 r_2 - r_6^2 r_3 r_1^2 r_4 - r_6^2 r_3^2 r_1 r_2 + r_6^2 r_3 r_1^2 r_4^2 \\
&+ r_6^2 r_3^2 r_1^2 r_4 - 3 r_6^2 r_3^2 r_1 r_2 r_4 - 3 r_6^2 r_3^2 r_1 r_2 r_5 r_4^2 + 3 r_3^2 r_5 r_4 r_6^2 r_2^2 \\
&- r_3 r_5 r_2^2 r_6^2 r_4^2 + r_3^2 r_5^2 r_1^2 r_4 + r_6 r_3^2 r_2^2 r_5^2 + r_6^2 r_1^2 r_5 r_4^2 + 6 r_6 r_3 r_1 r_5^2 r_2^2 r_4 \\
&- r_6 r_1 r_2^2 r_4^2 r_5^2 - 3 r_6 r_3 r_1^2 r_5 r_4^2 - 3 r_6 r_3^2 r_5 r_1 r_2^2 + 2 r_6 r_3 r_1^2 r_5 r_2 r_4^2 \\
&- r_6 r_3^2 r_5 r_1 r_2 r_4 - 3 r_6 r_3 r_1^2 r_5^2 r_2^2 r_4 + 2 r_6 r_3^2 r_5 r_1^2 r_4^2 + 2 r_6 r_3^2 r_1 r_5 r_4 r_2^2 \\
&+ 3 r_6 r_1^2 r_5^2 r_2 r_4^2 + r_6 r_3^2 r_1^2 r_5 r_2^2 r_4^2 - 3 r_6^2 r_3 r_2^2 r_5 r_4 + 6 r_6 r_3^2 r_1^2 r_5 r_2 r_4 \\
&- r_6 r_3 r_1^2 r_5 r_2 r_4 + 2 r_6 r_3 r_5^2 r_1 r_2 r_4^2 - 2 r_6 r_3 r_2^2 r_5^2 r_4 - 3 r_6 r_3^2 r_1^2 r_5 r_2 r_4^2 \\
&+ 2 r_6 r_3^2 r_1^2 r_5 r_2^2 - 3 r_3 r_1^2 r_5^2 r_2 r_4^2 r_6 - 2 r_6^2 r_1 r_2 r_5 r_4^2 - r_3 r_1 r_5 r_2^2 r_6^2 r_4^2 \\
&- r_3 r_1 r_5^2 r_2^2 r_6 r_4^2 + 2 r_6^2 r_3 r_1 r_4 r_2 + 6 r_6^2 r_3 r_1 r_2 r_5 r_4^2 + 2 r_6^2 r_3 r_1 r_2^2 r_5 r_4 \\
&- 3 r_3^2 r_1 r_5 r_4 r_6^2 r_2^2 + 2 r_6^2 r_3^2 r_1 r_2 r_4^2 + r_3^2 r_1 r_5 r_2^2 r_6^2 r_4 + r_1 r_2^2 r_4^2 r_5^2 \\
&- 2 r_3 r_1^2 r_5^2 r_4^2 - 2 r_1^2 r_5^2 r_2 r_4^2 + r_5^2 r_2^2 r_6 r_4^2 + r_5 r_2^2 r_6^2 r_4^2 - 3 r_3 r_1^2 r_5^2 r_2 r_4 \\
&+ 3 r_3 r_1^2 r_5^2 r_2 r_4^2 + 2 r_3 r_5^2 r_1 r_2 r_4 + r_6^2 r_3 r_4^2 r_2^2 + 2 r_3 r_1^2 r_5^2 r_2^2 r_4 \\
&- r_3^2 r_1 r_2^2 r_6^2 r_4^2 - 2 r_6^2 r_3^2 r_1 r_2^2 - r_3 r_1^2 r_5^2 r_2^2 r_4^2 + r_3 r_1^2 r_5^2 r_2^2 r_6 r_4^2 \\
&- 3 r_6 r_5^2 r_1 r_2 r_4^2 - 3 r_6 r_3^2 r_1^2 r_5 r_4 r_2^2 + 3 r_3^2 r_1 r_4 r_6^2 r_2^2 - r_6 r_2^2 r_4^2 r_5 \\
&- r_6^2 r_2^2 r_4 r_3 - 2 r_6^2 r_3^2 r_2^2 r_5 + 2 r_6^2 r_3 r_2^2 r_5^2 r_4 - r_6 r_2^2 r_3^2 r_5 + 2 r_6 r_2^2 r_4 r_5 r_3 \\
&+ 2 r_6 r_2 r_4^2 r_5 r_1 - r_6 r_4 r_1 r_2^2 r_5 r_3 - 2 r_5^2 r_4 r_1 r_2^2 r_3 - r_5^2 r_4^2 r_2 r_1 - r_6 r_2 r_3 r_4^2 r_5 r_1 \\
&- 2 r_6^2 r_2 r_3 r_4^2 r_1)
\end{aligned}
$$

$$
\begin{aligned}
X_3 = (&-r_6^2 r_3^2 r_4 r_2^2 + r_5^2 r_1^2 r_4^2 + r_6^2 r_3^2 r_2^2 - r_6^2 r_3^2 r_1 r_2 r_4 - r_6^2 r_3^2 r_1 r_2 r_5 r_4^2 \\
&+ r_3^2 r_5 r_4 r_6^2 r_2^2 - r_3 r_5 r_2^2 r_6^2 r_4^2 + 2 r_6 r_3 r_1 r_5^2 r_2^2 r_4 - r_6 r_1 r_2^2 r_4^2 r_5^2 \\
&- r_6 r_3 r_1^2 r_5 r_4^2 - r_6 r_3^2 r_5 r_1 r_2^2 + r_6 r_3 r_1^2 r_5 r_2 r_4^2 - r_6 r_3^2 r_5 r_1 r_2 r_4 \\
&- r_6 r_3 r_1^2 r_5^2 r_2^2 r_4 + r_6 r_3^2 r_5 r_1^2 r_4^2 + r_6 r_3^2 r_1 r_5 r_4 r_2^2 + r_6 r_1^2 r_5^2 r_2 r_4^2 \\
&+ r_6 r_3^2 r_1^2 r_5 r_2^2 r_4^2 - r_6^2 r_3 r_2^2 r_5 r_4 + 2 r_6 r_3^2 r_1^2 r_5 r_2 r_4 - r_6 r_3 r_1^2 r_5 r_2 r_4 \\
&+ r_6 r_3 r_5^2 r_1 r_2 r_4^2 - r_6 r_3 r_2^2 r_5^2 r_4 - 2 r_6 r_3^2 r_1^2 r_5 r_2 r_4^2 + r_6 r_3^2 r_1^2 r_5 r_2^2 \\
&- r_3 r_1^2 r_5^2 r_2 r_4^2 r_6 - r_6^2 r_1 r_2 r_5 r_4^2 - r_3 r_1 r_5 r_2^2 r_6^2 r_4^2 - r_3 r_1 r_5^2 r_2^2 r_6 r_4^2 \\
&+ r_6^2 r_3 r_1 r_4 r_2 + 2 r_6^2 r_3 r_1 r_2 r_5 r_4^2 + r_6^2 r_3 r_1 r_2^2 r_5 r_4 - r_3^2 r_1 r_5 r_4 r_6^2 r_2^2 \\
&+ r_6^2 r_3^2 r_1 r_2 r_4^2 + r_3^2 r_1 r_5 r_2^2 r_6^2 r_4^2 + r_1 r_2^2 r_4^2 r_5^2 - r_3 r_1^2 r_5^2 r_4^2 - r_1^2 r_5^2 r_2 r_4^2 \\
&+ r_5^2 r_2^2 r_6 r_4^2 + r_5 r_2^2 r_6^2 r_4^2 - r_3 r_1^2 r_5^2 r_2 r_4 + 2 r_3 r_1^2 r_5^2 r_2 r_4^2 + r_3 r_5^2 r_1 r_2 r_4 \\
&+ r_6^2 r_3 r_4^2 r_2^2 + r_3 r_1^2 r_5^2 r_2^2 r_4 - r_3^2 r_1 r_2^2 r_6^2 r_4^2 - r_6^2 r_3^2 r_1 r_2^2 - r_3 r_1^2 r_5^2 r_2^2 r_4^2 \\
&+ r_3 r_1^2 r_5^2 r_2^2 r_6 r_4^2 - r_6 r_5^2 r_1 r_2 r_4^2 - 2 r_6 r_3^2 r_1^2 r_5 r_4 r_2^2 + 2 r_3^2 r_1 r_4 r_6^2 r_2^2 \\
&- r_6 r_2^2 r_4^2 r_5 - r_6^2 r_2^2 r_4 r_3 + r_6 r_2^2 r_4 r_5 r_3 + r_6 r_2 r_4^2 r_5 r_1 - r_5^2 r_4 r_1 r_2^2 r_3 \\
&- r_5^2 r_4^2 r_2 r_1 - r_6^2 r_2 r_3 r_4^2 r_1) \Big/ (-2 r_6^2 r_3^2 r_4 r_2^2 - r_3^2 r_5^2 r_6^2 r_4 r_2^2 \\
&- r_3^2 r_1^2 r_5^2 r_2 r_4 - r_6^2 r_1^2 r_2 r_5^2 r_4^2 - 2 r_6 r_3^2 r_1^2 r_5 r_4 + 2 r_6^2 r_1 r_2 r_5^2 r_4^2 \\
&- r_3^2 r_1^2 r_6^2 r_2 r_4 - r_5^2 r_1^2 r_3^2 r_4^2 r_6 - r_3 r_1^2 r_5 r_6^2 r_4^2 + 3 r_3 r_1^2 r_5^2 r_4^2 r_6 \\
&+ 2 r_6 r_3 r_1^2 r_5 r_4 - 2 r_6 r_3^2 r_5 r_1^2 r_2 + 2 r_6 r_3^2 r_1 r_5 r_2 - r_6 r_3^2 r_2^2 r_1 r_5^2 \\
&+ 3 r_6^2 r_3^2 r_1 r_2^2 r_5 - r_6^2 r_3^2 r_2^2 r_1^2 r_5 + r_3^2 r_1^2 r_5^2 r_2 r_4^2 r_6 + r_3 r_1^2 r_5^2 r_6^2 r_2 r_4^2 \\
&- r_3 r_1^2 r_5 r_6^2 r_2 r_4^2 - r_6 r_3 r_2 r_5^2 r_1 r_4 + 2 r_6^2 r_3^2 r_1 r_2 r_5 r_4 + r_6^2 r_3 r_1^2 r_2^2 r_5^2 r_4 \\
&- 3 r_6^2 r_3 r_1 r_2 r_5^2 r_4^2 - r_6^2 r_3 r_1 r_2 r_5 r_4 - 3 r_6^2 r_3 r_1 r_2^2 r_5^2 r_4 + r_6^2 r_3^2 r_1 r_2 r_5^2 r_4^2 \\
&- r_6 r_1^2 r_5 r_4^2 + 2 r_6 r_3 r_2 r_1^2 r_5^2 r_4 - r_3^2 r_1 r_5^2 r_2^2 r_4 r_6 - r_3^2 r_1^2 r_5 r_6^2 r_2 r_4 \\
&+ r_3^2 r_1^2 r_5 r_4 r_6^2 r_2^2 - r_3^2 r_1^2 r_5^2 r_2 r_6 r_4 + r_3^2 r_1 r_5^2 r_6^2 r_4 r_2^2 + 3 r_5^2 r_1^2 r_4^2 \\
&+ 3 r_6^2 r_3^2 r_2^2 + r_3^2 r_2^2 r_1 r_5^2 - r_3 r_1^2 r_5^2 r_4 + r_3^2 r_2 r_1^2 r_5^2 - r_3^2 r_2 r_1 r_5^2 \\
&- 2 r_6 r_1^2 r_4^2 r_5^2 + r_6^2 r_3^2 r_1^2 r_2 - r_6^2 r_3 r_1^2 r_4 - r_6^2 r_3^2 r_1 r_2 + r_6^2 r_3 r_1^2 r_4^2
\end{aligned}
$$

$$
\begin{aligned}
&+ r_6^2 r_3^2 r_1^2 r_4 - 3 r_6^2 r_3^2 r_1 r_2 r_4 - 3 r_6^2 r_3^2 r_1 r_2 r_5 r_4^2 + 3 r_3^2 r_5 r_4 r_6^2 r_2^2 \\
&- r_3 r_5 r_2^2 r_6^2 r_4^2 + r_3^2 r_5^2 r_1^2 r_4 + r_6 r_3^2 r_2^2 r_5^2 + r_6^2 r_1^2 r_5 r_4^2 + 6 r_6 r_3 r_1 r_5^2 r_2^2 r_4 \\
&- r_6 r_1 r_2^2 r_4^2 r_5^2 - 3 r_6 r_3 r_1^2 r_5 r_4^2 - 3 r_6 r_3^2 r_5 r_1 r_2^2 + 2 r_6 r_3 r_1^2 r_5 r_2 r_4^2 \\
&- r_6 r_3^2 r_5 r_1 r_2 r_4 - 3 r_6 r_3 r_1^2 r_5^2 r_2^2 r_4 + 2 r_6 r_3^2 r_5 r_1^2 r_4^2 + 2 r_6 r_3^2 r_1 r_5 r_4 r_2^2 \\
&+ 3 r_6 r_1^2 r_5^2 r_2 r_4^2 + r_6 r_3^2 r_1^2 r_5 r_2^2 r_4^2 - 3 r_6^2 r_3 r_2^2 r_5 r_4 + 6 r_6 r_3^2 r_1^2 r_5 r_2 r_4 \\
&- r_6 r_3 r_1^2 r_5 r_2 r_4 + 2 r_6 r_3 r_5^2 r_1 r_2 r_4^2 - 2 r_6 r_3 r_2^2 r_5^2 r_4 - 3 r_6 r_3^2 r_1^2 r_5 r_2 r_4^2 \\
&+ 2 r_6 r_3^2 r_1^2 r_5 r_2^2 - 3 r_3 r_1^2 r_5^2 r_2 r_4^2 r_6 - 2 r_6^2 r_1 r_2 r_5 r_4^2 - r_3 r_1 r_5 r_2^2 r_6^2 r_4^2 \\
&- r_3 r_1 r_5^2 r_2^2 r_6 r_4^2 + 2 r_6^2 r_3 r_1 r_4 r_2 + 6 r_6^2 r_3 r_1 r_2 r_5 r_4^2 + 2 r_6^2 r_3 r_1 r_2^2 r_5 r_4 \\
&- 3 r_3^2 r_1 r_5 r_4 r_6^2 r_2^2 + 2 r_6^2 r_3^2 r_1 r_2 r_4^2 + r_3^2 r_1 r_5 r_2^2 r_6^2 r_4^2 + r_1 r_2^2 r_4^2 r_5^2 \\
&- 2 r_3 r_1^2 r_5^2 r_4^2 - 2 r_1^2 r_5^2 r_2 r_4^2 + r_5^2 r_2^2 r_6 r_4^2 + r_5 r_2^2 r_6^2 r_4^2 - 3 r_3 r_1^2 r_5^2 r_2 r_4 \\
&+ 3 r_3 r_1^2 r_5^2 r_2 r_4^2 + 2 r_3 r_5^2 r_1 r_2 r_4 + r_6^2 r_3 r_4^2 r_2^2 + 2 r_3 r_1^2 r_5^2 r_2^2 r_4 \\
&- r_3^2 r_1 r_2^2 r_6^2 r_4^2 - 2 r_6^2 r_3^2 r_1 r_2^2 - r_3 r_1^2 r_5^2 r_2^2 r_4^2 + r_3 r_1^2 r_5^2 r_2^2 r_6 r_4^2 \\
&- 3 r_6 r_5^2 r_1 r_2 r_4^2 - 3 r_6 r_3^2 r_1^2 r_5 r_4 r_2^2 + 3 r_3^2 r_1 r_4 r_6^2 r_2^2 - r_6 r_2^2 r_4^2 r_5 \\
&- r_6^2 r_2^2 r_4 r_3 - 2 r_6^2 r_3^2 r_2^2 r_5 + 2 r_6^2 r_3 r_2^2 r_5^2 r_4 - r_6 r_2^2 r_3^2 r_5 + 2 r_6 r_2^2 r_4 r_5 r_3 \\
&+ 2 r_6 r_2 r_4^2 r_5 r_1 - r_6 r_4 r_1 r_2^2 r_5 r_3 - 2 r_5^2 r_4 r_1 r_2^2 r_3 - r_5^2 r_4^2 r_2 r_1 - r_6 r_2 r_3 r_4^2 r_5 r_1 \\
&- 2 r_6^2 r_2 r_3 r_4^2 r_1)
\end{aligned}
$$